UNIVERSITÀ DEGLI STUDI DI PADOVA

Head Office: Università degli Studi di Padova

Department of Cardiac, Thoracic, Vascular Sciences and Public Health

Ph.D. Course in Translational Specialistic Medicine "G.B. Morgagni"
Curriculum: Cardiovascular Sciences
Series 38°

MULTIMODALITY IMAGING IN CARDIAC AMYLOIDOSIS: FROM HISTOPATHOLOGICAL BASIS TO RISK STRATIFICATION

Coordinator: Prof. Dario Gregori
Supervisor: Prof. Alberto Cipriani
Co-Supervisor: Prof. Martina Perazzolo Marra
Supervisor period abroad: Prof. Marianna Fontana

Ph.D. Student: Giulio Sinigiani

Table of contents

Non-standard abbreviations and acronyms

AL: light chains amyloidosis
ATTR: transthyretin amyloidosis
ATTR-CM: transthyretin-related cardiomyopathy
ATTRv: hereditary transthyretin amyloidosis
ATTRwt: wild-type transthyretin amyloidosis
BNP: B-type natriuretic peptide
CA: cardiac amyloidosis
CCTA: coronary computed tomography angiography
CI: confidence interval
cTn: cardiac troponin
eGFR: estimated glomerular filtration rate
EMB: endomyocardial biopsy
HR: hazard ratio
Hs-cTn: high-sensitivity cardiac troponin
HF: heart failure
LVEF: left ventricular ejection fraction
NT-proBNP: N-terminal pro B-type natriuretic peptide

List of thesis original contributions

1. Relative apical sparing in cardiac amyloidosis is not always explained by an amyloid gradient.
2. Atrial electrofunctional predictors of incident atrial fibrillation in cardiac amyloidosis.
3. Right ventricular to pulmonary artery uncoupling is an early predictor of poor outcome in wild-type transthyretin amyloid cardiomyopathy.
4. Outcome and Disease Progression in NYHA Functional Class I and II Patients With Wild-Type Transthyretin Cardiomyopathy Treated With Tafamidis.

Abstracts

Relative apical sparing in cardiac amyloidosis is not always explained by an amyloid gradient

Background and aim: myocardial longitudinal strain (LS) by two-dimensional (2D) speckle-tracking echocardiography has a diagnostic and prognostic role in cardiac amyloidosis (CA). Typically, the apical segments of the left ventricle (LV) are less affected by LS abnormalities, a finding called relative apical sparing (RELAPS). Whether a variable burden of CA might explain the RELAPS remains unknown. We aimed to evaluate the extent, distribution, and deposition pattern of amyloid in autopsy hearts of CA patients and to correlate the histopathology findings with 2D echocardiography.

Methods: this is a retrospective study of whole heart specimens of CA patients who died and underwent autopsy and 2D echocardiography. Amyloid burden quantification was assessed by histomorphometry in each segment at different LV levels. The LS analysis results were compared with the amyloid burden and the base-to-apex distribution.

Results: histopathology investigation of 27 hearts with CA [immunoglobulin light chains (AL) 17 cases and transthyretin (ATTR) 10 cases] demonstrated an amyloid base-to-apex gradient. In 11 CA patients with 2D echocardiography, analysis of LS and histological amyloid burden allowed to identify different patterns: RELAPS (8 cases, 73%), with (2) or without (6) amyloid gradient, normal or mildly reduced LS with diffuse low amyloid (2, 18%), and severely reduced LS with diffuse high amyloid (1, 9%).

Conclusions: the typical RELAPS pattern at echocardiography is not always explained by a base-to-apex gradient of amyloid burden at histopathology, suggesting that RELAPS might be an epiphenomenon of complex interactions among amyloid infiltration, myocardial structure, and adaptation.

Atrial electrofunctional predictors of incident atrial fibrillation in cardiac amyloidosis

Background and aim: atrial fibrillation (AF) is common in patients with cardiac amyloidosis (CA) and is a significant risk factor for heart failure hospitalization and thromboembolic events. This study was designed to investigate the atrial electrofunctional predictors of incident AF in CA.

Methods: a multicenter, observational study was conducted in 4 CA referral centers including sinus rhythm patients with light-chain (AL) and transthyretin (ATTR) CA undergoing electrocardiography and cardiac magnetic resonance imaging. The primary end point was new-onset AF occurrence.

Results: overall, 96 patients (AL-CA, n = 40; ATTR-CA, n = 56) were enrolled. During an 18-month median follow-up (Q1-Q3, 7-29 months), 30 patients (29%) had incident AF. Compared with those without AF, patients with AF were older (79 vs 73 years; P = .001). They more frequently had ATTR (87% vs 45%; P < .001); electrocardiographic interatrial block (IAB), either partial (47% vs 21%; P = .011) or advanced (17% vs 3%; P = .017); and lower left atrial ejection fraction (LAEF; 29% vs 41%; P = .004). Age (hazard ratio [HR], 1.059; 95% CI, 1.002-1.118; P = .042), any type of IAB (HR, 2.211; 95% CI, 1.03-4.75; P = .041), and LAEF (HR, 0.967; 95% CI, 0.936-0.998; P = .044) emerged as independent predictors of incident AF. Patients exhibiting any type of IAB, LAEF <40%, and age >78 years showed a cumulative incidence for AF of 40% at 12 months. This risk was significantly higher than that carried by 1 (8.5%) or none (7.6%) of these 3 risk factors.

Conclusions: in patients with CA, older age, IAB on 12-lead electrocardiography, and reduced LAEF on cardiac magnetic resonance imaging are significant and independent predictors of incident AF. A closer screening for AF is advisable in CA patients carrying these features.

Right ventricular to pulmonary artery uncoupling is an early predictor of poor outcome in wild-type transthyretin amyloid cardiomyopathy

Background and aim: non-invasive right ventricular to pulmonary artery (RV-PA) uncoupling assessment has prognostic value in patients with heart failure (HF). Little is known about its application in patients with wild-type transthyretin amyloid cardiomyopathy (wtATTR-CM).

Methods: this single-centre retrospective study included consecutive patients with wtATTR-CM diagnosis undergoing 2D echocardiogram. RV-PA uncoupling was evaluated with the ratios between tricuspid annular plane systolic excursion (TAPSE), RV free wall longitudinal strain (RVFWLS) or RV four-chamber longitudinal strain (RV4CLS) and pulmonary artery systolic pressure (sPAP). Primary endpoint was the composite of all-cause mortality and HF hospitalisation.

Results: overall, 100 patients (91% males, median age 81 years, 85% in National Amyloid Centre (NAC) stage ≤ 2, 18% in NAC stage Ia and 82% in New York Heart Association class ≤ II) were enrolled. Over a 16-months follow up (Q1-Q3:12-24), the primary endpoint occurred in 37 patients (37%). TAPSE/sPAP (HR 0.04, 95% CI 0.01-0.24, $p < 0.001$), RVFWLS/sPAP (HR 0.07, 95% CI 0.01-0.41, $p = 0.003$) and RV4CLS/sPAP (HR 0.06, 95% CI 0.01-0.53, $p = 0.011$) emerged as independent predictors of the primary endpoint and showed incremental risk prediction compared with TAPSE, RVFWLS and RV4CLS, considered as separate parameters. No differences in outcome risk prediction were observed among TAPSE/sPAP, RVFWLS/sPAP and RV4CLS/sPAP ($p > 0.05$).

Conclusions: in patients with CA, older age, IAB on 12-lead electrocardiography, and reduced LAEF on cardiac magnetic resonance imaging are significant and independent predictors of incident AF. A closer screening for AF is advisable in CA patients carrying these features.

Outcome and Disease Progression in NYHA Functional Class I and II Patients With Wild-Type Transthyretin Cardiomyopathy Treated With Tafamidis

Background and aim: Tafamidis has been the first and, for years, the only clinically available disease-modifying therapy for ATTRwt-CM, with the greatest benefit in NYHA class I–II. Monitoring the response remains an unmet need, as treatment options are expanding. We aimed to investigate outcomes and disease progression in NYHA class I–II patients with wild-type transthyretin cardiomyopathy (ATTRwt-CM) treated with tafamidis.

Methods: NYHA class I-II ATTRwt-CM patients receiving tafamidis were included. Treatment response was assessed based on: (1) occurrence of the primary endpoint, a composite of heart failure (HF) hospitalization and all-cause death; (2) clinical, biochemical, and echocardiographic criteria of 12-month disease progression.

Results: 683 patients were enrolled (median age 78 years; NAC/Mondor stage I, II and III: 64%, 29%, and 7%). Within 12 months, the primary endpoint occurred in 58 patients (9%), independently associated with higher daily loop diuretic dose (HR 1.29, 95% CI 1.14 – 1.46, $p < 0.001$) and NAC/Mondor stage III (HR 2.51, 95% CI 1.00 – 6.26, $p = 0.047$). After 12 months, worsening of NYHA class, NAC/Mondor stage, NT-proBNP, eGFR and outpatient diuretic intensification (ODI) occurred in 85/607 (14%), 109/591 (18%), 146/625 (23%), 117/591 (20%) and 210/625 (34%), respectively. Two predictive models were developed: the first including progression to NYHA class III (HR 4.81, 95% CI 2.52 – 9.20, $p < 0.001$) and NAC/Mondor stage worsening (HR 3.59, 95% CI 1.89 – 6.81, $p < 0.001$); the second including NT-proBNP progression (HR 3.32, 95% CI 1.73 – 6.38, $p < 0.001$), eGFR decline (HR 2.14, 95% CI 1.13 – 4.08, $p = 0.020$) and ODI (HR 1.92, 95% CI 1.01 – 3.68, $p = 0.046$) (Harrell's C 0.71 and 0.72).

Conclusions: in a large cohort of early-stage tafamidis-treated ATTRwt-CM patients, 9% experienced HF hospitalization or death, and up to one-third exhibited markers of disease

progression within 12-months. Two models accurately forecasted poor prognosis, offering potential to treatment optimization.

PART I: BACKGROUND

Chapter 1. Introduction to systemic amyloidosis

Systemic amyloidoses are protein misfolding disorders characterized by extracellular deposition of amyloid fibrils, ultimately leading to progressive organ dysfunction. The term “amyloid”, first introduced by Virchow to describe a substance he erroneously considered starch-like in nature[1], refers to highly organized, insoluble protein fibrils that display marked resistance to proteolytic degradation[2]. To date, more than 40 amyloidogenic proteins have been identified, and many of them may cause systemic disease, in which the precursor protein is synthesized at one site (e.g., bone marrow or liver) and deposited in distant organs (e.g., heart and kidneys)[3]. In recent years, systemic amyloidosis has undergone a profound revolution in both diagnostic approaches and therapeutic strategies. The pathogenic mechanisms underlying systemic amyloidosis can be broadly classified into three categories: (1) excess production of amyloidogenic proteins; (2) structural alterations of mutant proteins with increased propensity for misfolding; and (3) intrinsic amyloidogenicity of normal (wild-type) proteins[2]. Several forms of systemic amyloidosis are clinically relevant and may result in multi-organ involvement. Among these, the subtypes most frequently affecting the heart are light chain (AL) amyloidosis and transthyretin (ATTR) amyloidosis, the latter occurring either in hereditary (ATTRv) or wild-type (ATTRwt) forms. These three conditions represent distinct clinical entities with specific natural history, prognosis, and therapeutic strategies[4], and will be addressed in detail.

Cardiac involvement may also rarely occur in AA amyloidosis, or secondary amyloidosis, which is driven by chronic inflammatory activation and characterized by deposition of serum amyloid A (SAA), an acute-phase reactant[2].

1.1 Pathophysiology

The pathogenetic hallmark of amyloidosis is the transformation of soluble, globular proteins into insoluble amyloid fibrils, which progressively deposit in vital organs and impair their function[5]. This multifactorial process can be promoted by different mechanisms, including destabilizing

mutations that expose hydrophobic or protease-sensitive regions (as in ATTRv), elevated protein concentrations resulting from increased synthesis or impaired clearance (as in AL), or the intrinsic amyloidogenic propensity of certain proteins that becomes clinically evident with aging (as in ATTRwt)[5]. Normally, intracellular and extracellular proteostasis pathways counteract protein misfolding and aggregation; however, when these mechanisms fail—for instance, due to aging—protein aggregation and fibril formation may ensue. In vitro studies of AL amyloidosis have shown that fibrillogenesis begins with misfolding of monomeric native proteins into partially folded intermediates[5]. Once these species reach a threshold concentration, a critical nucleus forms, triggering rapid protein aggregation and fibril elongation. Notably, after nucleation, fibril growth accelerates, requiring lower concentrations of misfolded proteins, and amyloid fibrils themselves act as templates to further promote precursor protein misfolding and oligomer formation. Structurally, amyloid fibrils display a highly ordered cross-β-sheet arrangement, characterized by antiparallel β-strands oriented perpendicularly to the fibril axis, as demonstrated by X-ray diffraction. Their ultrastructure is further defined by a diameter of 7.5–10.0 nm on electron microscopy[5]. The diagnosis of systemic amyloidosis relies on the combination of a compatible clinical phenotype and histological confirmation of extracellular Congo red–positive deposits, which exhibit the pathognomonic apple-green birefringence under polarized light[2]. Since histological appearance does not distinguish among amyloidosis subtypes, precise identification of the precursor protein is required. Mass spectrometry–based proteomic analysis represents the gold standard, though its use is limited by high cost and availability. Immunohistochemistry and immunoelectron microscopy with antibody-directed techniques may serve as alternative typing methods in specialized laboratories, although in challenging cases mass spectrometry may still be necessary to establish a definitive diagnosis[6].

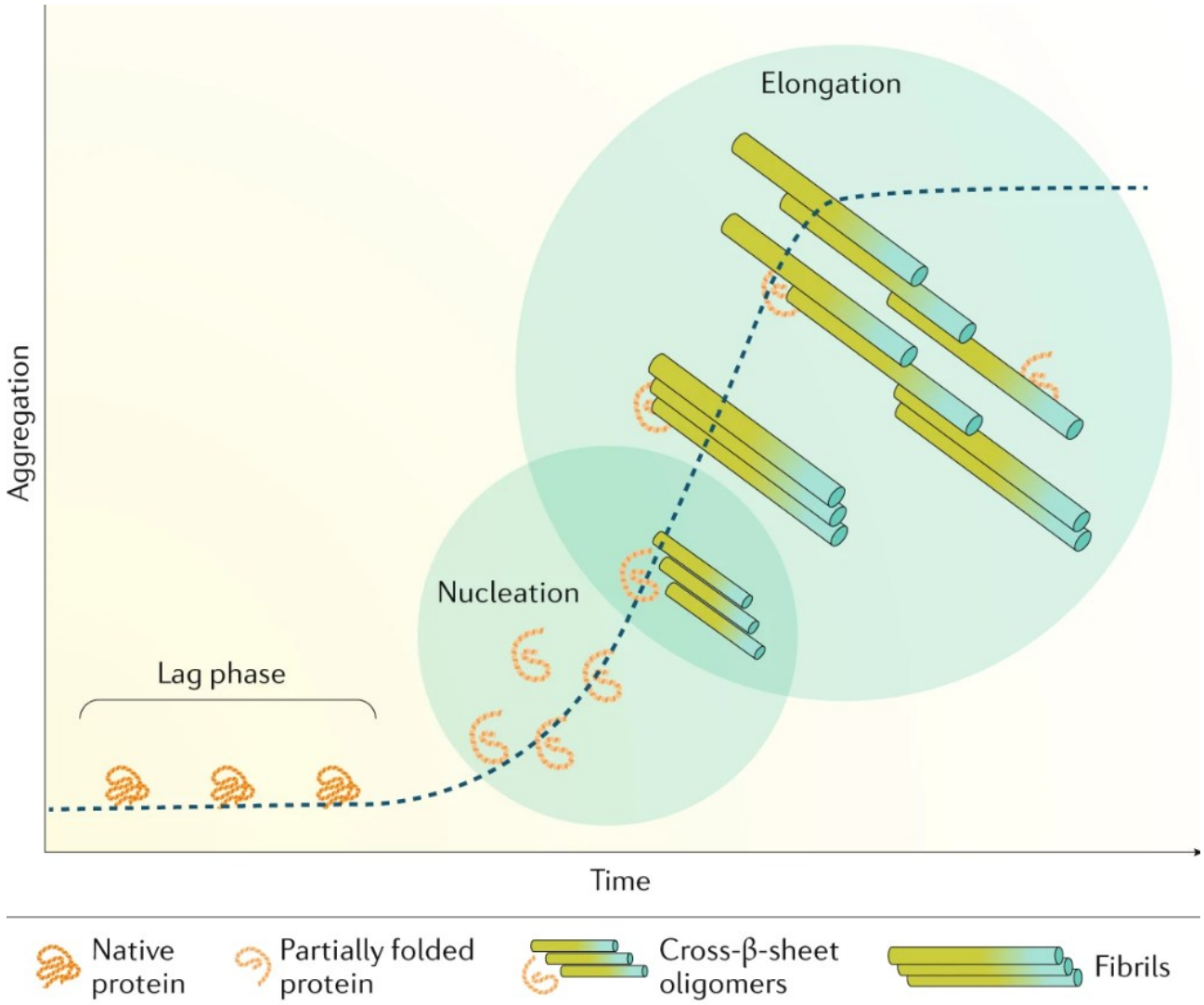

Figure 1. In vitro kinetics of amyloid fibrils formation. From Merlini et al[5].

1.2. Nomenclature

Amyloid fibrils are named according to their precursor protein, using an abbreviated form preceded by the letter "A" for amyloid. For instance, immunoglobulin light chain–derived amyloid is termed AL, while transthyretin-derived amyloid is designated ATTR. Further specification is possible, such as ATTRv for the hereditary variant, ATTRV30M for a specific mutation, or ATTRwt for the wild-type form. In 2024, the Nomenclature Committee recommended that mutations be numbered according to the sequence of the mature protein, excluding the leader sequence and propeptides. When referring to specific clinical conditions, the precursor protein abbreviation should be followed by the term "amyloidosis," for example, ATTR amyloidosis or AL amyloidosis. Additional

clinically relevant descriptors, such as ATTR cardiomyopathy or AL neuropathy, may also be used[3].

1.3 References

1. Kyle RA. Amyloidosis: a convoluted story. Br J Haematol. 2001;114(3):529-38.
2. Muchtar E, Dispenzieri A, Magen H, et al. Systemic amyloidosis from A (AA) to T (ATTR): a review. J Intern Med. 2021;289(3):268-292.
3. Buxbaum JN, Eisenberg DS, Fändrich M, et al. Amyloid nomenclature 2024: update, novel proteins, and recommendations by the International Society of Amyloidosis (ISA) Nomenclature Committee. Amyloid. 2024;31(4):249-256.
4. Rapezzi C, Merlini G, Quarta CC, et al. Systemic cardiac amyloidoses: disease profiles and clinical courses of the 3 main types. Circulation. 2009;120(13):1203-12.
5. Merlini G, Dispenzieri A, Sanchorawala V, et al. Systemic immunoglobulin light chain amyloidosis. Nat Rev Dis Primers. 2018;4(1):38.
6. Garcia-Pavia P, Rapezzi C, Adler Y, et al. Diagnosis and treatment of cardiac amyloidosis: a position statement of the ESC Working Group on Myocardial and Pericardial Diseases. Eur Heart J. 2021;42(16):1554-1568.

Chapter 2. Amyloidosis and the heart: AL and ATTR amyloidosis

When amyloid deposition affects the heart, the so-called cardiac amyloidosis occurs[1]. More than 98% of contemporary cases of cardiac amyloidosis are attributable to fibrils derived from either monoclonal immunoglobulin light chains (AL) or transthyretin (ATTR), the latter occurring in hereditary (ATTRv) or wild-type (ATTRwt) forms[2]. This chapter encompasses both these subtypes, describing their unique pathophysiological, clinical and treatment aspects.

2.1. AL amyloidosis pathophysiology

In AL amyloidosis, misfolding of immunoglobulin light chains arises from either proteolytic cleavage or amino acid sequence alterations that confer thermodynamic and kinetic instability, ultimately promoting self-aggregation[3]. These aggregates interact with glycosaminoglycans and serum amyloid P component, thereby facilitating fibril formation, stabilizing tissue deposits, and progressively disrupting organ architecture and function. Experimental evidence from in vitro models indicates that amyloidogenic precursor aggregates exert direct cytotoxic effects, adding to organ dysfunction[4,5,6].

AL amyloidosis is most often associated with an underlying plasma cell disorder that produces monoclonal immunoglobulin light chains, predominantly of the lambda subtype (75–80% of cases), with kappa chains accounting for the remaining 20–25%[6]. The chromosomal translocation t(11;14), which juxtaposes the immunoglobulin heavy-chain (IgH) locus and the oncogene cyclin D1, is a hallmark of AL amyloidosis and is identified in approximately 50% of cases[7], whereas hyperdiploidy—frequent in multiple myeloma—is observed in only ~10% of affected patients[8]. In addition, somatic mutations within the IGLV gene family, encoding the variable region of the light chain, further reduce protein stability and thereby enhance the propensity for amyloid fibril formation[9].

2.2. AL amyloidosis clinical manifestations

As shown in **Figure 1**, the heart is the most involved organ in AL amyloidosis. Other manifestations are nephropathy (>60% of patients), hepatomegaly (> 50% of patients), neuropathy (10-20% of patients), macroglossia (17% of patients) and periorbital purpura (15% of patients)[10]. Cardiac involvement represents the major determinant of prognosis in AL amyloidosis, accounting for more than 61% of deaths and constituting the leading cause of mortality[11]. Clinically, patients with heart involvement exhibits as progressive heart failure, atrial and ventricular arrhythmias, and advanced atrio-ventricular blocks[10]. Myocardial infiltration typically produces symmetrical biventricular wall thickening with nondilated or small ventricular cavities. Left ventricular ejection fraction is generally preserved until advanced stages, whereas systolic dysfunction primarily affects longitudinal rather than radial function[12]. This disproportionate reduction in longitudinal strain is more pronounced than in other hypertrophic cardiomyopathies and is characteristically accompanied by relative apical sparing, resulting in the well-recognized “bull’s-eye pattern” on longitudinal strain polar maps[13]. Early left ventricular involvement is marked by impaired relaxation, which invariably evolves into a restrictive filling pattern. Additional, though nonspecific, findings include thickening of atrioventricular valves and the interatrial septum, a speckled myocardial appearance, and the presence of pericardial and pleural effusions[12].

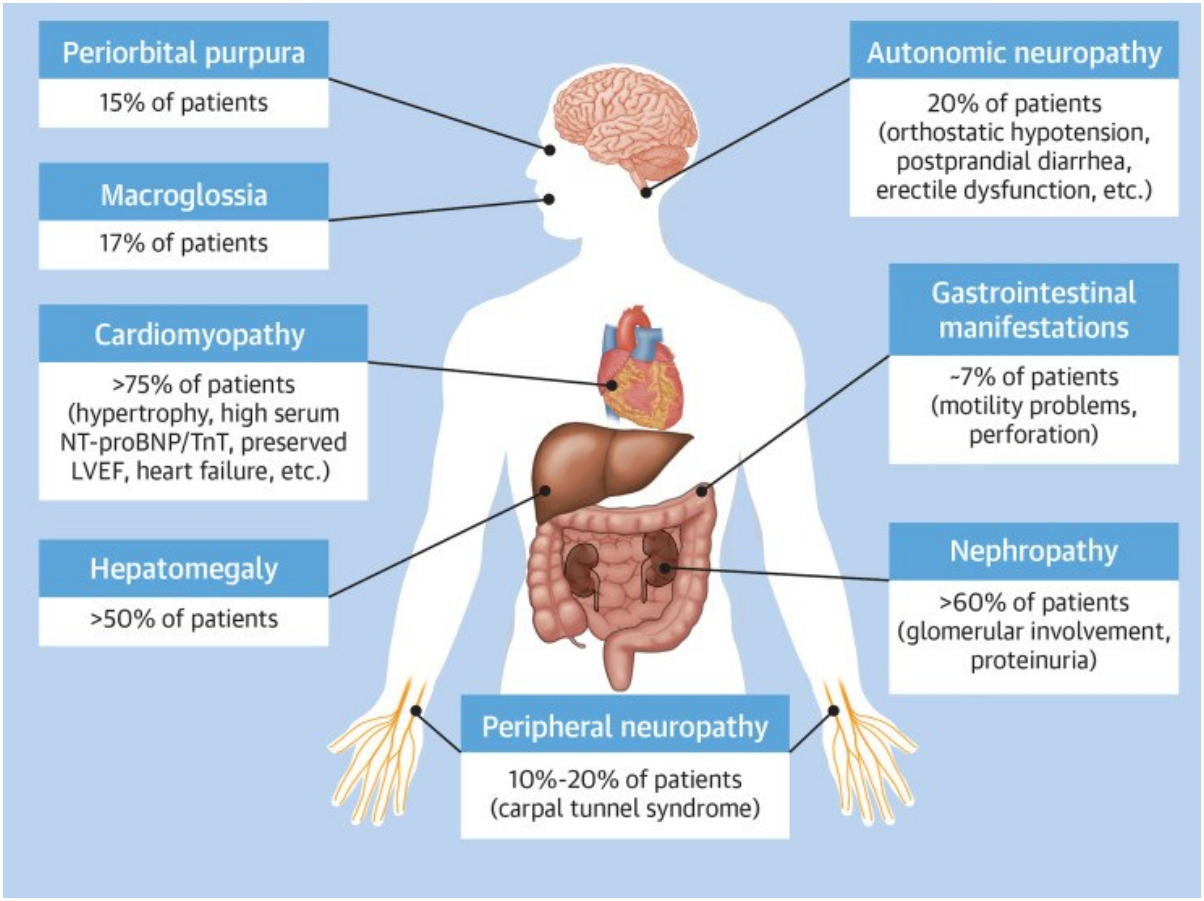

Figure 1. Common Pathologies Among Patients With Amyloid Light Chain Amyloidosis. From Wechalekar et al[10]. LVEF = left ventricular ejection fraction; NT-proBNP = N-terminal pro–brain natriuretic peptide; TnT = troponin T.

2.3. AL amyloidosis diagnosis and staging

The suspicion of the disease relies upon the so-called "red flags", signs and symptoms with high sensitivity and variable specificity for the diagnosis. Index of suspicion should be high for a patient presenting with heart failure and other extracardiac symptoms, as neuropathy, bleeding, carpal tunnel syndrome, nephrotic syndrome, proteinuria, diarrhea, hepatomegaly, peripheral and autonomic neuropathy, macroglossia, and periorbital purpura[14,15]. ECG and cardiac imaging are essential sources of red flags and will be discussed in detail in dedicated chapters. Regarding biomarkers, elevated serum cardiac troponin T and/or N-terminal pro-brain natriuretic peptide (NT-proBNP) are common in patients with cardiac AL amyloidosis[15,16]. Once amyloidosis is clinically suspected, the initial step is the evaluation for an underlying plasma cell disorder, typically performed through serum free light chain assessment and serum and urine immunofixation

electrophoresis. The absence of a detectable monoclonal protein by these exams makes AL amyloidosis less likely. Conversely, a positive result may reflect monoclonal gammopathy of undetermined significance, multiple myeloma, indolent B-cell lymphoma, Waldenström macroglobulinemia, or AL amyloidosis[17]. Definitive diagnosis, however, requires histological demonstration of amyloid deposits. Abdominal fat pad aspiration offers a rapid and safe biopsy option, although with limited sensitivity[18]. Bone marrow biopsy is mandatory, and when combined with fat pad biopsy, diagnostic sensitivity for AL amyloidosis reaches approximately 85%[19]. In cases with negative results, labial salivary gland biopsy may be considered. Ultimately, biopsy of the clinically affected organ—including the heart—should be performed if uncertainty persists. Congo red staining represents the initial approach for detecting amyloid deposits, but its limited sensitivity and inability to identify the precursor protein restrict its diagnostic value and may risk misclassification with serious clinical consequences. For improved sensitivity and reliable amyloid typing, immunohistochemistry is commonly employed; however, its accuracy is highly dependent on laboratory expertise and requires an extensive antibody panel[20]. Mass spectrometry–based proteomic analysis remains the diagnostic gold standard[20].

After diagnosis, disease staging is essential. The Mayo Clinic proposed a staging system in 2004, which classified patients into three stages based on troponin T and NT-proBNP levels, using thresholds of TnT <0.035 µg/L and NT-proBNP <332 ng/L. Patients were categorized as stage I when both markers were below threshold, stage II when only one was elevated, and stage III when both were elevated[21]. In 2012, this model was revised by incorporating different thresholds (TnT ≥ 0.025 ng/mL, NT-proBNP ≥ 1,800 pg/mL) and adding the difference in free light chains (dFLC ≥ 180 mg/L) as a measure of disease burden, thereby expanding stratification into four stages (I–IV)[22]. Moreover, to refine risk discrimination in advanced disease, stage III was further subdivided into IIIa and IIIb, based on an NT-proBNP cutoff of 8,500 pg/mL[23]. More recently, an alternative system employing BNP rather than NT-proBNP was proposed, thereby enabling disease staging in centers lacking NT-proBNP or TnT assays. This classification assigns patients to stage I when both

BNP (<81 pg/mL) and troponin I (TnI <0.1 ng/mL) are below threshold, stage II when only one is elevated, and stage III when both are elevated, with further subdivision into IIIa and IIIb depending on whether BNP is below or above 700 pg/mL[24].

2.4 AL amyloidosis disease-modifying treatment

At diagnosis, patients with AL amyloidosis are stratified to determine eligibility for autologous stem cell transplantation (ASCT), which is feasible in approximately 20% of cases, whereas the remaining ~80% are directed to combination chemotherapy. The eligibility criteria for ASCT are stringent to minimize treatment-related mortality, and from a cardiovascular standpoint, include a New York Heart Association class I-II, a left ventricular ejection fraction ≥40%, a systolic blood pressure ≥90 mmHg, NTproBNP < 5000 pg/mL, Troponin I <0.1 ng/mL and Troponin T <60 ng/L and hs-Troponin T <75 ng/mL[25]. In those undergoing ASCT as first-line therapy, complete or very good partial hematologic responses are achieved in nearly 73% of cases[26]. For patients ineligible for ASCT first-line management consists of plasma cell–directed therapy. Current guidelines endorse daratumumab in combination with cyclophosphamide, bortezomib, and dexamethasone (Dara-CyBorD) as the preferred regimen, with CyBorD or bortezomib–melphalan–dexamethasone serving as alternatives when access to daratumumab is limited[27]. The hematologic efficacy of Dara-CyBorD is remarkable, with ~78% of patients achieving a very good partial response or better[28]. Nonetheless, tolerability issues are common, as more than 20% of patients discontinue at least one drug and over 30% require dose reductions due to adverse events[29]. In patients with clinically significant neuropathy, treatment strategies that avoid bortezomib, including daratumumab monotherapy, may be considered. Currently, no consensus exists regarding the criteria for initiating second-line therapy in patients with progressive disease following first-line treatment. In cases of relapse, re-treatment with the initial regimen may be considered if the prior response was sustained for more than 12 months; however, these patients generally experience shorter subsequent remission durations, albeit without a significant impact on overall survival compared with those switched to alternative regimens. Therapeutic options for relapsed systemic AL amyloidosis include

proteasome inhibitors, anti–CD38 monoclonal antibodies, immunomodulatory agents, venetoclax for patients harboring t(11;14), bendamustine, high-dose melphalan with autologous stem cell transplantation, as well as emerging strategies such as bispecific antibodies and chimeric antigen receptor T-cell therapy. Although treatment sequencing cannot be standardized, two principles guide therapeutic decisions: the depth and durability of the initial response, and the use of drug classes not previously administered. Additionally, patient frailty, comorbidities, and end-organ damage must be carefully weighed.

2.5 AL amyloidosis disease monitoring

The criteria for disease monitoring, summarized in **Table 1**, rely exclusively on markers of plasma cell activity and organ response biomarkers. The therapeutic goal is to quickly achieve at least a very good partial hematologic response, as partial or absent responses are associated with unfavourable prognosis. The deep and rapidity in haematological response is also crucial for the subsequent, slower, organ response.

Table 1. Monitoring disease course in AL amyloidosis.

System	Response	Criteria
Haematologic[30]	CR	Absence of amyloidogenic light chains defined by negative IFE of both serum and urine AND Either an FLC ratio within the reference range or uninvolved FLC concentration greater than involved FLC concentration with or without an abnormal FLC ratio
	VGPR	dFLC <40 mg/L
	PR	dFLC decrease >50% from baseline
	NR	All other patients
Cardiac[31]	CarCR	Nadir NT-proBNP ≤ 350 pg/ml or BNP ≤ 80 pg/ml
	CarVGPR	>60% reduction in NT-proBNP/BNP form baseline level not meeting CarCR
	CarPR	31-60% reduction in NT-proBNP from baseline not meeting CarCR
	CarNR	≤30% reduction in NT-proBNP from baseline level
	Progression	NT-proBNP progression >30% and >300 pg/mL, not precipitated by infection, elevate creatinine or arrhythmias OR Troponin increase > 33% OR EF decrease ≥ 10%
Renal[32,33]	KidCR	Proteinuria ≤200 mg/24h
	KidVGPR	>60% reduction in proteinuria/24h
	KidPR	30 – 60% reduction in proteinuria/24h
	KidNR	≤30% reduction in proteinuria/24h
	Progression	≥25% decrease in eGFR

Hepatic[34]	Improvement	Decrease in ALP ≥50% OR ALP normalization

Abbreviations: ALP: alkaline phosphatase; BNP: B-type natriuretic peptide; Car: cardiac; CR: complete response; EF: ejection fraction; eGFR: estimated glomerular filtration rate; dFLC: difference free light chain; Kid: kidney; IFE: immunofixation electrophoresis; NR: non response; NT-proBNP: N-terminal pro B-type natriuretic peptide; PR: partial response; VGPR: very good partial response.

2.6 ATTR amyloidosis pathophysiology

Transthyretin, also known as prealbumin, is a 55-kDa transport protein that circulates as a homo-tetramer composed of four identical monomers. It is a carrier for thyroxine and retinol-binding protein. Approximately 95% of TTR is synthesized in the liver and secreted into the circulation, with smaller amounts produced by the choroid plexus and retinal pigment epithelium[35]. The most widely accepted mechanism of amyloid fibril formation involves tetramer dissociation into dimers and monomers, followed by protein misfolding and aggregation into amyloid fibrils[35]. Factors contributing to transthyretin destabilization include oxidative modifications, age-related decline in proteostatic capacity, metal cations, proteolysis and genetic mutations[35]. These mechanisms converge on the generation of a stable nucleus capable of growth through sequential monomer addition, in a process analogous to that described for AL amyloidosis. Once nucleation has occurred, the presence of preformed seeds can markedly accelerate fibril formation, a phenomenon known as seeding. During the subsequent elongation phase, progressive monomer incorporation leads to the development of mature amyloid fibrils. These fibrils may consist of both C-terminal transthyretin fragments and full-length protein (type A fibrils), or exclusively of full-length transthyretin (type B fibrils)[35]. When fibrils deposit in the extracellular space, transthyretin amyloidosis (ATTR) occurs. It arises either from age-related impairment of above-mentioned homeostatic mechanisms with a wild-type protein (ATTRwt), or from destabilizing mutations in variant ATTR (ATTRv)[36,37].

2.7 ATTR amyloidosis clinical manifestations

Clinical manifestations are substantially different between ATTRwt and ATTRv. ATTRwt predominantly affects older individuals (mean age ~75 years, typically >60 years) and occurs more frequently in men[38,39]. Until recently, ATTRwt was frequently under- or misdiagnosed. However, the advent of non-invasive diagnostic tools, the availability of disease-modifying therapies, and growing clinical awareness have led to a marked increase in reported incidence and a shift toward recognition of milder phenotypes[40]. ATTRwt involves both the heart and soft tissues, leading to ATTR cardiomyopathy (ATTR-CM) and to musculoskeletal manifestations[41]. Peripheral and autonomic neuropathies, generally mild, may occasionally occur.

ATTR-CM typically presents with signs and symptoms of heart failure (HF), accompanied by increased left ventricular wall thickness with impaired diastolic filling and longitudinal systolic dysfunction, fulfilling the criteria for HF with preserved ejection fraction (HFpEF)[42]. A subset of patients may manifest with mildly reduced or reduced ejection fraction, especially in advanced stages of the disease[42]. Furthermore, ATTR-CM manifests commonly with arrhythmias, that will be discussed in detail in a dedicated chapter. Notably, the risk of intracardiac thrombus is elevated even in sinus rhythm[43], and stroke or systemic embolization may occasionally represent the initial presentation. Among valvular diseases, the association between aortic stenosis and ATTR-CM is increasingly recognized[44]. Imaging characteristics of ATTR-CM will be discussed in detail in a dedicated chapter. On the other hand, musculoskeletal involvement is a hallmark of ATTRwt[41]. Carpal tunnel syndrome and its prior treatment often precede the cardiac diagnosis by 5–10 years[45]. Similarly, lumbar spinal stenosis is closely associated with ATTRwt, with frequent amyloid deposition in the ligamentum flavum of elderly patients undergoing surgery[46]. Other features may include atraumatic rupture of the brachial bicep tendon, trigger finger, and rotator cuff rupture.

By contrast, ATTRv typically presents at a younger age and shows greater heterogeneity in sex distribution and clinical phenotype[35]. The prevalence of genotypes is strongly influenced by geography. Val122Ile substitution is most frequent in the United States, Caribbean, and Africa

(present in 3–4% of Afro-Caribbean individuals), the Thr60Ala mutation is predominantly observed in the United Kingdom and Ireland, while the Val30Met mutation is highly prevalent in Portugal, Sweden, and Japan. In Italy, multiple variants have been reported, with Ile68Leu being the most common among patients with an exclusively cardiac phenotype. Clinical manifestations are more heterogeneous compared to ATTRwt, and largely dependent upon by genotype[47] (**Figure 2**). In addition to cardiac involvement, peripheral sensory-motor neuropathy is frequent, along with autonomic dysfunction and gastrointestinal symptoms (**Figure 3**)[48].

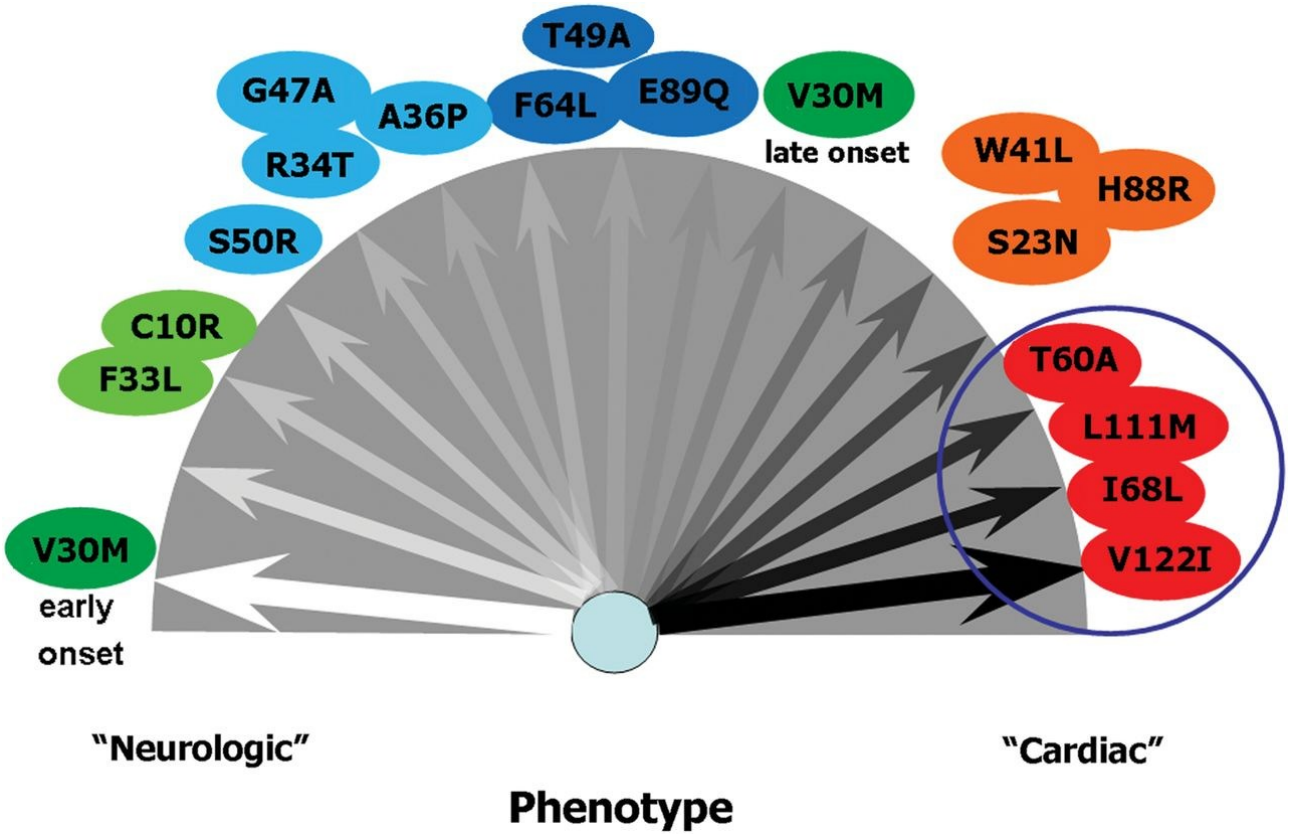

Figure 2. Possible spectrum of genotype–phenotype correlations in transthyretin-related amyloidosis. From Rapezzi et al.[47]

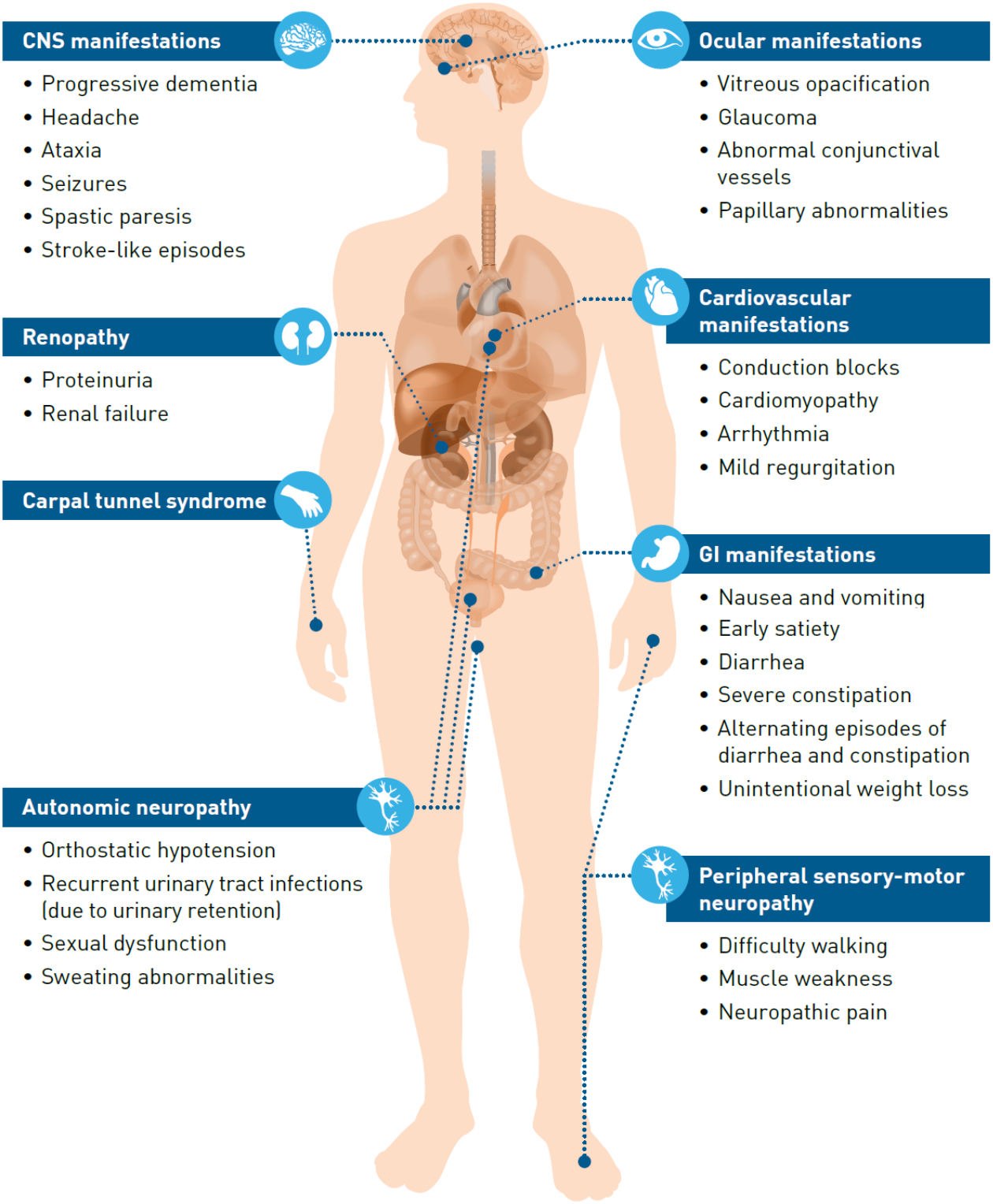

Figure 3. Clinical manifestations of ATTRv. From Gertz et al.[48]

2.8 ATTR amyloidosis diagnosis and staging

This chapter is focused on the diagnosis and staging of ATTR-CM, being the other ATTR-related clinical conditions beyond its scope.

Similarly to AL amyloidosis, the suspicion of the disease relies upon the so-called red flags. In ATTRwt-CM and ATTRv-CM, musculoskeletal and neurological manifestations, respectively, represent important clinical clues that in presence of suggestive imaging should heighten the index of suspicion[2]. Imaging red flags will be discussed in detail in a dedicated chapter. To confirm the suspicion, the European Society of Cardiology Consensus indicates either an invasive or a non-invasive diagnostic pathway[2]. Similarly to AL amyloidosis, invasive criteria require demonstration of amyloid fibrils within cardiac tissue, or alternatively, evidence of amyloid deposits in an extracardiac biopsy combined with characteristic imaging findings of cardiac amyloidosis. This pathway becomes mandatory when a plasma cell disorder is identified by serum free light chain analysis and serum or urine immunofixation, given the lack of specificity of non-invasive criteria for ATTR-CM in this context[2]. Otherwise, planar and single-photon emission computed tomography scintigraphy using bone-avid tracers such as 99mtechnetium-pyrophosphate (99mTc-PYP), 3,3-diphosphono-1,2-propanodicarboxylic acid (DPD), or hydroxymethylene diphosphonate (HMDP) enable the non-invasive diagnosis of ATTR-CM, with a Perugini score of grade 2 or 3 myocardial uptake is considered diagnostic[2]. False-negative scans may occur in specific ATTRv genotypes[49], whereas false-positive results can be observed in AL amyloidosis, recent myocardial infarction, long-term chloroquine therapy, or due to blood-pool activity within the left ventricle[50]. Further details on the diagnostic role of bone scintigraphy will be provided in a dedicated chapter.

Several staging systems for ATTR-CM were proposed. Between them, the National Amyloid Centre (NAC) staging system is the most used[51]. The score is based on NT-proBNP and estimated glomerular filtration rate (eGFR), with thresholds of NT-proBNP 3000 ng/L and eGFR 45 mL/min/1.73 m². Stage I is defined as NT-proBNP ≤ 3000 ng/L and eGFR ≥45 mL/min/1.73 m²; stage III as NT-proBNP >3000 ng/L and eGFR <45 mL/min/1.73 m²; and all other combinations

were classified as stage II[52]. More recently, stage I was further divided into stage Ia, defined as a daily intake of furosemide equivalent of <0.75 mg/kg and an NT-proBNP ≤500 ng/L or ≤1000 ng/L in the presence of atrial fibrillation, and stage Ib comprising all remaining stage I patients[53]. Moreover, the system was further expanded by the introduction of a new stage 4, defined as NT-proBNP ≥10 000 ng/L, irrespective of eGFR[54].

2.9 ATTR amyloidosis disease-modifying treatment

This paragraph is adapted from the manuscript: *De Michieli, L.; Lupi, A.; Sinigiani, G.; Tietto, A.; Salvalaggio, A.; Branca, A.; Da Pozzo, S.; Rizzo, S.; Cecchin, D.; Perazzolo Marra, M.; et al. Pharmacological Management of Transthyretin Amyloid Cardiomyopathy: Where We Are and Where We Are Going. J. Clin. Med. 2025, 14, 3481.*

ATTR disease modifying drugs aim to either stabilise transthyretin tetramer, stop its production, or actively promote amyloid clearance (**Figure 4**).

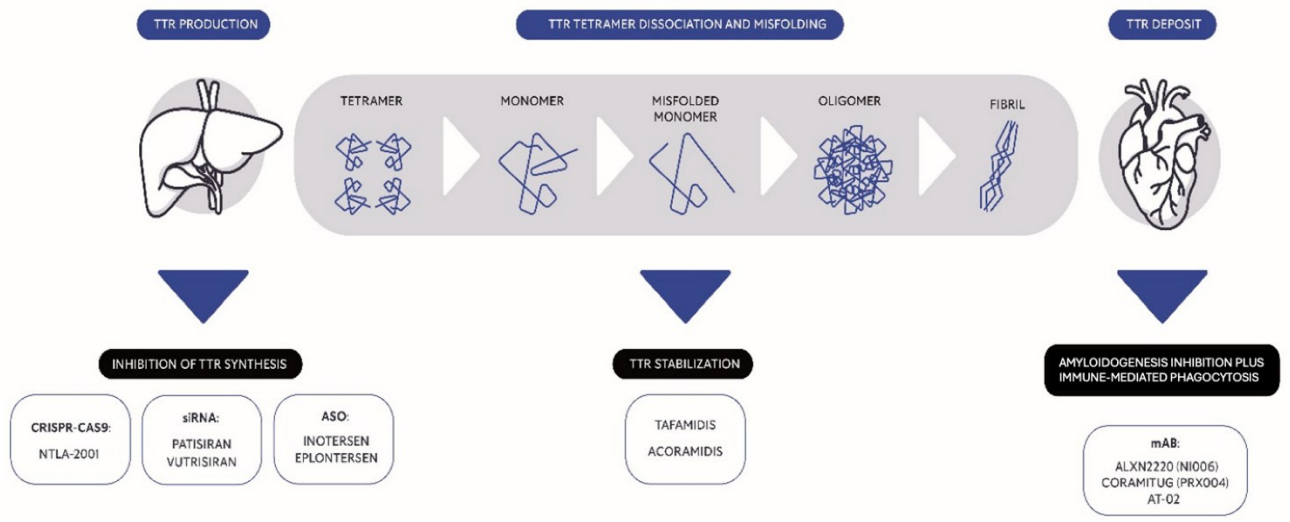

Figure 4. Present therapeutic landscape of transthyretin amyloid cardiomyopathy (ATTR-CM).. ASO: antisense oligonucleotides. CRISPR-CAS9: clustered regularly interspaced short palindromic repeats CAS9. mAb: monoclonal antibody. siRNA: short interfering ribonucleic acid. From De Michieli et al.

TTR stabilisation

Two main molecules have been investigated in randomised clinical trials with the purpose of TTR stabilisation: tafamidis and acoramidis. Diflunisal, which is a non-steroidal anti-inflammatory agent acting as a non-selective TTR stabiliser, has been investigated in non-randomised studies with small cohorts of patients and non-negligible adverse effects[55]; it is rarely clinically used nowadays and not

reported in recent Consensus Documents and Guidelines[56,57]. The following paragraphs will focus on tafamidis and acoramidis and their respective clinical trials.

Tafamidis

The ATTR-ACT (Tafamidis Treatment for Patients with Transthyretin Amyloid Cardiomyopathy) trial[58] was the first pivotal study investigating a disease-modifying therapy specifically in ATTR-CM; previous trials with tafamidis[59] and other molecules, such as inotersen[60] and patisiran[61], focused on ATTR-related neuropathy. The ATTR-ACT trial evaluated tafamidis, a benzoxazole derivative that binds to the thyroxine-binding sites of TTR with very high selectivity and inhibits the dissociation of tetramers into monomers[62]. In this phase III, multicentre, international, double-blind, parallel-design, placebo-controlled trial, 441 ATTR-CM patients were randomised to receive tafamidis (20 mg or 80 mg) or placebo for 30 months. These patients had biopsy-proven (from cardiac and noncardiac sites, such as fat aspirate, gastrointestinal sites, salivary glands, or bone marrow) ATTRwt-CM or ATTRv-CM; the majority were white males with a median age of 75 years. Overall, 25% were affected by ATTRv-CM, with Val122Ile, Thr60Ala, and Ile68Leu being the most common TTR mutations. The primary endpoint included a composite of all-cause mortality and frequency of CV-related hospitalisations (hierarchically assessed according to the Finkelstein–Schoenfeld method), while secondary endpoints assessed change from baseline in functional capacity (measured by distance walked on the 6 min walking test, 6MWT) and quality of life (assessed by the Kansas City Cardiomyopathy Questionnaire, KCCQ[63]). After a 30-month follow-up period, the trial demonstrated that tafamidis significantly reduced all-cause mortality by 30% and CV-related hospitalisations by 32% when compared to placebo. With Kaplan–Meier analysis, the curves for mortality started to diverge after approximately 18 months of treatment. Furthermore, patients receiving tafamidis experienced a slower decline in functional capacity and quality of life, with differences already observed at 6 months. A prespecified analysis showed that the reduction in mortality and functional decline was similar between ATTRwt-CM and ATTRv-CM patients treated with tafamidis[64], although untreated ATTRv-CM patients had the worst

prognosis. The open-label extension (OLE) study confirmed that patients initially randomised to placebo had worse long-term survival than those randomised to tafamidis[65], although there was a signal towards improved survival in patients transitioned from placebo to tafamidis during follow-up.

The ATTR-ACT trial represented the first, long-awaited, hope for disease-specific therapy for patients with ATTR-CM. Some limitations of the study must be highlighted, including that the study population was predominantly male and mostly affected by ATTRwt-CM. Secondly and importantly, the study focused on a cohort of patients whose characteristics were typical for the years during which the study was conducted, namely biopsy-proven ATTR-CM with advanced phenotype (with significantly elevated NT-proBNP) and with 30% of patients in NYHA class III. Fortunately, patients currently seen in clinical practice can benefit from a non-invasive diagnostic approach[66] when a monoclonal component has been excluded and are generally diagnosed at earlier stages[40] with milder phenotypes.

Interestingly, in the ATTR-ACT trial, there was no significant reduction of CV-related hospitalisations among the subgroup of patients with ATTR-CM and NYHA class III who received tafamidis compared to placebo. The authors speculated that the higher hospitalisation rate observed in this group was attributable to longer survival during a more severe phase of the disease, underscoring the importance of early diagnosis and treatment. Elliot et al.[65,67] subsequently analysed the impact of treatment with tafamidis in patients with ATTR-CM who presented advanced HF symptoms, classified as NYHA class III. Although tafamidis significantly enhanced all-cause survival in this group of patients, patients with NYHA class III experienced an increased risk of CV-related hospitalisations, compared to those with lower NYHA classes. This again highlights the importance of a timely diagnosis in patients with ATTR-CM in order to achieve not only a higher survival rate but also a better quality of life.

Currently, tafamidis represents the only approved treatment for ATTR-CM in several countries, making it a cornerstone therapy for clinicians managing this condition. Current real-life experiences

are being published[68,69,70,71] analysing the efficacy of tafamidis outside the controlled environment of a clinical trial, involving a more diverse and representative patient group. Debonnaire and colleagues[70] conducted a multicentre international study of 710 ATTRwt-CM patients to investigate the impact of tafamidis treatment in octogenarians and found that, after propensity score matching, this treatment was associated with lower mortality in patients > 80 years old. Neither age at diagnosis nor at treatment initiation interacted with tafamidis' mortality benefit. Survival was worse despite tafamidis in individuals ≥ 90 years, NAC stage ≥ 3, NYHA class ≥ III. A study from the Transthyretin Amyloidosis Outcomes Survey (THAOS) Registry[69], including both ATTRwt-CM and ATTRv-CM, compared tafamidis-treated and tafamidis-untreated patients and reported better survival in the first group. The survival rate at 30 months in tafamidis-treated patients (84.4%) was higher than that of the treatment arm of ATTR-ACT (70.5%), and a similar trend was noted between tafamidis-untreated patients (70.0%) and the placebo arm of ATTR-ACT (57.1%), underscoring once again the changing landscape of patients affected by ATTR-CM. Clearly, this study is limited by its observational nature, as treated patients had less severe disease, as indicated by lower median NT-proBNP values, than untreated patients and were more likely to have been enrolled in THAOS in 2019 or later. Masri et al.[72] reported a contemporary long-term outcomes analysis of patients with ATTR-CM treated with tafamidis. Among 624 treated patients, 39% died at 43 months and the probability of survival was closely related, among others, to age, NYHA class and disease stage at diagnosis.

Establishing clear criteria to evaluate therapeutic response remains a remarkable challenge. Ioannou et al.[73] suggested the role of an increase in NT-proBNP and outpatient diuretic intensification (ODI) as potential markers to detect disease progression in ATTR-CM. Furthermore, a decline in estimated glomerular filtration rate has been associated with increased risk of mortality[74]. It is noteworthy that these markers, while extremely promising, were derived from patients' cohorts with only a subset receiving treatment with tafamidis. As such, the applicability of these markers warrants further investigation to validate their relevance and reliability in this specific context.

Acoramidis

The ATTRIBUTE (Efficacy and Safety of Acoramidis in Transthyretin Amyloid Cardiomyopathy) trial[75] investigated acoramidis, a TTR stabiliser deemed to achieve almost complete stabilisation in both ATTRwt-CM and in the most common TTR variants[75,76,77]. A rare mutation in the gene encoding TTR, T119M, results in a variant protein characterised by a higher stability of the tetramer compared to wild-type TTR. Acoramidis was designed to mimic the activity of the T119M variant, thus reaching better potency, binding affinity and TTR stabilisation when compared to tafamidis[78]. In this phase III, multicentre, international, double-blind, placebo-controlled trial, 632 ATTR-CM patients were randomised to receive acoramidis 800 mg twice daily or placebo for 30 months. These patients presented alternatively with ATTRwt-CM or ATTRv-CM, which could either be biopsy proven (endomyocardial biopsy) or non-invasively diagnosed with a technetium-99m bone scintigraphy, with a Perugini grade equal to or greater than two and the exclusion of a monoclonal component. Like the ATTRACT trial, the study population was predominantly composed of white males, with a median age of 77 years. Only 10% of those who underwent randomisation were affected by ATTRv-CM, with V122I being the most frequent TTR variant. Treatment with tafamidis was not allowed during the initial 12 months of the trial but was permitted thereafter. The primary endpoint was represented by a four-step primary hierarchical analysis, which included all-cause mortality, frequency of CV-related hospitalisation, the change from baseline in NT-proBNP level, and the change from baseline in the 6MWT. Aside from evaluating functional capacity (via the 6MWT) and quality of life (via the KCCQ) as secondary endpoints, the trial also analysed the change from the baseline of serum TTR levels.

Treatment with acoramidis was associated with a reduced combined risk of all-cause mortality and CV-related hospitalisations when compared to placebo (Finkelstein–Schoenfeld test statistic, 5.015; $p < 0.001$; win ratio of 1.8 [1.4 to 2.2] 95% CI, $p < 0.05$); moreover, acoramidis was effective in slowing disease progression, as evidenced by meaningful improvements in quality of life and functional capacity (the decrease from baseline in the 6MWT had a mean difference of 39 metres

between the acoramidis and placebo group, favouring the former), as well as in maintaining favourable serum TTR levels compared to patients receiving placebo. Interestingly, the trial showed no statistically significant difference in all-cause mortality between patients who received acoramidis and those who were given a placebo. This outcome likely reflects the remarkable improvements in the overall care and management of ATTR-CM patients in recent years. To set this in perspective, patients in the ATTRIBUTE trial placebo group showed a better 30-month survival rate than the patients in the ATTR-ACT trial tafamidis group (30-month survival of 74.3% in the ATTRIBUTE placebo group vs. 70.5% in the combined tafamidis treatment groups in the ATTR-ACT trial). The increased awareness of the disease and the enhanced non-invasive diagnostic tools have led to earlier detection, and a more comprehensive supportive care has undeniably contributed to improved survival rates, even for patients who do not receive specific therapies[79]. Consequently, it is more challenging for new additional therapies to demonstrate survival benefits over a placebo in a clinical trial. A report of the first 12 months of the OLE study[80], whose participants were required to discontinue tafamidis, showed a significant difference in all-cause mortality as well as first CV hospitalisation between the continuous acoramidis and placebo-to-acoramidis group; while there may be a trend of reduction in the risk of all-cause mortality in the placebo arm following initiation of acoramidis, further ongoing follow-up will clarify the impact of acoramidis in this subset.

More insights into the mechanisms of clinical benefit of acoramidis were provided by the cardiac magnetic resonance (CMR) substudy[81], which reported that acoramidis trended toward improving or stabilising structural and biventricular functional CMR parameters compared to placebo. Notably, at 30 months, 12.5% of acoramidis recipients demonstrated amyloid regression, defined as a reduction of at least 5% in extracellular volume (ECV), suggesting that TTR stabilisation may allow the rate of innate amyloid clearance mechanisms to exceed the rate of amyloid formation.

Reduction in TTR synthesis

Another potential target in the pathophysiology of ATTR-CM is the reduction in TTR synthesis. Until recently, orthotopic liver transplantation was considered the only option to interrupt the synthesis of variant TTR in ATTRv patients; however, this is no longer a therapeutic tool in most centers, and it is not an option in ATTRwt-CM. The following paragraphs will focus on contemporary strategies for the reduction in TTR synthesis.

Antisense oligonucleotide inhibitors

Antisense oligonucleotide inhibitors (ASOs) are short, synthetic strands of ribonucleic acid (RNA) specifically designed to target a determined messenger RNA, thus halting its translation into protein. This precise mechanism allows ASOs to reduce or completely silence the production of a particular protein, such as TTR.

Inotersen

Inotersen is a 2′-O-methoxyethyl–modified ASO that targets TTR messenger RNA in hepatocytes, thus promoting its degradation through the RNAase H1 pathway, and reducing the overall TTR production[82,83]. The NEURO-TTR[83] (Inotersen Treatment for Patients with Hereditary Transthyretin Amyloidosis) was a phase III, international, randomised, double-blind, placebo-controlled trial analysing the safety and efficacy of treatment with inotersen in patients with ATTRv with polyneuropathy (ATTR-PN). After a 15-month follow-up period, the trial confirmed the efficacy of inotersen treatment in ATTR-PN, as it significantly reduced the neurological manifestation of the disease, along with increasing patients' quality of life, when compared to placebo. However, there were safety concerns regarding thrombocytopenia and glomerulonephritis, such that platelet count and kidney function require close monitoring during treatment in clinical practice. No significant changes in cardiac structure were documented between patients receiving inotersen compared to placebo. A dedicated trial on patients with ATTR-CM was not pursued by the company; an open-label study[84] reported a trend towards improvement of the cardiac structure and functional capacity in ATTR-CM patients treated with inotersen; however, this included a small cohort of patients (n = 33).

Eplontersen

A next-generation antisense oligonucleotide inhibitor, eplontersen, is currently under investigation for the treatment of ATTR-CM. This molecule is conjugated to a triantennary N-acetyl galactosamine (GalNAc) ligand for enhanced uptake by hepatocytes[85]. The phase 3, open-label, clinical trial for ATTRv patients with PN, NEURO-TTRansform trial, compared eplontersen with the placebo cohort of the NEURO-TTR trial, showing a significantly lowered serum TTR concentration, less neuropathy impairment and better QoL. The ongoing CARDIO-TTRansform trial (NCT04136171) will evaluate, enrolling more than 1400 patients, the impact of treatment with eplontersen in patients with ATTR-CM. This will be the largest ATTR-CM trial to date, and results are expected in 2026.

Short interfering RNAs

Short interfering RNAs, or siRNAs, aim to silence liver expression of TTR by targeting the messenger RNA in hepatocytes, thereby reducing TTR levels through an RNA interference mechanism[86,87,88]. By inhibiting the translation of TTR, these agents rapidly knock down its formation and subsequent misfolding, preventing deposition of further amyloid fibrils in the extracellular cardiac matrix[87,88,89].

Patisiran

The APOLLO-A (Patisiran, an RNAi Therapeutic, for Hereditary Transthyretin Amyloidosis) trial[90], evaluated the use of the siRNA patisiran in hereditary ATTR-PN. Treatment with patisiran was associated with significant quality of life improvement and neurological manifestation reduction when compared to placebo. In a prespecified subgroup of patients with ATTR-CM, measures of cardiac structure and function favoured patisiran over placebo at 18 months. The APOLLO-B (Patisiran Treatment in Patients with Transthyretin Cardiac Amyloidosis) trial[91] investigated specifically the use of patisiran in ATTR-CM. In this phase III, multicentre, international, double-blind, randomised trial, 360 ATTR-CM patients were randomised to receive either patisiran 0.3 mg/kg of body weight (maximum dose of 30 mg) intravenously or placebo once

every three weeks for 12 months. The study population was composed mostly of ATTRwt-CM (80%), and patients were diagnosed through tissue biopsy or by fulfilling validated non-invasive diagnostic criteria. Other key inclusion criteria were the history of HF and a baseline NTproBNP greater than 300 ng/L (600 ng/L in patients with atrial fibrillation) but lower than 8500 ng/L. Notably, patients with both NYHA III and NAC stage 3 were excluded, as were patients with NYHA IV. Both the patisiran group and the placebo group consisted predominantly of male patients, median age of 76 years; compared to other studies, such as the ATTRIBUTE trial, there was a more consistent percentage of ATTRv-CM (20%) and a greater ethnic diversity within the study population; however, white ethnicity remained the most represented demographic among participants. Interestingly, approximately 25% of patients undergoing randomisation received tafamidis at baseline treatment. Still, the size of the trial population precluded any formal evaluation of the patisiran treatment in this subgroup. The primary endpoint of the APOLLO-B trial was to investigate functional capacity, analysing the change from baseline in the distance walked on the 6MWT. Secondary key endpoints included modifications in quality of life and composite outcomes, including death from any cause, hospitalisations for any cause, and urgent HF visits over 12 months. Exploratory endpoints included changes in cardiac biomarkers and echocardiographic parameters. After a 12-month follow-up period, the trial reported how patisiran preserved functional status, both as 6MWT and KCCQ results; however, the decrease from baseline in the 6MWT had a mean difference of only 14 metres between the placebo and patisiran groups, favouring the latter. There were no statistically significant differences regarding the other secondary endpoints. This outcome may be attributed to the short duration of the trial, which may have been insufficient to capture long-term benefits in a slow progressive disease, such as ATTR-CM. Secondly, as mentioned before for the ATTRIBUTE trial results, the patient population is constantly evolving, and it is progressively more challenging to detect the beneficial impact of targeted therapies.

Vutrisiran

Vutrisiran is a next-generation subcutaneously administered RNA interference agent[88,89]. Vutrisiran siRNA is conjugated to a GalNAc ligand that binds the asialoglycoprotein receptor expressed on the surface of hepatocytes[88,89]. This conjugate provides enhanced stabilisation chemistry, allowing for subcutaneous (SC) injections every 3 months. In the HELIOS-A trial, including patients with ATTRv polyneuropathy, vutrisiran improved disease-relevant outcomes were compared to an external placebo cohort (from APOLLO trial)[92]. An exploratory analysis on cardiac parameters[93] showed that, at 18 months, vutrisiran was beneficial in terms of NT-proBNP values and some echocardiographic findings in the modified intent-to-treat (mITT) population and a cardiac subpopulation (n = 40). In a planned cohort undergoing bone scintigraphy assessments, most vutrisiran-treated patients experienced reduced or stabilised radiotracer uptake versus baseline. The HELIOS-B (Vutrisiran in Patients with Transthyretin Amyloidosis with Cardiomyopathy) trial[94] investigated the safety and efficacy of vutrisiran in ATTR-CM. In this phase III, multicentre, international, double-blind, randomised, placebo-controlled trial 655 ATTR-CM patients were randomised to receive either vutrisiran 25 mg subcutaneously once every twelve weeks or placebo for 36 months. The trial population included both ATTRv-CM or ATTRwt-CM patients, with the latter representing approximately 90% of the population. Like the APOLLO-B trial, inclusion criteria required either a biopsy-proven diagnosis of ATTR-CM or the fulfilment of non-invasive diagnostic criteria, and a history of HF with baseline NT-proBNP greater than 300 ng/L (600 ng/L in atrial fibrillation) but lower than 8500 ng/L. Of those who underwent randomisation, about 40% were receiving tafamidis treatment at baseline; for this reason, the results of the trial were, respectively, referred to as the general population and the monotherapy population (patients who were not receiving tafamidis at baseline). The primary endpoint of the HELIOS-B trial was represented by a composite of death from any cause and recurrent CV events, whereas secondary endpoints included death from any cause through 42 months, change from baseline in both functional capacity (measured by distance covered on the 6MWT) and quality of life (assessed by the KCCQ-OS). A subgroup analysis considering baseline disease severities in HELIOS-B (in terms

of NYHA class and NTproBNP values) showed that the greatest benefit was achieved in earlier, less severe disease[95].

The HELIOS-B trial marked a pivotal advancement in the therapeutic management of ATTR-CM, as it demonstrated, in a modern cohort, that vutrisiran treatment was associated with lower risk of the composite outcome of death from any cause and recurrent CV events when compared to placebo, both in the overall (HR 0.72; 95% CI, 0.56 to 0.93; p = 0.01) and monotherapy population (HR 0.67; 95% CI, 0.49 to 0.93; p = 0.02). Furthermore, this benefit was broadly consistent even for all the secondary endpoints, with reduced risk of death from any cause through 42 months when compared to placebo (HR, 0.65; 95% CI, 0.46 to 0.90; p = 0.01), reduced decline in functional capacity and quality of life. Similarly encouraging results were observed in the monotherapy population.

The HELIOS-B trial provided decisive data on the impact of vutrisiran in ATTR-CM, not only regarding performance status and quality of life but also on hard clinical endpoints such as hospitalisation and mortality from CV causes in a modern cohort of patients with earlier diagnoses and patients presenting in an overall better health state[40,96,97]. Compared to the ATTR-ACT trial population, the HELIOS-B patients presented generally a less severe disease at baseline, according to NYHA class (29% of NYHA class III patients in the ATTR-ACT population vs. 8% of NYHA class III patients in the HELIOS-B population), KCCQ overall score (mean value of 67 in the ATTR-ACT population vs. mean value of 73 in the HELIOS-B population), distance covered on 6MWT (mean value of 350 metres in the ATTR-ACT population vs. mean value of 377 metres in the HELIOS-B population), and NT-proBNP (mean value of 2995 ng/L in the ATTR-ACT population vs. mean value of 1801 ng/L in the HELIOS-B population), and could potentially benefit from a more robust arsenal of therapies, such as tafamidis or HF therapies. Despite these evolving population dynamics, vutrisiran has demonstrated clear efficacy over placebo, highlighting its potential as an effective treatment option even for patients at earlier disease stages. The favourable

safety profile and relatively infrequent dosing schedule of vutrisiran make it especially suitable for long-term use, further supporting its application in early-stage patients.

At present day, patisiran has not received Food and Drug Administration (FDA) authorisation for ATTR-CM treatment due to the limited treatment effects on 6MWT and KCCQ and the lack of documentation of improved all-cause mortality and CV events. Treatment with vutrisiran for ATTR-CM is now approved by the FDA and is currently under consideration by the European Medical Agency (EMA).

Gene editing

The clustered regularly interspaced short palindromic repeats and associated Cas9 endonuclease (CRISPR-Cas9) system is a Nobel-winning technology that has recently emerged as a revolutionary tool in the treatment of ATTR-CM; ATTRv-CM was the first disease treated in vivo with this method[98]. By enabling precise genetic editing, CRISPR-Cas9 targets the root cause of the disease at a genetic, DNA level. The CRISPR-Cas9 system has been applied to cleave the mutated TTR gene in hepatocytes, the primary source of TTR production, thereby preventing its translation and subsequent protein formation.

Gillmore et al.[98] have evaluated the safety and efficacy of in vivo CRISPR-Cas9 gene editing in humans with ATTRv with PN. In this phase I, open-label, multicentre study, six patients were given a single dose of NTLA-2001, a CRISPR-Cas9 system targeting TTR gene, at a dosage of either 0.1 mg/kg or 0.3 mg/kg. The authors demonstrated a significant reduction (up to 87%) in serum TTR levels compared to baseline at only 28 days of follow-up. No serious adverse events were observed in the study population. These findings provide strong evidence for the potential of CRISPR-Cas9 to achieve sustained therapeutic effects with only one infusion, representing a paradigm change when compared to other chronic treatments, such as TTR stabilisers or silencers. In the expanded phase 1 trial enrolling 36 patients receiving nexiguran ziclumeran (nex-z, also known as NTLA-2001)[99], infusion-related reactions (in five patients) and transient elevations in AST levels (in two patients) were reported. Serious adverse events (most of which were consistent with ATTR-CM)

were reported in 14 patients. Only one of these events was considered to be related to nex-z (serious infusion reaction). A single dose of this compound was associated with deep and durable TTR concentration reductions, as well as limited disease progression during the first 12 months of treatment. The ongoing phase III MAGNITUDE trial (NCT06128629) is investigating the efficacy and safety profile of NTLA-2001 in patients with ATTR-CM.

Nonetheless, uncertainties about the long-term effects of such gene-editing therapy remain. Potential risks include immune responses against the Cas9 enzyme or reactivation of the TTR gene due to natural hepatocyte turnover; these concerns will be addressed through extended clinical follow-up, which will be of paramount importance in establishing the long-term safety profile of NTLA-2001 and its viability as a targeted therapy for ATTR-CM.

Amyloid deposits removal

Monoclonal antibodies (mAbs) represent a fascinating novelty as potential therapies in ATTR-CM, as they display a new, distinct pharmacodynamic: amyloid clearance. The deposition of amyloid fibrils is not to be considered as a static process, but rather a dynamic interplay between two different mechanisms: formation of misfolded TTR monomers/oligomers/fibrils with subsequent infiltration, and amyloid clearance. mAb directly targeting amyloid fibrils within the myocardial tissue can promote active clearance through activation of innate immunity. Unlike stabilisers and silencers, which address amyloidogenesis upstream, mAbs aim to reduce the established amyloid burden, potentially halting and reversing disease progression.

ALXN2220 (NI006)

Garcia-Pavia et al.[100] recently investigated the safety of a recombinant human anti-ATTR monoclonal antibody, NI006, in ATTR-CM. NI006 is a recombinant human anti-ATTR monoclonal IgG1 antibody, generated through comprehensive immune repertoire analyses of memory B-cell complement obtained from healthy elderly[101]. NI006 selectively binds ATTRv and ATTRwt deposits, not physiologically folded TTR, and can promote ATTR depletion by inducing antibody-mediated phagocytosis of ATTR fibrils. In the phase I, double-blind, placebo-controlled, ascending

dose, randomised trial, 40 ATTR-CA patients were randomised in a 2:1 ratio to either receive intravenous infusions of NI006 (with ascending dose from 0.3 mg/kg to 60 mg/kg of body weight) or placebo every four weeks for a 4-month period. The 4-month placebo-controlled, ascending-dose phase was followed by an 8-month OLE phase in which all participating patients received NI006 with stepwise increases in the dose. Almost all patients enrolled in the study were male, with a median age of 72 years. ATTRwt-CM accounted for more than 80% of the entire population. Concomitant treatment with tafamidis was allowed, but treatment with other ATTR-specific drugs was not permitted. NI006 successfully achieved the primary endpoint of safety, as patients who received NI006 did not experience apparent drug-related serious adverse events. Most frequently, adverse events were HF and arrhythmias (expected complications in ATTR-CM) and musculoskeletal events, mainly arthralgias and arthritis; three patients experienced cytokine release syndrome with an associated increase in cardiac biomarker levels, and two patients had transient, asymptomatic decreases in the platelet count. Interestingly, the authors described a significant reduction in cardiac tracer uptake at bone scintigraphy in patients receiving high doses of NI006 compared to placebo, with a distinct difference already visible at 4 months, and a consistent further reduction at 12 months, also in patients switched to NI006 during the OLE phase. Similar results were achieved in terms of ECV reduction on cardiac MRI and of cardiac biomarkers, such as NT-proBNP and high-sensitivity troponin T (although available in a subset of patients). These conclusions are crucial, as they suggest the efficacy of NI006 in targeting the amyloid deposits already present in the myocardium, therefore reducing the already established disease burden, potentially with reversion of the structural and functional impairment.

The ongoing phase III DEPLETE-TTR trial (NCT06183931) is designed to investigate the safety and efficacy of ALXN2220 (new name for NI006) in patients with ATTR-CM, either ATTRwt-CM or ATTRv-CM, with an NTproBNP > 2000 ng/L and a history of HF; in case of positive results, the mAb approach could truly revolutionise the therapy for patients with ATTR-CM. Indeed, while TTR stabilisation and silencing therapies can slow down or prevent disease progression, this

approach could potentially lead to a regression of the ongoing process and a functional recovery of the cardiomyopathy.

Other mAbs

PRX004, now known as coramitug, is another humanised mAb designed to deplete TTR amyloid deposits via antibody-dependent phagocytosis and to inhibit fibril formation by binding misfolded TTR. The phase I clinical trial was recently published, including 21 ATTRv patients; the drug was well tolerated and, in seven patients, global longitudinal strain and neurological impairment were stable/slightly improved. Other phase I and phase II clinical trials (NCT05521022/NCT05951049) are ongoing for the pan-amyloid fibril-depleting AT-02.

2.10 ATTR amyloidosis disease monitoring

This paragraph is based on the manuscript: *Sinigiani G, Milani P, De Michieli L, Sanna GD, Perlini S, Cipriani A, Palladini G. Monitoring heart involvement in treated and untreated transthyretin amyloidosis. Submitted to the Journal Of Cardiac Failure.*

This paragraph focuses on monitoring the disease course of ATTR-CM. Describing the monitoring of the other ATTR amyloidosis manifestations is beyond its scope.

In untreated patients, the ESC has proposed a monitoring approach for ATTR with heart involvement, that largely mirrors conventional strategies for chronic HF management in 2021[56]. The ESC expert consensus identified three core domains for evaluation—clinical/functional status, biomarkers, and imaging—with the goal of achieving a practical yet holistic monitoring strategy (**Figure 5**). It is recommended that clinical assessments, biomarker testing, electrocardiographic and imaging evaluations be performed every six/twelve months. Disease progression was defined as the concurrent worsening of at least one parameter from each of the three categories. This model acknowledged the multifactorial nature of ATTR progression, also including the prognostic impact of frailty and non-cardiac comorbidities, although these two relevant factors did not enter the progression/regression algorithm. However, small retrospective studies have shown that this multiparametric approach lacks adequate sensitivity in real-world clinical settings, failing to reliably detect early disease progression in many cases[103,104,105]. In addition, most of the proposed variables

were selected based on expert consensus and their association with survival outcomes was unproven.

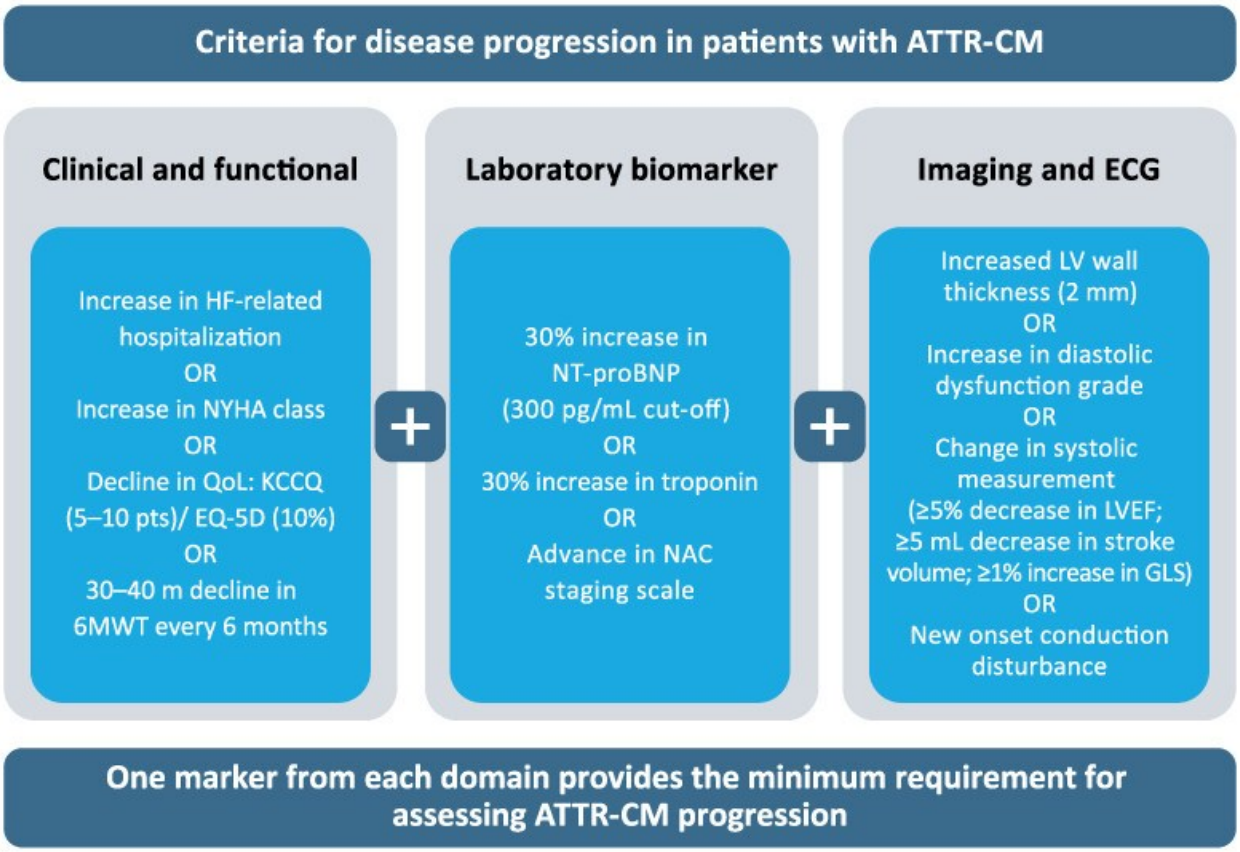

Figure 5. European Society of Cardiology ATTR-CM progression criteria. 6MWT, 6-min walk test; ECG, electrocardiogram; EQ-5D, EuroQol five dimensions; GLS, global longitudinal strain; HF, heart failure; KCCQ, Kansas City Cardiomyopathy Questionnaire; LV, left ventricular; LVEF, LV, left ventricular ejection fraction; NAC, UK National Amyloidosis Centre; NT-proBNP, N-terminal pro-B-type natriuretic peptide; NYHA, New York Heart Association; QoL, quality of life. From Garcia-Pavia et al[56].

Insights into the natural history of cardiac ATTR have been substantially enriched by longitudinal data from historical cohorts of largely untreated patients. A retrospective analysis of 877 patients followed at the NAC between 2000 and 2020 demonstrated progressive increases in left ventricular (LV) wall thickness, alongside worsening parameters of LV systolic and diastolic function at both 12- and 24-month follow-ups. Interestingly, among these echocardiographic markers – global longitudinal strain (GLS) included - only progressive mitral (MR), tricuspid regurgitation (TR) and stroke volume indexed (SVi) were independently associated with all-cause mortality and identified as a robust indicator of disease progression[106]. These results suggest that echocardiography, despite

high diagnostic utility, is not able to detect amyloid load changes in ATTR, but only their functional and haemodynamic consequences. On the other hand, biomarkers have emerged as a particularly valuable tool in disease monitoring. In a retrospective cohort of 945 patients with ATTR evaluated at NAC between 2011 and 2019, an increase in NAC stage—an integrated score based on NT-proBNP and eGFR—was independently associated with increased all-cause mortality at 6-, 12-, and 24-month intervals[107]. These data highlighted the central role of the cardio-renal axis in the natural history of ATTR and provided a rationale for incorporating serial biomarker measurements into clinical practice, as in AL amyloidosis where cardiac biomarkers are key for diagnosis, prognosis, and treatment response. Further evidence supporting the prognostic value of biomarker and therapy-response indicators comes from a large multicenter, retrospective study by Ioannou et al.[73], which analyzed 2275 patients with cardiac ATTR, including 321 (14%) receiving tafamidis. At 12 months, an increase in NT-proBNP >700 ng/L and >30%, as well as any initiation or up-titration of loop diuretics—referred to as "outpatient diuretic intensification" (ODI)—were independently predictive of subsequent all-cause mortality. The combination of these two parameters allowed for effective risk stratification and identification of patients at highest risk of poor outcomes. Notably, this study emphasized the potential value of ODI as a pragmatic and objective marker of clinical deterioration that may overcome potential limitations of the New York Heart Association (NYHA) classification, such as interobserver variability, subjectivity, and lack of standardization[108]. Renal function decline has also been shown to correlate with worse outcomes. In a single-center, retrospective study including 2001 ATTR patients—of whom only 78 (4%) were treated with tafamidis—a decline in eGFR ≥20% over 12 months was significantly associated with higher all-cause mortality[74]. Importantly, the combined occurrence of NT-proBNP elevation, ODI, and eGFR reduction identified a subgroup of patients at particularly high risk, further reinforcing the relevance of integrated cardio-renal monitoring. In addition to cardiac and renal markers, functional capacity and frailty are important prognostic indicators. A retrospective study of 2141 patients (97 of whom were treated with tafamidis) evaluated between 2011 and 2023 reported that a >35-meter decline in six-

minute walk test distance (6MWTD) over 12 months was significantly associated with increased mortality[109]. When considered alongside NT-proBNP progression and ODI, 6MWTD decline served as a third pillar in identifying patients at highest risk of adverse outcomes. These findings support the inclusion of functional measures in disease surveillance frameworks for cardiac ATTR. On the other hand, current evidence primarily relies on clinical and biochemical markers to assess disease progression during treatment with disease-modifying therapies. A prospective observational study of 339 cardiac ATTR patients from Germany[103], followed between 2020 and 2023, evaluated the effectiveness of the ESC monitoring criteria. After 12 months of tafamidis therapy, 25 patients (9%) were classified as "non-responders." However, no significant differences in survival were observed between responders and non-responders. These results should be interpreted with caution, considering the relatively short follow-up and the lack of functional and quality-of-life measures such as 6MWTD and validated questionnaires. Nevertheless, these findings also highlight the inherent complexity of monitoring tafamidis-treated patients, the limited sensitivity of the ESC multiparametric model in real-world clinical practice, and the need for validated monitoring tools that can reliably predict outcomes. Few studies have explored alternative approaches. In a single-center retrospective study involving 303 cardiac ATTR patients[110]—of whom 271 (90%) were receiving tafamidis—the occurrence of worsening HF, defined as either HF hospitalization or ODI, was assessed over a mean follow-up of 3.3 years. Worsening HF events occurred in 35 patients (11.6%) as hospitalizations and in 145 patients (47.9%) as ODI, both of which were associated with significantly increased all-cause mortality. This study reaffirmed the prognostic relevance of ODI in treated patients and emphasized the importance of HF hospitalization as a marker of disease progression. However, the lack of a standardized evaluation time point limits its utility for prospective, structured monitoring. Furthermore, the use of ODI as a surrogate for worsening heart failure is subject to limitations, primarily due to the heterogeneity in strategies for assessing euvolemia. As a result, diuretic management remains largely unstandardized and often dependent on clinical, subjective, judgment. A second retrospective single-center study, analyzing 238 cardiac

ATTR patients treated with tafamidis, applied the definitions of ODI and NT-proBNP progression proposed by Ioannou et al. Patients showing evidence of either ODI or NT-proBNP elevation at 12 months were at increased risk of all-cause mortality, with the highest risk observed in those who concurrently had both these markers present. The same pattern was noted for the composite endpoint of cardiovascular hospitalizations, defined as acute heart failure admission, use of intravenous diuretics in the emergency department, or unplanned admission for arrhythmia. However, the presence of cardiovascular hospitalizations during the first 12 months was not independently analyzed, limiting conclusions about its temporal relationship with treatment response[111]. By contrast, the role of ECG and imaging in assessing disease progression during treatment with disease-modifying therapies remains uncertain. In studies applying the ESC strategy for progression assessment, only a minority of patients met ECG-based progression criteria. Moreover, no dedicated investigations have systematically evaluated ECG parameters as tools for monitoring progression, representing a major gap in current knowledge. Conversely, more evidence is available for cardiac imaging. Ideally, an imaging parameter should not only quantify amyloid load and its progression, but also capture the resulting structural, functional, and biomarker alterations, and ultimately provide robust prognostic information. In this context, echocardiography has not proven capable of fulfilling this role, as its parameters mainly reflect secondary functional and hemodynamic consequences of amyloid load changes. By contrast, bone scintigraphy has demonstrated reliability in detecting amyloid burden at diagnosis. For longitudinal monitoring, data from clinical trials reported a reduction in cardiac tracer uptake after treatment with vutrisiran and with the NI006 antibody, suggesting a potential role in tracking changes in amyloid load. However, a subsequent case report showed that, despite a reduction in cardiac uptake, amyloid burden assessed by positron emission tomography remained unchanged after 13 months of vutrisiran therapy, and this finding was not associated with improvements in hemodynamic or laboratory parameters. These limitations were confirmed in a study of 66 treated patients (64% patisiran, 21% inotersen, and 15% tafamidis), in which 21% demonstrated a reduction in cardiac uptake on follow-

up scans after a median of 28 months. Notably, among the 28 patients with improved scans, many still exhibited disease progression according to established biochemical criteria. These findings underscore the controversial clinical utility of bone scintigraphy in tracking disease course, as it may fail to detect changes in amyloid load and to capture the accompanying structural, functional, and biomarker alterations. A potential role for tracking disease progression was suggested for extracellular volume (ECV) assessed on cardiac magnetic resonance (CMR). In light-chain (AL) amyloidosis, both an ECV increase and a reduction of at least 5% at 12 months were associated with clonal response—indirectly reflecting amyloid load—as well as with structural, functional, and biomarker alterations. Moreover, these changes demonstrated prognostic relevance. In ATTR, robust evidence is still lacking, except for a recent study of 189 patients, including 70 treated with patisiran, in which an ECV increase ≥5% was associated with adverse prognosis. In addition, among treated patients, structural and functional parameters—but not biomarkers—improved, and 6% demonstrated ECV regression, defined as a ≥5% reduction[112]. This coexistence of ECV reduction and morpho-functional improvement was also reported in patients treated with acoramidis[81]. These findings suggest that CMR-derived ECV may represent an optimal imaging parameter for ATTR amyloidosis monitoring, although confirmation in larger studies is warranted. In summary, available evidence confirms that several markers previously validated in untreated cardiac ATTR retain an important prognostic value in treated patients. However, an integrated, standardized, and widely applicable monitoring strategy remains to be fully defined.

2.11 References

1. Fontana M, Ćorović A, Scully P, Moon JC. Myocardial Amyloidosis: The Exemplar Interstitial Disease. JACC Cardiovasc Imaging. 2019;12(11 Pt 2):2345-2356.
2. Garcia-Pavia P, Rapezzi C, Adler Y, et al. Diagnosis and treatment of cardiac amyloidosis: a position statement of the ESC Working Group on Myocardial and Pericardial Diseases. Eur Heart J. 2021;42(16):1554-1568.
3. Morgan GJ, Wall JS. The Process of Amyloid Formation due to Monoclonal Immunoglobulins. Hematol Oncol Clin North Am. 2020;34(6):1041-1054.

4. Diomede L, Rognoni P, Lavatelli F, et al. A Caenorhabditis elegans-based assay recognizes immunoglobulin light chains causing heart amyloidosis. Blood. 2014;123(23):3543-52.
5. Mishra S, Guan J, Plovie E, et al. Human amyloidogenic light chain proteins result in cardiac dysfunction, cell death, and early mortality in zebrafish. Am J Physiol Heart Circ Physiol. 2013;305(1):H95-103.
6. Sanchorawala V. Systemic Light Chain Amyloidosis. N Engl J Med. 2024;390(24):2295-2307.
7. Bochtler T, Hegenbart U, Kunz C, et al. Translocation t(11;14) is associated with adverse outcome in patients with newly diagnosed AL amyloidosis when treated with bortezomib-based regimens. J Clin Oncol. 2015;33(12):1371-8.
8. Bochtler T, Hegenbart U, Heiss C, et al. Hyperdiploidy is less frequent in AL amyloidosis compared with monoclonal gammopathy of undetermined significance and inversely associated with translocation t(11;14). Blood. 2011 Apr 7;117(14):3809-15.
9. Morgan GJ, Kelly JW. The Kinetic Stability of a Full-Length Antibody Light Chain Dimer Determines whether Endoproteolysis Can Release Amyloidogenic Variable Domains. J Mol Biol. 2016;428(21):4280-4297.
10. Wechalekar AD, Fontana M, Quarta CC, et al. AL Amyloidosis for Cardiologists: Awareness, Diagnosis, and Future Prospects: *JACC: CardioOncology* State-of-the-Art Review. JACC CardioOncol. 2022;4(4):427-441.
11. Merlini G. AL amyloidosis: from molecular mechanisms to targeted therapies. Hematology Am Soc Hematol Educ Program. 2017;2017(1):1-12.
12. Falk RH. Diagnosis and management of the cardiac amyloidoses. Circulation. 2005;112(13):2047-60.
13. Phelan D, Collier P, Thavendiranathan P, et al. Relative apical sparing of longitudinal strain using two-dimensional speckle-tracking echocardiography is both sensitive and specific for the diagnosis of cardiac amyloidosis. Heart. 2012;98(19):1442-8.
14. Desport E, Bridoux F, Sirac C, et al; Centre national de référence pour l'amylose AL et les autres maladies par dépôts d'immunoglobulines monoclonales. Al amyloidosis. Orphanet J Rare Dis. 2012;7:54.
15. Griffin JM, Rosenblum H, Maurer MS. Pathophysiology and Therapeutic Approaches to Cardiac Amyloidosis. Circ Res. 2021;128(10):1554-1575.
16. De Michieli L, Cipriani A, Iliceto S, et al. Cardiac Troponin in Patients With Light Chain and Transthyretin Cardiac Amyloidosis: *JACC: CardioOncology* State-of-the-Art Review. JACC CardioOncol. 2024;6(1):1-15.

17. Palladini G, Russo P, Bosoni T, et al. Identification of amyloidogenic light chains requires the combination of serum-free light chain assay with immunofixation of serum and urine. Clin Chem. 2009;55(3):499-504.
18. Wisniowski B, Wechalekar A. Confirming the Diagnosis of Amyloidosis. Acta Haematol. 2020;143(4):312-321.
19. Gertz MA. Immunoglobulin light chain amyloidosis: 2016 update on diagnosis, prognosis, and treatment. Am J Hematol. 2016;91(9):947-56.
20. Schönland SO, Hegenbart U, Bochtler T, et al. Immunohistochemistry in the classification of systemic forms of amyloidosis: a systematic investigation of 117 patients. Blood. 2012;119(2):488-93.
21. Dispenzieri A, Gertz MA, Kyle RA, et al. Serum cardiac troponins and N-terminal pro-brain natriuretic peptide: a staging system for primary systemic amyloidosis. J Clin Oncol. 2004;22(18):3751-7.
22. Kumar S, Dispenzieri A, Lacy MQ, et al. Revised prognostic staging system for light chain amyloidosis incorporating cardiac biomarkers and serum free light chain measurements. J Clin Oncol. 2012;30(9):989-95.
23. Wechalekar AD, Schonland SO, Kastritis E, et al. A European collaborative study of treatment outcomes in 346 patients with cardiac stage III AL amyloidosis. Blood. 2013;121(17):3420-7.
24. Lilleness B, Ruberg FL, Mussinelli R, et al. Development and validation of a survival staging system incorporating BNP in patients with light chain amyloidosis. Blood. 2019;133(3):215-223.
25. Sanchorawala V, Boccadoro M, Gertz M, et al. Guidelines for high dose chemotherapy and stem cell transplantation for systemic AL amyloidosis: EHA-ISA working group guidelines. Amyloid. 2022;29(1):1-7.
26. Muchtar E, Gertz MA, Kumar SK, et al. Improved outcomes for newly diagnosed AL amyloidosis between 2000 and 2014: cracking the glass ceiling of early death. Blood. 2017;129(15):2111-2119.
27. Wechalekar AD, Cibeira MT, Gibbs SD, et al. Guidelines for non-transplant chemotherapy for treatment of systemic AL amyloidosis: EHA-ISA working group. Amyloid. 2023;30(1):3-17.
28. Kastritis E, Palladini G, Minnema MC, et al. Daratumumab-Based Treatment for Immunoglobulin Light-Chain Amyloidosis. N Engl J Med. 2021;385(1):46-58.

29. Rizio AA, White MK, McCausland KL, et al. Treatment Tolerability in Patients with Immunoglobulin Light-Chain Amyloidosis. Am Health Drug Benefits. 2018;11(8):430-437.
30. Palladini G, Schönland SO, Sanchorawala V, et al. Clarification on the definition of complete haematologic response in light-chain (AL) amyloidosis. Amyloid. 2021;28(1):1-2.
31. Muchtar E, Dispenzieri A, Wisniowski B, et al. Graded Cardiac Response Criteria for Patients With Systemic Light Chain Amyloidosis. J Clin Oncol. 2023;41(7):1393-1403.
32. Muchtar E, Wisniowski B, Geyer S, et al. Graded Organ Response and Progression Criteria for Kidney Immunoglobulin Light Chain Amyloidosis. JAMA Oncol. 2024;10(10):1362-1369.
33. Palladini G, Hegenbart U, Milani P, et al. A staging system for renal outcome and early markers of renal response to chemotherapy in AL amyloidosis. Blood. 2014;124(15):2325-32.
34. Gertz MA, Comenzo R, Falk RH, et al. Definition of organ involvement and treatment response in immunoglobulin light chain amyloidosis (AL): a consensus opinion from the 10th International Symposium on Amyloid and Amyloidosis, Tours, France, 18-22 April 2004. Am J Hematol. 2005;79(4):319-28.
35. Porcari A, Fontana M, Gillmore JD. Transthyretin cardiac amyloidosis. Cardiovasc Res. 2023;118(18):3517-3535.
36. Muchtar E, Dispenzieri A, Magen H, et al. Systemic amyloidosis from A (AA) to T (ATTR): a review. *J Intern Med*. 2021;289(3):268-292.
37. Griffin JM, Rosenthal JL, Grodin JL, et al. ATTR Amyloidosis: Current and Emerging Management Strategies. *JACC CardioOncology*. 2021;3(4):488-505.
38. Ruberg FL, Grogan M, Hanna M, et al. Transthyretin Amyloid Cardiomyopathy. *J Am Coll Cardiol*. 2019;73(22):2872-2891.
39. Grogan M, Scott CG, Kyle RA, et al. Natural History of Wild-Type Transthyretin Cardiac Amyloidosis and Risk Stratification Using a Novel Staging System. *J Am Coll Cardiol*. 2016;68(10):1014-1020.
40. Ioannou A, Patel RK, Razvi Y, et al. Impact of Earlier Diagnosis in Cardiac ATTR Amyloidosis Over the Course of 20 Years. Circulation. 2022;146(22):1657-1670.
41. Perfetto F, Zampieri M, Bandini G, et al. Transthyretin Cardiac Amyloidosis: A Cardio-Orthopedic Disease. *Biomedicines*. 2022;10(12):3226.
42. Aimo A, Tomasoni D, Porcari A, et al. Left ventricular wall thickness and severity of cardiac disease in women and men with transthyretin amyloidosis. *Eur J Heart Fail*. 2023;25(4):510-514.

43. Vilches S, Fontana M, Gonzalez-Lopez E, et al. Systemic embolism in amyloid transthyretin cardiomyopathy. Eur J Heart Fail. 2022;24(8):1387-1396.
44. Aimo A, Camerini L, Fabiani I, et al. Valvular heart disease in patients with cardiac amyloidosis. Heart Fail Rev. 2024 Jan;29(1):65-77.
45. Westin O, Fosbøl EL, Maurer MS, et al. Screening for Cardiac Amyloidosis 5 to 15 Years After Surgery for Bilateral Carpal Tunnel Syndrome. *J Am Coll Cardiol*. 2022;80(10):967-977.
46. Eldhagen P, Berg S, Lund LH, et al. Transthyretin amyloid deposits in lumbar spinal stenosis and assessment of signs of systemic amyloidosis. *J Intern Med*. 2021;289(6):895-905.
47. Rapezzi C, Quarta CC, Obici L, et al. Disease profile and differential diagnosis of hereditary transthyretin-related amyloidosis with exclusively cardiac phenotype: an Italian perspective. *Eur Heart J*. 2013;34(7):520-528.
48. Gertz MA. Hereditary ATTR amyloidosis: burden of illness and diagnostic challenges. Am J Manag Care. 2017 ;23(7 Suppl):S107-S112.
49. Musumeci MB, Cappelli F, Russo D, et al. Low Sensitivity of Bone Scintigraphy in Detecting Phe64Leu Mutation-Related Transthyretin Cardiac Amyloidosis. *JACC Cardiovasc Imaging*. 2020;13(6):1314-1321.
50. Dorbala S, Ando Y, Bokhari S, et al. ASNC/AHA/ASE/EANM/HFSA/ISA/SCMR/SNMMI Expert Consensus Recommendations for Multimodality Imaging in Cardiac Amyloidosis: Part 2 of 2—Diagnostic Criteria and Appropriate Utilization. *J Card Fail*. 2019;25(11):854-865.
51. Porcari A, Sinagra G, Gillmore JD, et al. Breakthrough advances enhancing care in ATTR amyloid cardiomyopathy. Eur J Intern Med. 2024;123:29-36.
52. Gillmore JD, Damy T, Fontana M, et al. A new staging system for cardiac transthyretin amyloidosis. Eur Heart J. 2018;39(30):2799-2806.
53. Law S, Bezard M, Petrie A, et al. Characteristics and natural history of early-stage cardiac transthyretin amyloidosis. Eur Heart J. 2022;43(27):2622-2632.
54. Nitsche C, Ioannou A, Patel RK, et al. Expansion of the National Amyloidosis Centre staging system to detect early mortality in transthyretin cardiac amyloidosis. Eur J Heart Fail. 2024;26(9):2008-2012.
55. Tomasoni D, Bonfioli GB, Aimo A, et al. Treating amyloid transthyretin cardiomyopathy: lessons learned from clinical trials. Front Cardiovasc Med. 2023;10:1154594.

56. Garcia-Pavia P, Bengel F, Brito D, et al. Expert consensus on the monitoring of transthyretin amyloid cardiomyopathy. Eur J Heart Fail. 2021;23(6):895-905.
57. Arbelo E, Protonotarios A, Gimeno JR, et al. 2023 ESC Guidelines for the management of cardiomyopathies. Eur Heart J. 2023;44(37):3503-3626.
58. Maurer MS, Schwartz JH, Gundapaneni B, et al. Tafamidis Treatment for Patients with Transthyretin Amyloid Cardiomyopathy. N Engl J Med. 2018;379(11):1007-1016.
59. Cruz MW. Tafamidis for autonomic neuropathy in hereditary transthyretin (ATTR) amyloidosis: a review. Clin Auton Res. 2019;29(Suppl 1):19-24.
60. Gertz MA, Scheinberg M, Waddington-Cruz M, et al. Inotersen for the treatment of adults with polyneuropathy caused by hereditary transthyretin-mediated amyloidosis. Expert Rev Clin Pharmacol. 2019;12(8):701-711.
61. Adams D, Gonzalez-Duarte A, O'Riordan WD, et al. Patisiran, an RNAi Therapeutic, for Hereditary Transthyretin Amyloidosis. N Engl J Med. 2018;379(1):11-21.
62. Maurer MS, Grogan DR, Judge DP, et al. Tafamidis in transthyretin amyloid cardiomyopathy: effects on transthyretin stabilization and clinical outcomes. Circ Heart Fail. 2015;8(3):519-26.
63. Green CP, Porter CB, Bresnahan DR, et al. Development and evaluation of the Kansas City Cardiomyopathy Questionnaire: a new health status measure for heart failure. J Am Coll Cardiol. 2000;35(5):1245-55.
64. Rapezzi C, Elliott P, Damy T, et al. Efficacy of Tafamidis in Patients With Hereditary and Wild-Type Transthyretin Amyloid Cardiomyopathy: Further Analyses From ATTR-ACT. JACC Heart Fail. 2021;9(2):115-123.
65. Elliott P, Drachman BM, Gottlieb SS, et al. Long-Term Survival With Tafamidis in Patients With Transthyretin Amyloid Cardiomyopathy. Circ Heart Fail. 2022 Jan;15(1):e008193.
66. Gillmore JD, Maurer MS, Falk RH, et al. Nonbiopsy Diagnosis of Cardiac Transthyretin Amyloidosis. Circulation. 2016;133(24):2404-12.
67. Elliott P, Gundapaneni B, Sultan MB, et al. Improved long-term survival with tafamidis treatment in patients with transthyretin amyloid cardiomyopathy and severe heart failure symptoms. Eur J Heart Fail. 2023 Nov;25(11):2060-2064.
68. Ghoneem A, Bhatti AW, Khadke S, et al. Real-World Efficacy of Tafamidis in Patients With Transthyretin Amyloidosis and Heart Failure. Curr Probl Cardiol. 2023 Jun;48(6):101667.
69. Garcia-Pavia P, Kristen AV, Drachman B, et al. Survival in a Real-World Cohort of Patients With Transthyretin Amyloid Cardiomyopathy Treated With Tafamidis: An Analysis From

the Transthyretin Amyloidosis Outcomes Survey (THAOS). J Card Fail. 2025 Mar;31(3):525-533.

70. Debonnaire P, Dujardin K, Verheyen N, et al. Tafamidis in octogenarians with wild-type transthyretin cardiac amyloidosis: an international cohort study. Eur Heart J. 2025 Mar 13;46(11):1057-1070.
71. Müller ML, Latinova E, Brand A, et al. Outcomes in Cardiac Transthyretin Amyloidosis and Association With New York Heart Association Class: Real-World Data. J Am Heart Assoc. 2024 Jul 16;13(14):e033478.
72. Masri A, Bhattacharya P, Medoff B, et al. A Multicenter Study of Contemporary Long-Term Tafamidis Outcomes in Transthyretin Amyloid Cardiomyopathy. JACC CardioOncol. 2025 Apr;7(3):282-293.
73. Ioannou A, Cappelli F, Emdin M, et al. Stratifying Disease Progression in Patients With Cardiac ATTR Amyloidosis. J Am Coll Cardiol. 2024 Mar 1;83(14):1276–91.
74. Ioannou A, Razvi Y, Porcari A, et al. Kidney Outcomes in Transthyretin Amyloid Cardiomyopathy. JAMA Cardiol. 2025 Jan 1;10(1):50-58.
75. Gillmore JD, Judge DP, Cappelli F, et al. Efficacy and Safety of Acoramidis in Transthyretin Amyloid Cardiomyopathy. N Engl J Med. 2024 Jan 11;390(2):132-142.
76. Penchala SC, Connelly S, Wang Y, et al. AG10 inhibits amyloidogenesis and cellular toxicity of the familial amyloid cardiomyopathy-associated V122I transthyretin. Proc Natl Acad Sci U S A. 2013 Jun 11;110(24):9992-7.
77. Miller M, Pal A, Albusairi W, et al. Enthalpy-Driven Stabilization of Transthyretin by AG10 Mimics a Naturally Occurring Genetic Variant That Protects from Transthyretin Amyloidosis. J Med Chem. 2018 Sep 13;61(17):7862-7876.
78. Wong, P.W.; Ji, A.X.; Fox, J.; et al. Differential ex vivo stabilization of transthyretin by AG10 and tafamidis in samples from patients with moderately or severely destabilizing mutations. Circulation 2019, 140, A13964.
79. Fontana M, Berk JL, Drachman B, et al. Changing Treatment Landscape in Transthyretin Cardiac Amyloidosis. Circ Heart Fail. 2025 Aug;18(8):e012112.
80. Judge DP, Gillmore JD, Alexander KM, et al. Long-Term Efficacy and Safety of Acoramidis in ATTR-CM: Initial Report From the Open-Label Extension of the ATTRibute-CM Trial. Circulation. 2025 Mar 4;151(9):601-611.
81. Razvi Y, Judge DP, Martinez-Naharro A, et al. Effect of Acoramidis on Myocardial Structure and Function in Transthyretin Amyloid Cardiomyopathy: Insights From the

ATTRibute-CM Cardiac Magnetic Resonance (CMR) Substudy. Circ Heart Fail. 2024 Dec;17(12):e012135.
82. Keam SJ. Inotersen: First Global Approval. Drugs. 2018 Sep;78(13):1371-1376.
83. Benson MD, Waddington-Cruz M, Berk JL, et al. Inotersen Treatment for Patients with Hereditary Transthyretin Amyloidosis. N Engl J Med. 2018 Jul 5;379(1):22-31.
84. Dasgupta NR, Rissing SM, Smith J, et al. Inotersen therapy of transthyretin amyloid cardiomyopathy. Amyloid. 2020 Mar;27(1):52-58.
85. Coelho T, Marques W Jr, Dasgupta NR, et al. Eplontersen for Hereditary Transthyretin Amyloidosis With Polyneuropathy. JAMA. 2023 Oct 17;330(15):1448-1458.
86. Friedrich, M.; Aigner, A. Therapeutic siRNA: State-of-the-Art and Future Perspectives. BioDrugs 2022, 36, 549–557
87. Hoy, S.M. Patisiran: First Global Approval. Drugs 2018, 78, 1625–1631.
88. Keam, S.J. Vutrisiran: First Approval. Drugs 2022, 82, 1419–1425.
89. Aimo A, Castiglione V, Rapezzi C, et al. RNA-targeting and gene editing therapies for transthyretin amyloidosis. Nat Rev Cardiol. 2022 Oct;19(10):655-667.
90. Adams D, Gonzalez-Duarte A, O'Riordan WD, et al. Patisiran, an RNAi Therapeutic, for Hereditary Transthyretin Amyloidosis. N Engl J Med. 2018 Jul 5;379(1):11-21.
91. Maurer, M.S.; Kale, P.; Fontana, M. Patisiran Treatment in Patients with Transthyretin Cardiac Amyloidosis. N. Engl. J. Med. 2023, 389, 1553–1565.
92. Adams D, Tournev IL, Taylor MS, et al. Efficacy and safety of vutrisiran for patients with hereditary transthyretin-mediated amyloidosis with polyneuropathy: a randomized clinical trial. Amyloid. 2023 Mar;30(1):1-9.
93. Garcia-Pavia P, Grogan M, Kale P, et al. Impact of vutrisiran on exploratory cardiac parameters in hereditary transthyretin-mediated amyloidosis with polyneuropathy. Eur J Heart Fail. 2024 Feb;26(2):397-410.
94. Fontana M, Berk JL, Gillmore JD, et al. Vutrisiran in Patients with Transthyretin Amyloidosis with Cardiomyopathy. N Engl J Med. 2025 Jan 2;392(1):33-44.
95. Maurer MS, Witteles RM, Garcia-Pavia P, et al. Impact of Heart Failure Severity on Vutrisiran Efficacy in Transthyretin Amyloidosis With Cardiomyopathy. J Am Coll Cardiol. 2025 May 27;85(20):1927-1939.
96. Fumagalli C, Zampieri M, Perfetto F, et al. Early Diagnosis and Outcome in Patients With Wild-Type Transthyretin Cardiac Amyloidosis. Mayo Clin Proc. 2021 Aug;96(8):2185-2191.

97. Rozenbaum MH, Large S, Bhambri R, et al. Estimating the health benefits of timely diagnosis and treatment of transthyretin amyloid cardiomyopathy. J Comp Eff Res. 2021 Aug;10(11):927-938.
98. Gillmore JD, Gane E, Taubel J, et al. CRISPR-Cas9 In Vivo Gene Editing for Transthyretin Amyloidosis. N Engl J Med. 2021 Aug 5;385(6):493-502.
99. Fontana M, Solomon SD, Kachadourian J, et al. CRISPR-Cas9 Gene Editing with Nexiguran Ziclumeran for ATTR Cardiomyopathy. N Engl J Med. 2024 Dec 12;391(23):2231-2241.
100. Garcia-Pavia, P.; Aus dem Siepen, F.; Donal, E. Phase 1 Trial of Antibody NI006 for Depletion of Cardiac Transthyretin Amyloid. N. Engl. J. Med. 2023, 389, 239–250.
101. Michalon A, Hagenbuch A, Huy C, et al. A human antibody selective for transthyretin amyloid removes cardiac amyloid through phagocytic immune cells. Nat Commun. 2021 May 25;12(1):3142.
102. Suhr OB, Grogan M, Silva AMD, et al. PRX004 in variant amyloid transthyretin (ATTRv) amyloidosis: results of a phase 1, open-label, dose-escalation study. Amyloid. 2025 Mar;32(1):14-21.
103. Aus dem Siepen F, Meissner C, Hofmann E, et al. Response to therapy with tafamidis 61 mg in patients with cardiac transthyretin amyloidosis: real-world experience since approval. Amyloid. 2024;31(3):226-231
104. Itzhaki Ben Zadok O, Kornowski R. 18-Month effect of tafamidis on the progression of cardiac amyloidosis evaluated according to a multiparametric expert consensus tool. Acta Cardiol. 2023 Jun;78(4):417-422
105. Ney S, Gertz RJ, Pennig L, et al. Multiparametric Monitoring of Disease Progression in Contemporary Patients with Wild-Type Transthyretin Amyloid Cardiomyopathy Initiating Tafamidis Treatment. J Clin Med. 2024 Jan 4;13(1):284.
106. Chacko L, Karia N, Venneri L, et al. Progression of echocardiographic parameters and prognosis in transthyretin cardiac amyloidosis. Eur J Heart Fail. 2022 Sep;24(9):1700-1712.
107. Law S, Petrie A, Chacko L, et al. Disease progression in cardiac transthyretin amyloidosis is indicated by serial calculation of National Amyloidosis Centre transthyretin amyloidosis stage. ESC Heart Fail. 2020 Dec;7(6):3942-3949.
108. Zimerman A, da Silveira AD, Solomon SD, et al. NYHA classification for decision-making in heart failure: Time to reassess? Eur J Heart Fail. 2023 Jul;25(7):929-932.

109. Ioannou A, Fumagalli C, Razvi Y, et al. Prognostic Value of a 6-Minute Walk Test in Patients With Transthyretin Cardiac Amyloidosis. J Am Coll Cardiol. 2024 Jul 2;84(1):43-58.
110. Zeldin L, Eichler JBS, Teruya SL, et al. Outpatient worsening of heart failure and mortality in transthyretin amyloid cardiomyopathy. Eur J Heart Fail. 2024 Dec 5.
111. Bampatsias D, Wardhere A, Zeldin L, et al. Cardiac disease monitoring measures in patients with transthyretin amyloid cardiomyopathy treated with tafamidis. Heart. 2025 Mar 23:heartjnl-2024-324826
112. Patel RK, Ioannou A, Sheikh A, et al. Transthyretin amyloid cardiomyopathy: natural history and treatment response assessed by cardiovascular magnetic resonance. Eur Heart J. 2025 Jul 11:ehaf412.

Chapter 3. Electrocardiogram in cardiac amyloidosis

This chapter is based on the manuscript: *Martini N*, Sinigiani G*, De Michieli L, Mussinelli R, Perazzolo Marra M, Iliceto S, Zorzi A, Perlini S, Corrado D, Cipriani A. Electrocardiographic features and rhythm disorders in cardiac amyloidosis. Trends Cardiovasc Med. 2024;34(4):257-264.*

3.1 Introduction

Cardiac amyloidosis (CA) is an increasingly recognized cardiac disease caused by extracellular deposition of amyloid fibrils, mainly derived from transthyretin, either wild-type or hereditary variants (ATTRwt-CA and ATTRv-CA), or immunoglobulin light chains (AL-CA) misfolding[1]. CA is an infiltrative cardiomyopathy, characterized by an increased left ventricular (LV) mass and diastolic dysfunction, which can clinically manifest as heart failure with preserved ejection fraction (HFpEF) and rhythm or conduction disturbances[2]. According to the most recent expert consensus[3,4], the diagnosis relies on the detection of amyloid in the heart, and this is possible either invasively using biopsy for demonstration and typing of amyloid deposits, or non-invasively (only for ATTR) using radiolabeled bisphosphonates bone scintigraphy after careful monoclonal protein assessment; a peculiar role is played also by echocardiography and cardiac magnetic resonance (CMR), which can raise a concrete suspicion of cardiac amyloid infiltration[5], and allow diagnosis of CA in the presence of positive extracardiac biopsies[6]. In this diagnostic scenario, dominated by advanced cardiovascular imaging techniques, capable of comprehensive morphologic, functional and tissue characterization of the heart, the reading and interpretation of 12-lead electrocardiogram (ECG) may lose importance and be considered unnecessary. Conversely, ECG remains a good and trusted friend in the assessment of patients with CA, since they can manifest peculiar features such as low QRS voltages (LQRSV) in discordance with the increased LV mass, but also pseudo-infarction patterns, sinus node dysfunction (SND), atrioventricular (AV) blocks, premature supraventricular and ventricular beats, which support the presence of a myocardium disease[7]. Great awareness of these common ECG characteristics and their possible imaging/pathology determinants is needed to increase the understanding of the pathophysiology of CA, allow early recognition of this complex

disease and improve patient's outcome. In this review, we discuss the current role of the ECG in the diagnosis, risk stratification, and management of CA, focusing on the most common ECG abnormalities and rhythm disorders.

3.2 The QRS complex: low voltages and pseudo-infarction patterns

The most peculiar ECG abnormality in patients with CA is the reduction of QRS voltages, and the disproportion between QRS voltages and left ventricular thickness or mass on cardiac imaging[7,8,9,10,11,12,13,14,15,16]. Prevalence of LQRSV in patients with CA is various, ranging from 25% to 90% of cases, mostly depending on the method of LQRSV assessment and CA subtype. The most used LQRSV definitions are the presence of QRS voltage ≤ 0.5 mV in each limb lead[7,8,9], with or in alternative to QRS voltage ≤ 1 mV in each precordial lead or Sokolow/Lyon index <1.5 mV (i.e. the sum of the S wave in V1 and R wave in V5 or V6)[10,11,12,13]. An interesting study by Mussinelli et al.[14] aimed to identify the LQRSV index having the best diagnostic value in identifying cardiac involvement in AL amyloidosis. The results showed that LQRSV sensitivity for AL-CA can range from 27% when defined as "low total voltages" (i.e., combination of ≤ 0.5 mV peripheral and ≤ 1 mV precordial QRS voltages) to 90% when defined as "≤ 0.5 mV peripheral voltages or ≤ 1.5 mV Sokolow/Lyon index". This combined definition, however, showed low specificity, since up to 55% of patients with non-cardiac AL amyloidosis had this ECG pattern. Using "≤ 0.5 mV peripheral QRS voltages" only, the diagnostic accuracy was acceptable given a 66% sensitivity and 81% specificity. Moreover, among the quantitative (or continuous) definitions, peripheral QRS score (the sum of Q, R, and S heights, each taken as absolute value in mm), and peripheral QRS amplitude (total amplitude of the whole QRS complex, from its nadir to its zenith) were those showing the highest diagnostic performance[14]. LQRSV prevalence in CA depends not only on LQRSV definition, but also on CA etiology. It is well-established that LQRSV are more frequently detected in AL- than ATTR-CA[7,11,12,15]. From a recent multicenter study including 411 patients with CA, the LQRSV prevalence (defined as ≤ 0.5 mV in each limb lead, only) was reported as 55% in AL and 35% in ATTR[15]. This difference is intriguing from a pathogenetic point

of view, given that the mechanisms leading to LQRSV should be similar among the two CA forms and represented by the impairment of electrical signals generation or transmission to body surface, due to cardiac amyloid infiltration. The rule "the greater the amyloid burden, the lower the QRS voltages" should be valid across all the CA subtypes, but this is not the case. Indeed, patients with ATTR-CA usually present greater LV thickness and LV mass, possibly due to a higher amyloid infiltration, compared with patients with AL-CA[7,16]; however, LQRSV are more common in AL patients, so that other pathogenetic mechanisms must be involved, such as the worse myocardial inflammation secondary to light chains fibrils cytotoxic effects or peripheral tissue deposits which could increase electric impedance[15]. Clinical, echocardiographic features associated with LQRSV have been also investigated in depth, with the result that LQRSV are a marker of more advanced disease stages and poor prognosis, being associated with higher New York Heart Association (NYHA) class, higher natriuretic peptides and poorer right ventricular (RV) systolic function[11,12,15]. Voltage-to-mass ratio, defined as Sokolow/Lyon index divided by the LV cross-sectional area, is generally more pronounced in ATTR- than AL-CA, reflecting the relatively higher LV thickness, mass and QRS voltages of the former[7,17]. As a key feature of myocardial infiltration, an increased voltage-to-mass ratio could be more sensitive than LQRSV in the differential diagnosis between CA and other causes of LV hypertrophy[8,19,20]. Moreover, voltage-to-mass ratio has been demonstrated to have some prognostic significance, with regard of disease progression, hospitalizations for heart failure and pacemaker implantation[18,21,22].

The ECG evaluation of CA patients and LQRSV may be often hampered by the coexistence of conduction disorders such as bundle branch blocks. A study by Sharma et al. attempted to overcome this issue and found that, in patients with bundle branch blocks, a total QRS score/LV wall thickness ratio < 92.5 mV/cm (total QRS score defined as the sum of QRS amplitude in all 12 ECG leads) was 100% sensitive and 83% specific in the diagnosis of CA[23]. Differences in total QRS score/LV wall thickness between ATTR- and AL-CA were also reported, although not significant[15].

Another common QRS abnormality of CA is the so-called pseudo-infarction or pseudo-necrosis pattern, defined as pathological Q waves or QS complexes in two consecutive leads, in the absence of previous myocardial infarction or echocardiographic akinetic areas[11]. It can be identified in up to 70% of patients with CA, without significant differences among CA subtypes, mostly reflecting increased wall thickness and myocardial tissue abnormalities. This pattern is a frequent cause of coronary artery disease overdiagnosis[7,11] and is associated with poorer survival in patients with AL-CA[24]. In patients with AL-CA, it is common to note other QRS complex abnormalities, such as notches and RsR′ pattern in the absence of QRS prolongation, also known as QRS fragmentation. Perlini et al.[25] investigated this pattern in a cohort of 264 patients with AL-CA (those with coronary artery disease were excluded) and found a prevalence of about 30%. No associations were found between QRS fragmentation and PQ, QRS, and QTc intervals, presence of LQRSV or pseudo-infarction patterns, NT-proBNP serum levels or cardiac wall thickness. Follow-up analysis revealed that QRS fragmentation carried an independent prognostic value for mortality[25]. The coexistence of CA and other causes of LV hypertrophy (i.e., aortic stenosis and arterial hypertension) has been recently shown to be common, particularly in older men with ATTR-CA, and contributes to further complicate the diagnostic process of CA[26]. The ECG can reveal the typical abnormalities of pressure overload and LV hypertrophy conditions, such as high QRS voltages, long QRS duration, QRS axis deviation and repolarization abnormalities[27], in the early stages of CA. However, with the progression of CA, these can partially or completely regress and be substituted by LQRSV, pseudo-infarct pattern and conduction abnormalities[26,28]. Recognition of CA in these conditions is challenging, thus ECG algorithms have been developed to help the differential diagnosis. In detail, the association of corrected QT duration > 440 ms and Sokolow/Lyon index < 1.5 mV has showed high sensitivity and specificity in distinguishing CA from hypertensive heart disease and aortic stenosis. Another index ([PQ interval minus P-wave duration in lead II multiplied by corrected QT duration]/Sokolow-Lyon index) has been proved to be highly diagnostic for the differentiation of amyloidosis and another cause of LV hypertrophy such as Anderson-Fabry disease[29].

3.3 Conduction abnormalities and brady-arrhythmias

Sinus node dysfunction manifesting with sinus pauses and severe sinus bradycardia have been reported in CA[30,31]. Pathogenetic mechanisms may include fibrosis and amyloid infiltration involving the sinoatrial node and the sinus node artery, even if these findings have been described also in patients without ECG abnormalities[32,33].

Disorders of the cardiac conduction system are highly prevalent in the ECG of patients with CA[30]. Typical manifestations include AV blocks of different degree and His-Purkinje disease, including non-specific intraventricular conduction delays, fascicular blocks, or complete bundle branch blocks[34,35,36]. The etiology is related to amyloid infiltration of both specialized conduction system and cardiac ganglia, although a concomitant senile degeneration of conduction pathways is also worth considering, particularly in older wild-type ATTR patients[33,37,38]. Other pathogenetic mechanisms include myocardial ischemia due to perivascular amyloid deposition and impaired vasoactive function[39].

One of the most particular electrophysiological abnormalities in patients with CA is the possible evidence of narrow ECG QRS complexes despite demonstrated prolonged H-V intervals, likely due to equal and homogeneous infiltration of both bundle branches and distal conduction system[39,40]. Prolongation of the H-V interval is more common in ATTR- than AL-CA, and is associated to a higher risk of complete AV blocks, and sudden cardiac death (SCD) due to electromechanical dissociation[40,41]. True bundle branch blocks are also observed in patients with CA, with differences among subtypes: while left bundle branch block is more frequent in ATTR- than AL-CA, right bundle branch block and left anterior fascicular block are equally prevalent among the two groups[42].

Sinus node dysfunction and AV blocks are among the most frequent causes of pacemaker (PM) implantation in patients with CA. A recent multicenter study by Porcari et al.[43] investigated the incidence, the indications and clinical predictors of PM implantation in a large cohort of patients with AL- (n = 119), ATTRv- (n = 59) and ATTRwt-CA (n = 227). A definitive PM was already present at the time of CA diagnosis in 5 (3.9%), 6 (9.1%) and 30 (11.3%) patients with AL-,

ATTRv- and ATTRwt-CA, respectively. During a median follow-up of 33 months, 36 (8.9%) patients underwent PM implantation, of whom 24 ATTRwt-CA. More frequent indications were paroxysmal or permanent AV block (n = 16), atrial fibrillation (AF) with symptomatic low heart rate (n = 9), and syncope with bifascicular block (n = 6). At multivariable analysis, history of AF, longer PR interval and QRS >120 ms on baseline ECG were independently associated with subsequent PM implantation, and the presence of these three risk factors conferred the highest risk of PM implantation during follow-up[43].

3.4 Ventricular repolarization abnormalities and QT interval

ST-T segment abnormalities are common in CA. T-wave inversion (TWI) is a recognized feature of hypertrophic cardiomyopathy and, during screening, should prompt an accurate evaluation with available imaging techniques. In patients with hypertrophic cardiomyopathy phenotypes, TWI commonly involves the inferior and lateral leads and can be associated with ST-segment depression (strain pattern), reflecting either subendocardial ischemia due to coronary artery disease, or myocardial tissue abnormalities due to interstitial expansion[44]. In CA, TWI is observed more frequently in AL- than ATTR-CA[15,43], likely because of different infiltration patterns and toxic effects to the myocardium.

Cardiac hypertrophy can be associated with greater QT interval duration and dispersion[45]. Parthenakis et al. investigated the QT interval of a group of 30 patients with CA and found it to be longer than that of healthy controls[46]. Interestingly, the QT dispersion was not different among the two groups, suggesting a more uniform repolarization than other hypertrophic cardiomyopathy phenotypes[46]. The clinical significance of QTc duration in patients with CA and the relationship between QTc and risk of VAs is yet to be clarified.

3.5 Rhythm disorders: supraventricular arrhythmias

Patients with CA usually experience symptomatic supraventricular arrhythmias (SVAs), which are in most of the cases clinically relevant and difficult to treat[34]. SVAs are ordinary events, more frequent in ATTR- than AL-CA[35]. As occurs in the general population, AF is the most common

tachyarrhythmia in patients with CA; specifically, it was reported in 9%, 11% and 38% of AL-, ATTRv- and ATTRwt-CA patients, respectively[47]. Multiple mechanisms are involved in the pathogenesis of AF in amyloid cardiomyopathy, first and foremost the amyloid infiltration of the atrial walls, leading to structural, electrical, and contractile impairment of the atria. Atrial amyloid infiltration can occur in the setting of both AL- and ATTR-CA, but also in an isolated form, so-called "isolated atrial amyloidosis"[48]. In this particular disease subtype, the deposits are located in the left and right appendages in an interstitial patchy or diffuse pattern and showed a peculiar immunoreaction for atrial natriuretic peptide (ANP), supporting the role of ANP as a precursor of the fibrils. Accordingly, all cardiac and extracardiac chronic stimuli of synthesis and secretion of ANP such as exercise, hypoxia, ischemia, heart failure, mitral valve disease, may support amyloidogenesis and contribute to the deposition of atrial amyloid[48]. A second important determinant of AF in amyloid cardiomyopathy is represented by its restrictive hemodynamics, characterized by severe diastolic dysfunction and high ventricular filling pressures leading to atrial dilatation and AV valves regurgitations[34]. However, whether atrial amyloidosis or remodeling is the cause or the consequence of AF is not fully understood[36,49].

AF prediction and detection are crucial in the management of patients with CA. In a retrospective study including both AL- and ATTR-CA patients, age, HF, LVEF, renal involvement, left atrial size and right atrial pressure emerged as independent predictors of AF[47]. However, AF did not seem to impact all-cause mortality, but rather the hospitalization for HF[47,50].

AF increases the risk of intracardiac thrombus formation and the occurrence of ischemic stroke[51,52]; this is a non-rare complication of CA[53], in which a prothrombotic state is observed even in sinus rhythm[51,52, 53, 54], and often resistant to anticoagulation therapy. A study by El-Am et al.[50] in 58 patients scheduled to undergo electrical cardioversion revealed a high incidence of intracardiac thrombus (13 out of 16, 81%), even among patients receiving adequate anticoagulation (4 out of 13, 31%). For this reasons, current expert consensus documents recommend the anticoagulation therapy in patients with CA and AF, regardless of the CHA2DS2-VASc score[3,4].

Less frequently, patients with CA can present with other types of SVAs including atrial flutter, atrial tachycardia and atrioventricular nodal reentry tachycardias, whose cycle length or atrial organization and conduction may be affected by the extension of amyloid infiltration[41,55].

3.6 Rhythm disorders: ventricular arrhythmias

Though less common than SVAs, ventricular arrhythmias (VAs) can be recorded in patients with CA.

Previous studies using 24-hour ambulatory ECG monitoring or intracardiac device telemetry showed that non-sustained ventricular tachycardia (NSVT) can occur in up to 74% of patients[33,56,57,58], without significant differences between CA subtypes[59–60]. Multiple potential mechanisms can account for the occurrence of VAs in the CA population, including abnormal autonomic balance[61], myocardial ischemia due to amyloid infiltration of capillaries and subsequent coronary microvascular dysfunction[62] and the inhomogeneous distributions of amyloid within myocardial layers, as shown in multiple CMR studies[63–65]. NSVTs are more commonly associated with more advanced HF stages, characterized by higher NYHA class, higher natriuretic peptides and lower LVEF[59]. However, their predictive value for major arrhythmic events and mortality is still controversial[56–60].

Other than NSVT, VAs may also manifest as sustained ventricular tachycardia, electrical storm and ventricular fibrillation, possibly leading to SCD[66]. Although the mechanism of SCD in patients with CA has been traditionally attributed to pulseless electrical activity or bradyarrhythmias[30,67], increasingly recognized association between CA and ventricular tachyarrhythmias, including several reports of successful defibrillation in patients with CA, have raised concerns regarding this occurrence, and prompted the research of the high-risk profiles and of the possible benefit from prophylactic implantable cardioverter-defibrillator (ICD)[56,58,67]. To date, however, the efficacy of primary prevention ICD implantation for prolonging survival of patients with CA is still uncertain[68–70].

3.7 Conclusions

The standard 12-lead ECG remains a valuable tool for the diagnosis and management of CA (**Figure 1**). Despite the growing dominance of cardiac imaging techniques in the diagnostic work-up of patients with cardiomyopathy, a careful and focused interpretation of the ECG provides precious clues in the early identification of the disease, disease staging and mortality risk stratification.

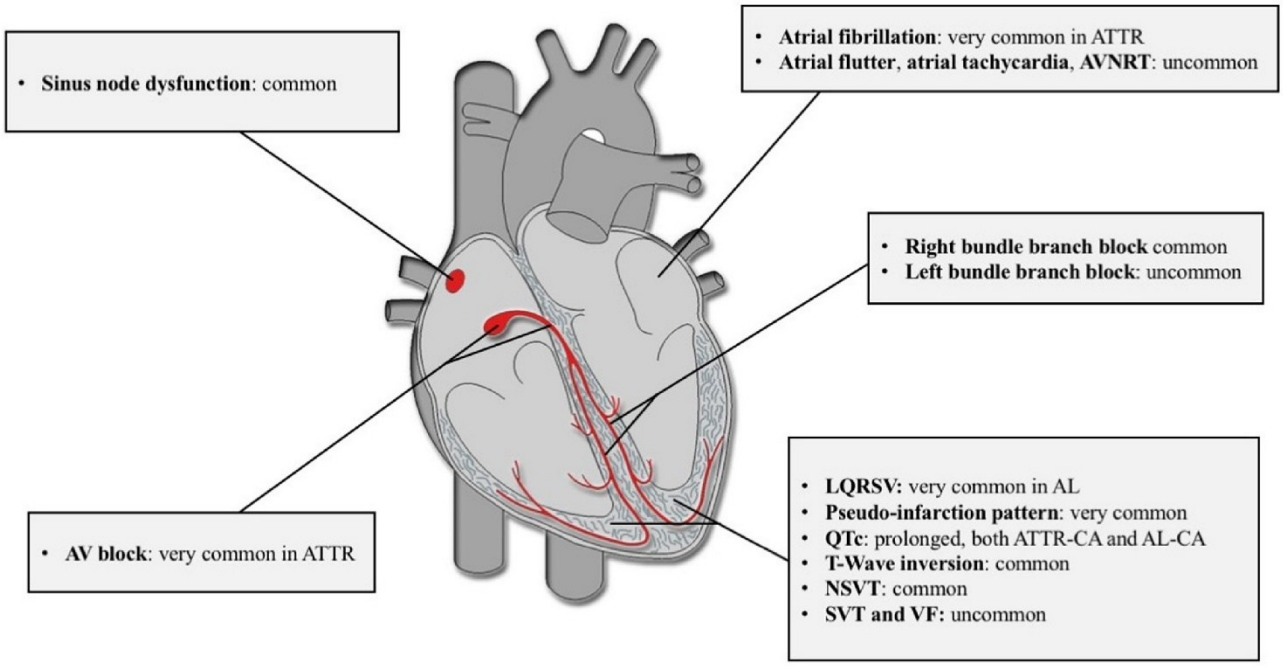

Figure 1. Electrocardiographic and rhythm abnormalities in cardiac amyloidosis. From Martini, Sinigiani et al.

3.8 References

1. Wechalekar AD, Gillmore JD, Hawkins PN. Systemic amyloidosis. Lancet North Am Ed 2016;387(10038):2641–54 Jun.
2. Gertz MA, Dispenzieri A, Sher T. Pathophysiology and treatment of cardiac amyloidosis. Nat Rev Cardiol 2015;12(2):91–102 Feb.
3. Garcia-Pavia P, Rapezzi C, Adler Y, Arad M, Basso C, Brucato A, et al. Diagnosis and treatment of cardiac amyloidosis: a position statement of the ESC working group on myocardial and pericardial diseases. Eur Heart J 2021;42(16):1554–68 Apr 21.

4. Maurer MS, Bokhari S, Damy T, Dorbala S, Drachman BM, Fontana M, et al. Expert consensus recommendations for the suspicion and diagnosis of transthyretin cardiac amyloidosis. Circ Heart Fail 2019;12(9):e006075 Sep.
5. Dorbala S, Ando Y, Bokhari S, Dispenzieri A, Falk RH, Ferrari VA, et al. ASNC/AHA/ASE/EANM/HFSA/ISA/SCMR/SNMMI expert consensus recommendations for multimodality imaging in cardiac amyloidosis: part 2 of 2—diagnostic criteria and appropriate utilization. Circ Cardiovasc Imaging 2021;14(7) Jul.
6. Dorbala S, Ando Y, Bokhari S, Dispenzieri A, Falk RH, Ferrari VA, et al. ASNC/AHA/ASE/EANM/HFSA/ISA/SCMR/SNMMI expert consensus recommendations for multimodality imaging in cardiac amyloidosis: part 1 of 2—evidence base and standardized methods of imaging. Circ Cardiovasc Imaging 2021;14(7) Jul.
7. Rapezzi C, Merlini G, Quarta CC, Riva L, Longhi S, Leone O, et al. Systemic cardiac amyloidoses: disease profiles and clinical courses of the 3 main types. Circulation 2009;120(13):1203–12 Sep 29.
8. Cheng Z, Kang L, Tian Z, Chen W, Guo W, Xu J, et al. Utility of combined indexes of electrocardiography and echocardiography in the diagnosis of biopsy proven primary cardiac amyloidosis: noninvasive diagnosis of primary cardiac amyloidosis. Ann Noninvasive Electrocardiol 2011;16(1):25–9 Jan.
9. Dubrey SW, Bilazarian S, LaValley M, Reisinger J, Skinner M, Falk RH. Signal-averaged electrocardiography in patients with AL (primary) amyloidosis. Am Heart J 1997;134(6):994–1001 Dec.
10. Murtagh B, Hammill SC, Gertz MA, Kyle RA, Tajik AJ, Grogan M. Electrocardiographic findings in primary systemic amyloidosis and biopsy-proven cardiac involvement. Am J Cardiol 2005;95(4):535–7 Feb.
11. Cyrille NB, Goldsmith J, Alvarez J, Maurer MS. Prevalence and prognostic significance of low QRS voltage among the three main types of cardiac amyloidosis. Am J Cardiol 2014;114(7):1089–93 Oct.
12. Kristen AV, Perz JB, Schonland SO, Hegenbart U, Schnabel PA, Kristen JH, et al. Non-invasive predictors of survival in cardiac amyloidosis. Eur J Heart Fail 2007;9(6–7):617–24 Jun 7.
13. Quarta CC, Borghi C, Perlini S, Musca F, Salinaro F. A simple voltage/mass index improves diagnosis of cardiac amyloidosis in patients with unexplained left ventricular “hypertrophy”: an electrocardiographic and echocardiographic study of more than 500 patients. Circulation 2018;122 Mar.

14. Mussinelli R, Salinaro F, Alogna A, Boldrini M, Raimondi A, Musca F, et al. Diagnostic and prognostic value of low QRS voltages in cardiac AL amyloidosis: low QRS voltages in cardiac AL amyloidosis. Ann Noninvasive Electrocardiol 2013;18(3):271–80 May.
15. Cipriani A, De Michieli L, Porcari A, Licchelli L, Sinigiani G, Tini G, et al. Low QRS voltages in cardiac amyloidosis. JACC Cardio Oncol 2022:S2666087322003854 Sep.
16. Quarta CC, Solomon SD, Uraizee I, Kruger J, Longhi S, Ferlito M, et al. Left ventricular structure and function in transthyretin-related versus light-chain cardiac amyloidosis. Circulation 2014;129(18):1840–9 May 6.
17. Carroll JD, Gaasch WH, McAdam KPWJ. Amyloid cardiomyopathy: characterization by a distinctive voltage/mass relation. Am J Cardiol 1982;49(1):9–13 Jan.
18. Slivnick JA, Wallner AL, Vallakati A, Truong VT, Mazur W, Elamin MB, et al. Indexed left ventricular mass to QRS voltage ratio is associated with heart failure hospitalizations in patients with cardiac amyloidosis. Int J Cardiovasc Imaging 2021;37(3):1043–51 Mar.
19. Rahman JE, Helou EF, Gelzer-Bell R, Thompson RE, Kuo C, Rodriguez ER, et al. Noninvasive diagnosis of biopsy-proven cardiac amyloidosis. J Am Coll Cardiol 2004;43(3):410–15 Feb.
20. Madias JE. Low QRS voltage and its causes. J Electrocardiol 2008;41(6):498–500 Nov.
21. Cueto-Garcia L, Tajik AJ, Kyle RA, Edwards WD, Greipp PR, Callahan JA, et al. Serial echocardiographic observations in patients with primary systemic amyloidosis: an introduction to the concept of early (Asymptomatic) amyloid infiltration of the heart. Mayo Clin Proc 1984;59(9):589–97 Sep.
22. Kinugasa Y, Nakamura K, Kamitani H, Hirai M, Yanagihara K, Kato M, et al. Left ventricular mass index-to-QRS-voltage ratio predicts outcomes in heart failure with preserved ejection fraction. ESC Heart Fail 2022;9(2):1098–106 Apr.
23. Sharma S, Labib SB, Shah SP. Electrocardiogram criteria to diagnose cardiac amyloidosis in men with a bundle branch block. Am J Cardiol 2021;146:89–94 May.
24. Zhao L, Li J, Tian Z, Fang Q. Clinical correlates and prognostic values of pseudoinfarction in cardiac light-chain amyloidosis. J Cardiol 2016;68(5):426–30 Nov.
25. Perlini S, Salinaro F, Cappelli F, Perfetto F, Bergesio F, Alogna A, et al. Prognostic value of fragmented QRS in cardiac AL amyloidosis. Int J Cardiol 2013;167(5):2156–61 Sep.
26. Ternacle J, Krapf L, Mohty D, Magne J, Nguyen A, Galat A, et al. Aortic stenosis and cardiac amyloidosis. J Am Coll Cardiol 2019;74(21):2638–51 Nov.

27. Hancock EW, Deal BJ, Mirvis DM, Okin P, Kligfield P, Gettes LS. AHA/ACCF/HRS recommendations for the standardization and interpretation of the electrocardiogram. J Am Coll Cardiol 2009;53(11):992–1002 Mar.
28. Higashi H, Inaba S, Inoue K, Ikeda S, Yamaguchi O. Pseudo-electrocardiographic regression of left ventricular hypertrophy in aortic stenosis: concomitant cardiac amyloidosis. Eur Heart J - Cardiovasc Imaging 2021;22(11):e155 Oct19–e155.
29. Namdar M, Steffel J, Jetzer S, Schmied C, Hürlimann D, Camici GG, et al. Value of electrocardiogram in the differentiation of hypertensive heart disease, hypertrophic cardiomyopathy, aortic stenosis, amyloidosis, and fabry disease. Am J Cardiol 2012;109(4):587–93 Feb.
30. Hartnett J, Jaber W, Maurer M, Sperry B, Hanna M, Collier P, et al. Electrophysiological manifestations of cardiac amyloidosis. JACC CardioOncology 2021;3(4):506–15 Oct.
31. Eriksson P, Karp K, Bjerle P, Olofsson BO. Disturbances of cardiac rhythm and conduction in familial amyloidosis with polyneuropathy. Heart 1984;51(6):658–62 Jun 1.
32. Ridolfi RL, Bulkley B, Hutchins G. The conduction system in cardiac amyloidosis. Am J Med 1977;62(5):677–86 May.
33. Reisinger J, Dubrey SW, Lavalley M, Skinner M, Falk RH. Electrophysiologic abnormalities in AL (Primary) amyloidosis with cardiac involvement. J Am Coll Cardiol 1997;30(4):1046–51 Oct.
34. Giancaterino S, Urey MA, Darden D, Hsu JC. Management of arrhythmias in cardiac amyloidosis. JACC Clin Electrophysiol 2020;6(4):351–61 Apr.
35. Cappelli F, Vignini E, Martone R, Perlini S, Mussinelli R, Sabena A, et al. Baseline ECG features and arrhythmic profile in transthyretin versus light chain cardiac amyloidosis. Circ Heart Fail 2020;13(3):e006619 Mar.
36. Thijssen VLJL, Ausma J, Liu GS, Allessie MA, van Eys GJJM, Borgers M. Structural changes of atrial myocardium during chronic atrial fibrillation. Cardiovasc Pathol 2000;9(1):17–28 Jan.
37. Bharati S, Lev M, Denes P, Modlinger J, Wyndham C, Bauernfeind R, et al. Infiltrative cardiomyopathy with conduction disease and ventricular arrhythmia: electrophysiologic and pathologic correlations. Am J Cardiol 1980;45(1):163–73 Jan.
38. Mathew V, Olson LJ, Gertz MA, Hayes DL. Symptomatic conduction system disease in cardiac amyloidosis. Am J Cardiol 1997;80(11):1491–2 Dec.
39. James TN. Pathology of the cardiac conduction system in amyloidosis. Ann Intern Med 1966;65(1):28 Jul 1.

40. Alreshq R, Tugal D, Siddiqi O, Ruberg F. Conduction abnormalities and role of cardiac pacing in cardiac amyloidosis: a systematic review. Pacing Clin Electrophysiol 2021;44(12):2092–9 Dec.
41. Barbhaiya CR, Kumar S, Baldinger SH, Michaud GF, Stevenson WG, Falk R, et al. Electrophysiologic assessment of conduction abnormalities and atrial arrhythmias associated with amyloid cardiomyopathy. Heart Rhythm 2016;13(2):383–90 Feb.
42. Goldsmith YB, Liu J, Chou J, Hoffman J, Comenzo RL, Steingart RM. Frequencies and types of arrhythmias in patients with systemic light-chain amyloidosis with cardiac involvement undergoing stem cell transplantation on telemetry monitoring. Am J Cardiol 2009;104(7):990–4 Oct.
43. Porcari A, Rossi M, Cappelli F, Canepa M, Musumeci B, Cipriani A, et al. Incidence and risk factors for pacemaker implantation in light-chain and transthyretin cardiac amyloidosis. Eur J Heart Fail 2022;24(7):1227–36 Jul.
44. Rodrigues JCL, Amadu AM, Ghosh Dastidar A, McIntyre B, Szantho GV, Lyen S, et al. ECG strain pattern in hypertension is associated with myocardial cellular expansion and diffuse interstitial fibrosis: a multi-parametric cardiac magnetic resonance study. Eur Heart J - Cardiovasc Imaging 2017;18(4):441–50 Apr 1.
45. Vassallo JA, Cassidy DM, Kindwall KE, Marchlinski FE, Josephson ME. Nonuniform recovery of excitability in the left ventricle. Circulation 1988;78(6):1365–72 Dec.
46. Parthenakis FI, Vardas PE, Ralidis L, Dritsas A, Nihoyannopoulos P. QT interval in cardiac amyloidosis. Clin Cardiol 1996;19(1):51–4 Jan.
47. Longhi S, Quarta CC, Milandri A, Lorenzini M, Gagliardi C, Manuzzi L, et al. Atrial fibrillation in amyloidotic cardiomyopathy: prevalence, incidence, risk factors and prognostic role. Amyloid 2015;22(3):147–55 Jul 3.
48. Röcken C, Peters B, Juenemann G, Saeger W, Klein HU, Huth C, et al. Atrial amyloidosis: an arrhythmogenic substrate for persistent atrial fibrillation. Circulation 2002;106(16):2091–7 Oct 15.
49. Leone O. Amyloid deposition as a cause of atrial remodelling in persistent valvular atrial fibrillation. Eur Heart J 2004;25(14):1237–41 Jul.
50. El-Am EA, Dispenzieri A, Melduni RM, Ammash NM, White RD, Hodge DO, et al. Direct current cardioversion of atrial arrhythmias in adults with cardiac amyloidosis. J Am Coll Cardiol 2019;73(5):589–97 Feb.

51. Feng D, Edwards WD, Oh JK, Chandrasekaran K, Grogan M, Martinez MW, et al. Intracardiac thrombosis and embolism in patients with cardiac amyloidosis. Circulation 2007;116(21):2420–6 Nov 20.
52. Martinez-Naharro A, Gonzalez-Lopez E, Corovic A, Mirelis JG, Baksi AJ, Moon JC, et al. High prevalence of intracardiac thrombi in cardiac amyloidosis. J Am Coll Cardiol 2019;73(13):1733–4 Apr.
53. Russo D, Limite LR, Arcari L, Autore C, Musumeci MB. Predicting the unpredictable. J Am Coll Cardiol 2019;73(22):2910–11 Jun.
54. Cappelli F, Tini G, Russo D, Emdin M, Del Franco A, Vergaro G, et al. Arterial thrombo-embolic events in cardiac amyloidosis: a look beyond atrial fibrillation. Amyloid 2021;28(1):12–18 Jan 2.
55. Kanazawa H, Ito M, Kawahara Y, Hoshiyama T, Takashio S, Tsujita K. Multiple focal atrial tachycardia as a characteristic finding of intractable arrhythmia associated with wild-type transthyretin amyloid cardiomyopathy. Hear Case Rep 2022;8(6):420–4 Jun.
56. Varr BC, Zarafshar S, Coakley T, Liedtke M, Lafayette RA, Arai S, et al. Implantable cardioverter-defibrillator placement in patients with cardiac amyloidosis. Heart Rhythm 2014;11(1):158–62 Jan.
57. Palladini G, Malamani G, Co F, Pistorio A, Recusani F, Anesi E, et al. Holter monitoring in AL amyloidosis: prognostic implications. Pacing Clin Electrophysiol 2001;24(8):1228–33 Aug.
58. Hamon D, Algalarrondo V, Gandjbakhch E, Extramiana F, Marijon E, Elbaz N, et al. Outcome and incidence of appropriate implantable cardioverter-defibrillator therapy in patients with cardiac amyloidosis. Int J Cardiol 2016;222:562–8 Nov.
59. Cappelli F, Cipriani A, Russo D, Tini G, Zampieri M, Zocchi C, et al. Prevalence and prognostic role of nonsustained ventricular tachycardia in cardiac amyloidosis. Amyloid 2022;29(3):211–12 Sep.
60. Halawa A, Woldu HG, Kacey KG, Alpert MA. Effect of ICD implantation on cardiovascular outcomes in patients with cardiac amyloidosis: a systematic review and meta-anaylsis. J Cardiovasc Electrophysiol 2020;31(7):1749–58 Jul.
61. Reyners AKL, Hazenberg BPC, Reitsma WD, Smit AJ. Heart rate variability as a predictor of mortality in patients with AA and AL amyloidosis. Eur Heart J 2002;23(2):157–61 Jan 15.

62. Dorbala S, Vangala D, Bruyere J, Quarta C, Kruger J, Padera R, et al. Coronary microvascular dysfunction is related to abnormalities in myocardial structure and function in cardiac amyloidosis. JACC Heart Fail 2014;2(4):358–67 Aug.
63. Hashimura H, Ishibashi-Ueda H, Yonemoto Y, Ohta-Ogo K, aki MT, Ikeda Y, et al. Late gadolinium enhancement in cardiac amyloidosis: attributable both to interstitial amyloid deposition and subendocardial fibrosis caused by ischemia. Heart Vessels 2016;31(6):990–5 Jun.
64. Syed IS, Glockner JF, Feng D, Araoz PA, Martinez MW, Edwards WD, et al. Role of cardiac magnetic resonance imaging in the detection of cardiac amyloidosis. JACC Cardiovasc Imaging 2010;3(2):155–64 Feb.
65. Martinez-Naharro A, Treibel TA, Abdel-Gadir A, Bulluck H, Zumbo G, Knight DS, et al. Magnetic resonance in transthyretin cardiac amyloidosis. J Am Coll Cardiol 2017;70(4):466–77 Jul.
66. Falk RH, Rubinow A, Cohen AS. Cardiac arrhythmias in systemic amyloidosis: correlation with echocardiographic abnormalities. J Am Coll Cardiol 1984;3(1):107–13 Jan.
67. Hess EP, White RD. Out-of-hospital cardiac arrest in patients with cardiac amyloidosis: presenting rhythms, management and outcomes in four patients. Resuscitation 2004;60(1):105–11 Jan.
68. Kim EJ, Holmes BB, Huang S, Lugo R, Al Aboud A, Goodman S, et al. Outcomes in patients with cardiac amyloidosis and implantable cardioverter-defibrillator. EP Eur 2020;22(8):1216–23 Aug 1.
69. Donnellan E, Wazni OM, Hanna M, Saliba W, Jaber W, Kanj M. Primary prevention implantable cardioverter-defibrillators in transthyretin cardiac amyloidosis. Pacing Clin Electrophysiol 2020;43(11):1401–3 Nov.
70. Higgins AY, Annapureddy AR, Wang Y, Minges KE, Lampert R, Rosenfeld LE, et al. Survival following implantable cardioverter-defibrillator implantation in patients with amyloid cardiomyopathy. J Am Heart Assoc 2020;9(18):e016038 Sep 15.
71. Goto S, Mahara K, Beussink-Nelson L, Ikura H, Katsumata Y, Endo J, et al. Artificial intelligence-enabled fully automated detection of cardiac amyloidosis using electrocardiograms and echocardiograms. Nat Commun 2021;12(1):2726 Dec.
72. Grogan M, Lopez-Jimenez F, Cohen-Shelly M, Dispenzieri A, Attia ZI, Abou Ezzedine OF, et al. Artificial intelligence–enhanced electrocardiogram for the early detection of cardiac amyloidosis. Mayo Clin Proc 2021;96(11):2768–78 Nov.

73. Schrutka L, Anner P, Agibetov A, Seirer B, Dusik F, Rettl R, et al. Machine learning-derived electrocardiographic algorithm for the detection of cardiac amyloidosis. Heart 2022;108(14):1137–47 Jul.

Chapter 4. Multimodality imaging in cardiac amyloidosis

This chapter is based on the manuscript: *Sinigiani G, De Michieli L, Lupi A, Cecchetto A, Nistri S, De Conti G, Berno T, Cecchin D, Mele D, Perazzolo Marra M, Cipriani A. Multimodality Imaging for Cardiac Amyloidosis: Clinical Applications and Future Directions. Under review on the European Journal of Internal Medicine.*

4.1 Introduction

Systemic amyloidosis are a group of disorders characterized by the extracellular deposition of misfolded protein fibrils[1]. When the heart is involved, the condition is referred to as cardiac amyloidosis (CA)[2]. The majority of CA are caused by either immunoglobulin light-chain (AL-CA) or transthyretin-related (ATTR-CA) amyloidosis[2]. ATTR-CA can be hereditary (ATTRv-CA) or wild-type (ATTRwt-CA), depending on the presence of pathogenic variants in the transthyretin gene[2]. The disease is characterized by increased left ventricular (LV) mass and diastolic dysfunction, often progressing to heart failure with preserved ejection fraction, along with rhythm and conduction abnormalities[2,3].

Historically, the diagnosis of CA relied on histological confirmation[4], often leading to late recognition and a poor prognosis. In recent years, advances in cardiac imaging have markedly improved both the accuracy and timeliness of diagnosis. Techniques such as tissue Doppler and strain imaging by echocardiography, as well as multiparametric mapping with cardiac magnetic resonance (CMR), have facilitated earlier disease detection[2,5]. Moreover, bone scintigraphy has emerged as a highly sensitive and specific non-invasive tool for detecting transthyretin amyloid deposits[6], particularly in the absence of monoclonal proteins[7].

These imaging advancements have contributed to earlier diagnosis, increased disease awareness, and improved patient outcomes[8,9]. The introduction of disease-modifying therapies for both ATTR-CA[10,11,12,13] and AL-CA[14] has further enhanced prognosis, highlighting the importance of early risk stratification. In this evolving clinical landscape, a comprehensive understanding of cardiac imaging is crucial for timely diagnosis and optimal management of patients with CA. Such knowledge is essential not only for cardiologists but also for internists, geriatricians, and general practitioners,

who frequently serve as the first point of medical contact and play a central role in patient management. This narrative review examines the role of various imaging modalities in the diagnosis, risk stratification, and therapeutic monitoring of CA, with a focus on their current clinical value and future perspectives.

4.2 Echocardiography

Echocardiography is pivotal in CA diagnosis and management, offering safe, low-cost hemodynamic evaluation. Its main limitations are operator dependency and image quality, which strongly relies on the patient's acoustic window.

Diagnostic value

Echocardiography represents a cornerstone for the identification of "red flags" suggestive of CA. Typical findings include biventricular wall thickening[15] with discordantly low QRS voltages[16], biatrial enlargement, increased atrial septal thickness, and pericardial effusion. In ATTR-CA, valvular involvement is common and frequently associated with aortic stenosis[17], often presenting with low transvalvular gradients[18,19,20,21], though the pathophysiological link remains unclear. Functionally, patients usually present with at least grade II diastolic dysfunction with preserved ejection fraction, with evidence of elevated filling pressures and impaired left atrial (LA) function across all phases[22,23], which may culminate in atrial standstill[24]. Subclinical systolic dysfunction is also detectable through reduced tissue Doppler velocities, lower stroke volume index, and decreased global longitudinal strain (GLS), with the apical sparing pattern[25] serving as a recognized, albeit non-specific, feature[26,27]. The combined assessment of multiple echocardiographic abnormalities enhances diagnostic accuracy, and dedicated scoring systems—based on wall thickness, diastolic parameters, right ventricular function, and GLS—have been developed to stratify the likelihood of CA in both systemic AL amyloidosis and unexplained left ventricular hypertrophy[28].

Prognostic value

ATTR-CA

Several echocardiographic parameters have been identified as independent predictors of outcome in ATTR-CA. In a large cohort, baseline SVi, E/e' ratio, right atrial area index, LV GLS, and severe aortic stenosis were associated with mortality[19]. RV function also carries strong prognostic value: TAPSE and RV free wall longitudinal strain predict adverse events[29,30,31], while a TAPSE/sPAP ratio <0.45 mm/mmHg correlates with higher mortality risk[32], even in early disease[33]. LA function analysis further refines risk assessment, with LA stiffness predicting mortality[23], reduced LA strain indices linked to arterial thromboembolism[34], and impaired LA ejection fraction or strain correlating with thrombus formation[35]. For longitudinal monitoring, European Society of Cardiology (ESC) criteria consider LV wall thickening ≥2 mm, worsening diastolic dysfunction, or declining systolic function (≥5% EF reduction, ≥5 ml decrease in SVi, or ≥1% GLS increase) as markers of progression[36]. However, Chacko et al. found that only worsening valvular regurgitation over 12–24 months predicted prognosis[37], highlighting the need for validation in dedicated, prospective studies.

AL-CA

In AL-CA, LV function is a key prognostic determinant despite preserved ejection fraction. LV GLS has consistently shown independent prognostic value: identified in a single-centre cohort[38], later confirmed in larger multicentre studies, together with SVi as an additional predictor of mortality[39,40]. RV function also holds prognostic significance. TAPSE independently predicts mortality and heart failure hospitalizations[41,42], and RV free wall strain provides similar prognostic value[41]. The prognostic role of RV–pulmonary artery coupling remains less defined, though TAPSE/sPAP has been associated with short-term mortality in a small AL-CA cohort[43], consistent with findings from larger mixed ATTR- and AL-CA populations[44].

LA function also contributes to risk stratification. In a single-centre cohort of patients with systemic AL amyloidosis, Lohrmann et al. found that mechanical LA dispersion was associated with the onset of atrial fibrillation[45]. Additionally, Akintoye et al. reported that LA strain predicted thrombotic events in AL-CA patients[34].

For longitudinal assessment, Cohen et al. found that an absolute improvement in LV GLS ≥2% at 12 months, in addition to a cardiac biomarker response, identified a subgroup of patients with a more favourable prognosis compared with those achieving a biomarker response alone[40].

In summary, current evidence supports the comprehensive evaluation of LV systolic and diastolic function, RV systolic performance, and LA function as valuable sources of prognostic information in CA. However, caution is warranted when interpreting these parameters using fixed cut-off values, as available studies span a broad timeframe during which substantial changes in the clinical phenotype of both ATTR- and AL-CA have occurred[8,9].

Future perspectives

The future of echocardiography in CA is increasingly shaped by the integration of artificial intelligence (AI) algorithms, which holds the potential to enhance efficiency and standardization while preserving diagnostic accuracy. In an exploratory analysis, Cotella et al. demonstrated that AI-assisted echocardiographic evaluation in CA improved measurement reproducibility and workflow efficiency[46]. Similarly, Goto et al. reported that an AI model combining electrocardiography and echocardiography achieved high sensitivity and specificity for the early detection of CA in a multicentre setting[47]. Moreover, in a study including 229 patients with ATTR-CA and 224 controls without left ventricular hypertrophy, a radiomics-derived model enabled myocardial texture analysis and accurately distinguished ATTR-CA from controls[48].

4.3 Cardiac Magnetic Resonance

CMR enables precise morpho-functional assessment and tissue characterization in CA, detecting typical late gadolinium enhancement (LGE) patterns, quantifying infiltration with mapping techniques and offering prognostic insights. In selected cases, it may replace biopsy and distinguish CA from other hypertrophic phenotypes. Limitations include reduced image quality in elderly patients with arrhythmias or devices, and contraindications to gadolinium use in chronic kidney disease.

Diagnostic value

CMR provides detailed morpho-functional assessment in CA and overcomes some echocardiographic limitations. In LGE imaging, difficulty in "nulling" the myocardium—particularly when the myocardium nulls before the blood pool—strongly suggests amyloid infiltration, with near-100% sensitivity[49,50]. Typical enhancement patterns are global subendocardial or transmural[51], although focal or patchy forms can also occur[52]. Native T1 and T2 values are elevated[5,52], and post-contrast extracellular volume (ECV) quantifies amyloid burden non-invasively[53]. Since neither LGE nor mapping can distinguish AL- from ATTR-CA[54,49], CMR plays a complementary role, guiding suspicion and histological confirmation in the ESC position statement on CA[55]. In cases where bone scintigraphy is inconclusive, but a monoclonal component is present, CMR may reveal early myocardial amyloid deposition, supporting the decision to perform endomyocardial biopsy. It can also confirm cardiac involvement when extracardiac amyloid is documented. Furthermore, even in the absence of a monoclonal component, CMR can detect cardiac involvement in those ATTRv-CA showing low sensitivity to bone scintigraphy, as well as in other rare amyloidogenic protein variants, such as apolipoprotein A-I, thereby providing an additional rationale for cardiac biopsy[56,57].

Prognostic value

ATTR-CA

On CMR, both LV and RV systolic function have emerged as independent predictors of mortality[58]. Additionally, impaired LA contractile function has been linked to worse outcomes[59] and incident atrial fibrillation[60]. In tissue characterization, transmural LGE predicts mortality[51], while elevated native T1 and ECV independently correlate with poor outcomes[54,61]. ECV is the most robust marker and is increasingly used for longitudinal monitoring of amyloid burden. Notably, Fontana et al. reported a significant 12-month reduction in ECV following patisiran therapy[62]. Similar findings were observed in three patients with natural anti-ATTR antibodies[63], suggesting a potential role for ECV in detecting amyloid regression.

AL-CA

LGE—particularly with a transmural pattern—and baseline native T1 and ECV values are associated with an increased risk of mortality in AL-CA[51,64]. Moreover, myocardial T2 mapping has emerged as an independent predictor of all-cause mortality[65] with a value >55 ms associated with significantly worse survival[52]. Longitudinal changes in mapping parameters are attracting increasing interest as potential indicators of response to anti-clonal therapies. In a single-centre AL-CA cohort, an increase in native T1 ≥50 ms at 6 or 12 months after treatment initiation was associated with increased mortality[66]. Similarly, in a prospective observational study of 176 patients, Martinez-Naharro et al. found that an ECV increase ≥5% at 6 months predicted poor prognosis and provided additive prognostic value beyond hematologic biomarkers. Conversely, ECV regression ≥5% was observed in 3%, 22%, and 38% of patients at 6, 12, and 24 months, respectively, all of whom achieved at least a haematological very good partial response[67]. In a large cohort of 560 patients with systemic AL amyloidosis, Porcari et al. demonstrated that survival at 1 and 6 months depended on the depth of hematologic response, but only in those with baseline ECV >40%, suggesting that baseline amyloid burden may help guide individualized treatment targets[68]. In summary, current evidence supports the combined assessment of morpho-functional parameters and tissue characterization for prognostic evaluation in CA. Notably, T2 mapping has been reported as a prognostic marker exclusively in AL-CA, potentially reflecting distinct pathophysiological mechanisms of myocardial injury compared with ATTR-CA[69].

Future perspectives

Despite its strengths, CMR has relevant limitations. A major one is the inability to reliably differentiate AL-CA from ATTR-CA, a gap that future advances in imaging science and contrast biology may help close. In addition, atrial fibrillation and intracardiac devices often reduce image quality, and overcoming these issues could markedly expand the prognostic and clinical utility of CMR. Artificial intelligence also holds promise as a means of overcoming other limitations, notably the time-consuming nature of image acquisition and reporting. Nonetheless, important challenges remain before AI can be safely and reliably integrated into routine clinical practice[70].

4.4 Nuclear medicine imaging

Nuclear imaging is central to CA diagnosis, with bone tracer scintigraphy enabling non-invasive identification of ATTR-CA in patients without monoclonal component. The technique combines high diagnostic accuracy with broad availability, good tolerability, and applicability even in frail patients or those with arrhythmias or devices. However, it lacks morpho-functional information, underscoring the need for integration with echocardiography or CMR in a multimodality approach.

Diagnostic value

Scintigraphy with bone tracers plays a pivotal role in the non-invasive diagnosis of ATTR-CA. In a landmark study, Perugini et al. introduced a visual scoring system using 99mTc-diphosphono-propanodicarboxylic acid (DPD) scintigraphy, assessing cardiac uptake three hours post-injection. Scores range from 0 (no uptake) to 3 (intense cardiac uptake with reduced or absent bone signal). This technique demonstrated high sensitivity and specificity in ATTR-CA and high specificity (but low sensitivity) in AL-CA, confirming its strong differential diagnostic capacity[6].

Subsequent studies validated the use of other bone tracers, including 99mTc-pyrophosphate (PYP) and 99mTc-hydroxy-methyl-diphosphonate (HMDP)[71,72]. Based on these findings, Gillmore et al. proposed a diagnostic algorithm combining bone scintigraphy with monoclonal protein screening, in which a Perugini score ≥2 and absence of monoclonal protein yielded 100% specificity and 74% sensitivity for ATTR-CA[7]. This approach has been endorsed by the ESC position statement, paving the way for non-invasive diagnosis in selected clinical scenarios[55]. Among available tracers, 99mTc-DPD appears to offer the highest sensitivity[73] for detecting cardiac amyloid deposits. However, planar imaging alone may produce false positives due to blood pool artifacts, rib fractures, calcifications, or recent myocardial infarction. For this reason, SPECT or SPECT/CT is highly recommended to improve diagnostic accuracy[74].

Bone tracers are not reliable for the diagnosis of AL-CA or rarer amyloidosis subtypes. This limitation has prompted investigation of amyloid-binding tracers for positron emission tomography (PET)—such as ^{11}C-Pittsburgh compound B, ^{18}F-florbetapir, ^{18}F-florbetaben, and ^{124}I-evuzamitide—

which can detect early amyloid deposition, quantify disease burden, and potentially differentiate ATTR- from AL-CA[75,76,77,78,79,80]. In a recent single-centre retrospective study including 46 patients — 12 affected by AL-CA, 14 by ATTR-CA and 20 control subjects — PET/CT with ^{124}I-evuzamitide and ^{18}F-florbetapir was performed. No tracer uptake was observed in the control group. Both tracers showed comparable diagnostic accuracy for AL-CA, whereas ^{124}I-evuzamitide demonstrated superior accuracy for ATTRwt-CA[79]. Furthermore, ^{18}F-florbetapir has also been compared with ^{18}F-fluorodeoxyglucose. In a study of 66 patients with AL-CA or plasma cell disorders undergoing PET/CT, ^{18}F-florbetapir showed higher diagnostic accuracy for detecting cardiac amyloid deposition[81].

Incidental cardiac uptake on bone scintigraphy

Incidental cardiac uptake ≥ grade 2 on bone scintigraphy, suggestive of ATTR-CA, is not uncommon[82]. A meta-analysis of eleven studies, including approximately 63,000 patients undergoing bone scans for non-cardiac indications, reported that around 1% showed cardiac uptake ≥ grade 2, consistent with possible ATTR-CA[83]. From a clinical perspective, a large multicentre Italian study found that between January 2016 and December 2021 up to 4% of ATTR-CA diagnoses were triggered by incidental cardiac uptake detected during bone scintigraphy performed for other indications[84]. Furthermore, in a large international cohort of early, asymptomatic ATTR-CA patients, incidental cardiac tracer uptake was identified in one-quarter of cases and was associated with a significantly increased risk of cardiovascular mortality over a median follow-up of 37 months[85].

Collectively, these findings highlight the clinical importance of recognizing and reporting cardiac uptake on bone scintigraphy, regardless of the scan's initial indication, as this may enable earlier diagnosis and management in patients at elevated risk.

Lung uptake on bone scintigraphy

In addition to cardiac uptake, pulmonary uptake has also been described in CA patients. In a single-centre study involving 93 patients undergoing 99mTc-HMDP scintigraphy as part of a non-invasive

diagnostic workup, CA was confirmed in 82 patients — 20 with AL-CA and 62 with ATTR-CA. Lung uptake was assessed using a three-grade visual scoring system: no significant uptake (grade 0), mild diffuse uptake less than the ribs (grade 1), and intense and/or inhomogeneous uptake (grade 2). According to this system, only one patient with AL-CA demonstrated grade 1 pulmonary uptake, whereas 36 patients with ATTR-CA showed pulmonary involvement, 81% of them graded as level 1. Notably, lung uptake significantly correlated with the degree of cardiac tracer retention, while no pulmonary uptake was observed in control subjects[86].

Further evidence was provided by a single-centre study of 20 patients with ATTR-CA, in which lung uptake on bone scintigraphy was inversely correlated with peak VO_2 on cardiopulmonary exercise testing[87], a parameter known to be associated with poor prognosis in this population[88]. Taken together, these findings suggest that identifying and reporting pulmonary uptake on bone scintigraphy may contribute to the diagnostic process and provide additional value for risk stratification, ultimately supporting more tailored patient management.

Prognostic Value

ATTR-CA

Prognostic findings from nuclear imaging in ATTR-CA have been somewhat mixed. Hutt et al. found no survival difference among patients with varying 99mTc-DPD uptake levels[89], whereas Castano et al. reported worse outcomes in those with higher cardiac 99mTc-PYP uptake[90]. More recently, Rettl et al. observed correlations between cardiac DPD uptake and ECV, disease stage, and troponin, suggesting that higher tracer retention may reflect more advanced disease[91]. Supporting this, patients with incidental cardiac uptake on bone scintigraphy have shown worse outcomes[92]. RV uptake also appears prognostically relevant: in a multicentre study, Porcari et al. reported that patients with diffuse RV uptake on SPECT had significantly lower survival than those with focal uptake[93].

Monitoring therapy response

Bone scintigraphy may also hold potential for monitoring response to therapy. In a single-centre study of 14 patients treated with tafamidis for a mean duration of 44 months, a reduction in cardiac tracer uptake was observed in 5 patients on follow-up imaging, despite stable NT-proBNP levels and unchanged echocardiographic findings[94]. Similarly, Rettl et al. reported decreased cardiac uptake after 9 months of tafamidis therapy in a cohort of 40 patients with ATTRwt-CA, with greater reductions associated with significant improvements in NT-proBNP levels and echocardiographic parameters[95].

However, the role of bone scintigraphy in treatment monitoring remains uncertain. In a single-centre study of 66 patients receiving various therapies (64% patisiran, 21% inotersen, and 15% tafamidis), 21% showed a reduction in Perugini grade on follow-up scans after a median interval of 28 months. Reductions were more frequent in patients treated with tafamidis compared with those receiving TTR gene silencers. Nevertheless, among 28 patients with improved DPD scans, many demonstrated disease progression according to established biochemical and CMR criteria[96]. Collectively, these findings suggest that the utility of bone scintigraphy for therapy monitoring may depend on the specific agent used. Further studies, integrating all validated disease progression criteria, are needed before bone scintigraphy can be reliably adopted for this purpose.

AL-CA

In AL-CA, PET imaging has shown prognostic potential. In a small monocentric cohort, Choi et al. found that ^{11}C-PiB uptake was associated with poorer survival[97]. Similarly, Clerc et al. reported that higher LV ^{18}F-florbetapir uptake predicted major adverse cardiac events, although not independently of Mayo stage[98]. RV ^{18}F-florbetapir uptake was likewise associated with poor outcomes[99]. In another study, Vergaro et al. found that higher biventricular ^{18}F-florbetaben uptake correlated with significantly worse prognosis[100]. While these findings are promising, they require validation in larger, prospective studies.

Future perspectives

Despite its established diagnostic value, bone scintigraphy remains limited by the unclear pathophysiological mechanisms underlying cardiac tracer uptake. A better understanding of this process could enhance its diagnostic accuracy. Artificial intelligence may also help optimize diagnostic workflows by enabling more accurate detection and precise quantification of cardiac tracer uptake[101]. Furthermore, planar imaging and conventional SPECT may show excessive blood pool uptake in the LV cavity, resulting in a high rate of false-positive or equivocal studies. To overcome this limitation, fusion imaging with SPECT/CT has been proposed. In a retrospective study of 176 patients, SPECT/CT fusion significantly reduced both equivocal and false-positive cases[102]. Further research is warranted to validate this promising approach. On the other hand, PET imaging with amyloid-binding tracers offers the potential for earlier detection, quantitative disease assessment, and subtype differentiation; however, their widespread adoption remains limited by high cost, potential technical complexity, and radiation exposure, with most evidence still at the exploratory stage.

4.5 Cardiac computed tomography

Diagnostic value

Compared with other imaging modalities, evidence on the use of cardiac computed tomography (CCT) in the diagnosis of CA remain limited. However, advances such as dual-energy techniques and late-phase imaging have enabled the quantification of myocardial iodine concentration and ECV, potentially overcoming some of the limitations of CMR, including claustrophobia, atrial fibrillation, and the presence of intracardiac devices. Myocardial iodine concentration has shown promising diagnostic performance in differentiating CA from phenocopies, with reported sensitivity and specificity of 100% and 92%, respectively[103].

Further supporting this role, a study of 26 patients with biopsy-confirmed CA and 27 control subjects demonstrated significantly elevated CCT-derived ECV in CA patients, with good correlation to CMR-based ECV measurements[104]. CCT-derived ECV has also been investigated in patients undergoing evaluation for transcatheter aortic valve replacement due to severe aortic

stenosis, a population with a higher prevalence of ATTR-CA. In a single-centre study of 109 such patients, 16 were diagnosed with ATTR-CA. CCT-based ECV was significantly higher in this subgroup, and a threshold of 31% yielded a negative predictive value of 98%, effectively excluding CA in this clinical context[105].

Prognostic value

Evidence regarding the prognostic value of CCT-derived parameters in CA remain limited. In a single-centre study of 72 patients (35 with AL-CA and 37 with ATTR-CA), CCT-based ECV was significantly higher in patients with ATTR-CA. During a median follow-up of 5.3 years, 40 patients died. CCT-derived ECV emerged as an independent predictor of all-cause mortality in ATTR-CA, whereas no such association was observed in AL-CA[106]. It should be noted, however, that this study was limited by its relatively small sample size, and none of the ATTR-CA patients received disease-modifying therapy, in contrast to the AL-CA group, which was treated with specific therapy. Conversely, in another single-centre study including 84 patients with CA, CCT-based ECV was also found to be independently predictive of mortality[107].

Future perspectives

Despite its promise, further studies are warranted to fully clarify the role of CCT-derived parameters in CA and to address technical limitations. A major drawback of CCT is its reduced reliability in patients with a high calcium burden—particularly relevant in older individuals and those with multiple risk factors for atherosclerotic disease, as is often the case in ATTR-CA—where ECV estimation may be less accurate. The recent introduction of photon-counting CT (PCCT) has partially mitigated this limitation. PCCT provides improved spatial resolution while maintaining temporal resolution, thereby enhancing image quality and potentially increasing the accuracy of tissue characterization in heavily calcified hearts. In a study of 30 patients with ATTR-CA, PCCT-derived ECV showed excellent correlation with CMR-derived values, with only minimal discrepancies. Moreover, PCCT enabled simultaneous assessment of coronary artery disease in a cohort characterized by a high mean Agatston score and frequent arrhythmias, with a

low proportion of nondiagnostic scans[108]. Given that chest pain and coronary artery disease are often encountered in clinical practice[109], PCCT may represent a valuable tool for both the diagnosis and management of patients with ATTR-CA.

Another limitation of CCT-derived ECV is its reliance on delayed-phase imaging, which is not part of standard clinical protocols. Radiomics — a computational approach that allows rapid, non-invasive extraction of high-dimensional quantitative features from imaging data — offers a potential solution by allowing tissue characterization without the need for delayed acquisitions. In a study of 378 patients with LV hypertrophy, a radiomics-based model was developed and validated in an independent cohort. The model demonstrated high accuracy in identifying CA and outperforming conventional myocardial CT attenuation metrics[110].

4.6 Conclusions

Multimodality imaging provides essential insights into the morpho-functional and tissue characteristics of amyloid-infiltrated hearts. Echocardiography remains the first-line tool, offering wide availability, safety, and the ability to identify key "red flags" and raise suspicion of CA. After exclusion of a monoclonal component through appropriate serum and urine testing, bone scintigraphy represents the next step, enabling the non-invasive diagnosis of ATTR-CA. Conversely, in the presence of a monoclonal component and a clinical scenario suggestive of AL amyloidosis, biopsy of affected organs remains the gold standard for diagnosis. CMR offers high-resolution morpho-functional evaluation and detailed tissue characterization through LGE and mapping techniques, with established prognostic value, although it does not allow amyloid subtype differentiation. Finally, PET tracers have shown promise for early detection, quantification, and subtype differentiation, particularly in AL-CA, though their application remains, for now, mostly investigational.

In recent years, several disease-modifying therapies have demonstrated significant improvements in clinical outcomes for patients with both ATTR-CA and AL-CA, and additional agents are expected

to become available soon. Within this evolving therapeutic landscape, the ability to monitor treatment response has gained increasing importance, allowing clinicians to promptly identify non-responders, optimize supportive care, or consider a change in therapy. As outlined in previous sections, a variety of imaging parameters have been investigated for this purpose. Among them, CMR-derived ECV has emerged as one of the most robust and reproducible tools for longitudinal assessment. An increase in ECV ≥5% at follow-up has been proposed as a marker of disease progression and has demonstrated prognostic value in stratifying subsequent mortality risk—after 12 months of therapy in ATTR-CA and after 6 or 12 months in AL-CA[71,66].

Recognizing the strengths and limitations of each imaging modality is essential for timely diagnosis, precise risk stratification, and tailored management in CA. A multimodal approach enhances diagnostic and prognostic accuracy and supports therapy monitoring, ultimately promoting earlier intervention and improved outcomes.

4.7 References

1. Wechalekar AD, Gillmore JD, Hawkins PN. Systemic amyloidosis. Lancet. 2016;387(10038):2641-2654.
2. Quarta CC, Kruger JL, Falk RH. Cardiac amyloidosis. Circulation. 2012;126(12):e178-82.
3. Martini N, Sinigiani G, De Michieli L, et al. Electrocardiographic features and rhythm disorders in cardiac amyloidosis. Trends Cardiovasc Med. 2024;34(4):257-264.
4. Falk RH. Diagnosis and management of the cardiac amyloidoses. Circulation. 2005;112(13):2047-60.
5. Fontana M, Banypersad SM, Treibel TA, et al. Native T1 mapping in transthyretin amyloidosis. JACC Cardiovasc Imaging. 2014;7(2):157-65.
6. Perugini E, Guidalotti PL, Salvi F, et al. Noninvasive etiologic diagnosis of cardiac amyloidosis using 99mTc-3,3-diphosphono-1,2-propanodicarboxylic acid scintigraphy. J Am Coll Cardiol. 2005;46(6):1076-84.
7. Gillmore JD, Maurer MS, Falk RH, et al. Nonbiopsy Diagnosis of Cardiac Transthyretin Amyloidosis. Circulation. 2016;133(24):2404-12.
8. Ioannou A, Patel RK, Razvi Y, et al. Impact of Earlier Diagnosis in Cardiac ATTR Amyloidosis Over the Course of 20 Years. Circulation. 2022;146(22):1657-1670.

9. Tini G, Cristiano E, Zampieri M, et al. Impact of the Noninvasive Diagnostic Algorithm on Clinical Presentation and Prognosis in Cardiac Amyloidosis. JACC Adv. 2024;3(10):101232.
10. Maurer MS, Schwartz JH, Gundapaneni B, et al. Tafamidis Treatment for Patients with Transthyretin Amyloid Cardiomyopathy. N Engl J Med. 2018;379(11):1007-1016.
11. Fontana M, Berk JL, Gillmore JD, et al. Vutrisiran in Patients with Transthyretin Amyloidosis with Cardiomyopathy. N Engl J Med. 2024.
12. Gillmore JD, Judge DP, Cappelli F, et al. Efficacy and Safety of Acoramidis in Transthyretin Amyloid Cardiomyopathy. N Engl J Med. 2024;390(2):132-142.
13. De Michieli L, Lupi A, Sinigiani G, et al. Pharmacological Management of Transthyretin Amyloid Cardiomyopathy: Where We Are and Where We Are Going. J Clin Med. 2025;14(10):3481.
14. Kastritis E, Palladini G, Minnema MC, et al. Daratumumab-Based Treatment for Immunoglobulin Light-Chain Amyloidosis. N Engl J Med. 2021;385(1):46-58.
15. Ioannou A, Patel RK, Razvi Y, et al. Multi-Imaging Characterization of Cardiac Phenotype in Different Types of Amyloidosis. JACC Cardiovasc Imaging. 2023;16(4):464-477.
16. Cipriani A, De Michieli L, Porcari A, et al. Low QRS Voltages in Cardiac Amyloidosis: Clinical Correlates and Prognostic Value. JACC CardioOncol. 2022;4(4):458-470.
17. Aimo A, Fabiani I, Maccarana A, et al. Valve disease in cardiac amyloidosis: an echocardiographic score. Int J Cardiovasc Imaging. 2023;39(10):1873-1887.
18. Annabi MS, Carter-Storch R, Zaroui A, et al. Prevalence, Characteristics, and Impact on Prognosis of Aortic Stenosis in Patients With Cardiac Amyloidosis. J Am Heart Assoc. 2024;13(13):e034723.
19. Chacko L, Martone R, Bandera F, et al. Echocardiographic phenotype and prognosis in transthyretin cardiac amyloidosis. Eur Heart J. 2020;41(14):1439-1447.
20. Nitsche C, Scully PR, Patel KP, et al. Prevalence and Outcomes of Concomitant Aortic Stenosis and Cardiac Amyloidosis. J Am Coll Cardiol. 2021;77(2):128-139.
21. Treibel TA, Fontana M, Gilbertson JA, et al. Occult Transthyretin Cardiac Amyloid in Severe Calcific Aortic Stenosis: Prevalence and Prognosis in Patients Undergoing Surgical Aortic Valve Replacement. Circ Cardiovasc Imaging. 2016;9(8):e005066.
22. Nochioka K, Quarta CC, Claggett B, et al. Left atrial structure and function in cardiac amyloidosis. Eur Heart J Cardiovasc Imaging. 2017;18(10):1128-1137.
23. Bandera F, Martone R, Chacko L, et al. Clinical Importance of Left Atrial Infiltration in Cardiac Transthyretin Amyloidosis. JACC Cardiovasc Imaging. 2022;15(1):17-29.

24. Zhao J, He Z, Chen T. Atrial electromechanical dissociation in cardiac amyloidosis. Eur Heart J Cardiovasc Imaging. 2024;25(9):e211.
25. Phelan D, Collier P, Thavendiranathan P, et al. Relative apical sparing of longitudinal strain using two-dimensional speckle-tracking echocardiography is both sensitive and specific for the diagnosis of cardiac amyloidosis. Heart. 2012;98(19):1442-8.
26. De Gaspari M, Sinigiani G, De Michieli L, et al. Relative apical sparing in cardiac amyloidosis is not always explained by an amyloid gradient. Eur Heart J Cardiovasc Imaging. 2023;24(9):1258-1268.
27. Abecasis J, Lopes P, Santos RR, et al. Prevalence and significance of relative apical sparing in aortic stenosis: insights from an echo and cardiovascular magnetic resonance study of patients referred for surgical aortic valve replacement. Eur Heart J Cardiovasc Imaging. 2023;24(8):1033-1042.
28. Boldrini M, Cappelli F, Chacko L, et al. Multiparametric Echocardiography Scores for the Diagnosis of Cardiac Amyloidosis. JACC Cardiovasc Imaging. 2020;13(4):909-920.
29. Bodez D, Ternacle J, Guellich A, et al. Prognostic value of right ventricular systolic function in cardiac amyloidosis. Amyloid. 2016;23(3):158-167.
30. Ozbay B, Satyavolu BS, Rearick C, et al. Right Ventricular Strain Improves the Echocardiographic Diagnosis and Risk Stratification of Transthyretin Cardiac Amyloidosis Among Other Phenotypes of Left Ventricular Hypertrophy. J Am Soc Echocardiogr. 2024;37(10):947-959.
31. Istratoaie S, Bourg C, Lee KC, et al. Right Ventricular Free Wall Strain Predicts ATTR Prognosis as Well as Biomarker- Based Staging Systems. Eur Heart J Cardiovasc Imaging. 2024:jeae242.
32. Meucci MC, Laenens D, Lillo R, et al. Right Ventricular to Pulmonary Artery Coupling and Prognosis in Transthyretin Cardiac Amyloidosis. J Am Soc Echocardiogr. 2024;37(12):1188-1190.e3.
33. Sinigiani G, De Michieli L, d'Addazio M, et al. Right ventricular to pulmonary artery uncoupling is an early predictor of poor outcome in wild-type transthyretin amyloid cardiomyopathy. Int J Cardiovasc Imaging. 2025;41(6):1119-1130.
34. Akintoye E, Majid M, Klein AL, et al. Prognostic Utility of Left Atrial Strain to Predict Thrombotic Events and Mortality in Amyloid Cardiomyopathy. JACC Cardiovasc Imaging. 2023;16(11):1371-1383.

35. Donnellan E, Hussain M, Marrouche N, et al. Left Atrial Strain May Predict Thrombus Formation in Patients With Transthyretin Cardiac Amyloidosis. JACC Clin Electrophysiol. 2023;9(8 Pt 1):1418-1420.
36. Garcia-Pavia P, Bengel F, Brito D, et al. Expert consensus on the monitoring of transthyretin amyloid cardiomyopathy. Eur J Heart Fail. 2021;23(6):895-905.
37. Chacko L, Karia N, Venneri L, et al. Progression of echocardiographic parameters and prognosis in transthyretin cardiac amyloidosis. Eur J Heart Fail. 2022;24(9):1700-1712.
38. Barros-Gomes S, Williams B, Nhola LF, et al. Prognosis of Light Chain Amyloidosis With Preserved LVEF: Added Value of 2D Speckle-Tracking Echocardiography to the Current Prognostic Staging System. JACC Cardiovasc Imaging. 2017;10(4):398-407.
39. Milani P, Dispenzieri A, Scott CG, et al. Independent Prognostic Value of Stroke Volume Index in Patients With Immunoglobulin Light Chain Amyloidosis. Circ Cardiovasc Imaging. 2018;11(5):e006588.
40. Cohen OC, Ismael A, Pawarova B, et al. Longitudinal strain is an independent predictor of survival and response to therapy in patients with systemic AL amyloidosis. Eur Heart J. 2022;43(4):333-341.
41. Cappelli F, Porciani MC, Bergesio F, et al. Right ventricular function in AL amyloidosis: characteristics and prognostic implication. Eur Heart J Cardiovasc Imaging. 2012;13(5):416-22.
42. Ghio S, Perlini S, Palladini G, et al. Importance of the echocardiographic evaluation of right ventricular function in patients with AL amyloidosis. Eur J Heart Fail. 2007;9(8):808-13.
43. Yu F, Cui Y, Shi J, et al. Association between the TAPSE to PASP ratio and short-term outcome in patients with light-chain cardiac amyloidosis. Int J Cardiol. 2023;387:131108.
44. Tomasoni D, Adamo M, Porcari A, et al. Right ventricular to pulmonary artery coupling and outcome in patients with cardiac amyloidosis. Eur Heart J Cardiovasc Imaging. 2023;24(10):1405-1414.
45. Lohrmann G, Patel MA, Brauneis D, et al. Left Atrial Mechanics Associates With Paroxysmal Atrial Fibrillation in Light-Chain Amyloidosis Following Stem Cell Transplantation. JACC CardioOncol. 2020;2(5):721-731.
46. Cotella JI, Slivnick JA, Sanderson E, et al. Artificial intelligence based left ventricular ejection fraction and global longitudinal strain in cardiac amyloidosis. Echocardiography. 2023;40(3):188-195.

47. Goto S, Mahara K, Beussink-Nelson L, et al. Artificial intelligence-enabled fully automated detection of cardiac amyloidosis using electrocardiograms and echocardiograms. Nat Commun. 2021;12(1):2726.
48. Mori S, Montobbio N, Sormani MP, et al. Echocardiographic Tissue Characterization Using Radiomics in Patients With Transthyretin-Related Cardiac Amyloidosis. JACC Adv. 2025;4(6 Pt 1):101755.
49. Dorbala S, Cuddy S, Falk RH. How to Image Cardiac Amyloidosis: A Practical Approach. JACC Cardiovasc Imaging. 2020;13(6):1368-1383.
50. White JA, Kim HW, Shah D, et al. CMR imaging with rapid visual T1 assessment predicts mortality in patients suspected of cardiac amyloidosis. JACC Cardiovasc Imaging. 2014;7(2):143-56.
51. Fontana M, Pica S, Reant P, et al. Prognostic Value of Late Gadolinium Enhancement Cardiovascular Magnetic Resonance in Cardiac Amyloidosis. Circulation. 2015;132(16):1570-9.
52. Kotecha T, Martinez-Naharro A, Treibel TA, et al. Myocardial Edema and Prognosis in Amyloidosis. J Am Coll Cardiol. 2018;71(25):2919-2931.
53. Mongeon FP, Jerosch-Herold M, Coelho-Filho OR, et al. Quantification of extracellular matrix expansion by CMR in infiltrative heart disease. JACC Cardiovasc Imaging. 2012;5(9):897-907.
54. Martinez-Naharro A, Treibel TA, Abdel-Gadir A, et al. Magnetic Resonance in Transthyretin Cardiac Amyloidosis. J Am Coll Cardiol. 2017;70(4):466-477.
55. Garcia-Pavia P, Rapezzi C, Adler Y, et al. Diagnosis and treatment of cardiac amyloidosis: a position statement of the ESC Working Group on Myocardial and Pericardial Diseases. Eur Heart J. 2021;42(16):1554-1568.
56. Musumeci MB, Cappelli F, Russo D, et al. Low Sensitivity of Bone Scintigraphy in Detecting Phe64Leu Mutation-Related Transthyretin Cardiac Amyloidosis. JACC Cardiovasc Imaging. 2020;13(6):1314-1321.
57. Nuvolone M, Sanna GD, Palladini G. AL or ATTR Amyloidosis? Never Two Without Three. Circulation. 2025;151(3):274-281.
58. Knight DS, Zumbo G, Barcella W, et al. Cardiac Structural and Functional Consequences of Amyloid Deposition by Cardiac Magnetic Resonance and Echocardiography and Their Prognostic Roles. JACC Cardiovasc Imaging. 2019;12(5):823-833.

59. Aquaro GD, Morini S, Grigoratos C, et al. Electromechanical dissociation of left atrium in patients with Cardiac Amyloidosis by Magnetic Resonance: Prognostic and clinical correlates. Int J Cardiol Heart Vasc. 2020;31:100633.
60. Sinigiani G, De Michieli L, Porcari A, et al. Atrial electrofunctional predictors of incident atrial fibrillation in cardiac amyloidosis. Heart Rhythm. 2024;21(6):725-732.
61. Martinez-Naharro A, Kotecha T, Norrington K, et al. Native T1 and Extracellular Volume in Transthyretin Amyloidosis. JACC Cardiovasc Imaging. 2019;12(5):810-819.
62. Patel RK, Ioannou A, Sheikh A, et al. Transthyretin amyloid cardiomyopathy: natural history and treatment response assessed by cardiovascular magnetic resonance. Eur Heart J. 2025:ehaf412.
63. Fontana M, Gilbertson J, Verona G, et al. Antibody-Associated Reversal of ATTR Amyloidosis-Related Cardiomyopathy. N Engl J Med. 2023;388(23):2199-2201.
64. Banypersad SM, Fontana M, Maestrini V, et al. T1 mapping and survival in systemic light-chain amyloidosis. Eur Heart J. 2015 Jan 21;36(4):244-51.
65. Sinigiani G, De Michieli L, De Conti G, et al. Cardiac Magnetic Resonance-Detected Acute Myocardial Edema as Predictor of Favourable Prognosis: A Comprehensive Review. J Cardiovasc Dev Dis. 2023;10(8):319.
66. Ioannou A, Patel RK, Martinez-Naharro A, et al. Tracking Treatment Response in Cardiac Light-Chain Amyloidosis With Native T1 Mapping. JAMA Cardiol. 2023;8(9):848-852.
67. Martinez-Naharro A, Patel R, Kotecha T, et al. Cardiovascular magnetic resonance in light-chain amyloidosis to guide treatment. Eur Heart J. 2022;43(45):4722-4735.
68. Porcari A, Masi A, Martinez-Naharro A, et al. Redefining Cardiac Involvement and Targets of Treatment in Systemic Immunoglobulin AL Amyloidosis. JAMA Cardiol. 2024;9(11):982-989.
69. Schilling JD, Nuvolone M, Merlini G. The Pathophysiological and Therapeutic Implications of Cardiac Light-Chain Amyloidosis Compared With Transthyretin Amyloidosis. JACC Heart Fail. 2024;12(10):1781-1787.
70. Zhang Q, Fotaki A, Ghadimi S, et al. Improving the efficiency and accuracy of cardiovascular magnetic resonance with artificial intelligence-review of evidence and proposition of a roadmap to clinical translation. J Cardiovasc Magn Reson. 2024;26(2):101051.
71. Bokhari S, Castaño A, Pozniakoff T, et al. (99m)Tc-pyrophosphate scintigraphy for differentiating light-chain cardiac amyloidosis from the transthyretin-related familial and senile cardiac amyloidoses. Circ Cardiovasc Imaging. 2013;6(2):195-201.

72. Galat A, Rosso J, Guellich A, et al. Usefulness of (99m)Tc-HMDP scintigraphy for the etiologic diagnosis and prognosis of cardiac amyloidosis. Amyloid. 2015;22(4):210-20.
73. Porcari A, Hutt DF, Grigore SF, et al. Comparison of different technetium-99m-labelled bone tracers for imaging cardiac amyloidosis. Eur J Prev Cardiol. 2023;30(3):e4-e6.
74. Dorbala S, Ando Y, Bokhari S, et al. ASNC/AHA/ASE/EANM/HFSA/ISA/SCMR/SNMMI Expert Consensus Recommendations for Multimodality Imaging in Cardiac Amyloidosis:Part 1 of 2-Evidence Base and Standardized Methods of Imaging. Circ Cardiovasc Imaging. 2021;14(7):e000029.
75. Lee SP, Lee ES, Choi H, et al. 11C-Pittsburgh B PET imaging in cardiac amyloidosis. JACC Cardiovasc Imaging. 2015;8(1):50-59.
76. Rosengren S, Skibsted Clemmensen T, Tolbod L, et al. Diagnostic Accuracy of [11C]PIB Positron Emission Tomography for Detection of Cardiac Amyloidosis. JACC Cardiovasc Imaging. 2020;13(6):1337-1347.
77. Cuddy SAM, Bravo PE, Falk RH, et al. Improved Quantification of Cardiac Amyloid Burden in Systemic Light Chain Amyloidosis: Redefining Early Disease? JACC Cardiovasc Imaging. 2020;13(6):1325-1336.
78. Genovesi D, Vergaro G, Giorgetti A, et al. [18F]-Florbetaben PET/CT for Differential Diagnosis Among Cardiac Immunoglobulin Light Chain, Transthyretin Amyloidosis, and Mimicking Conditions. JACC Cardiovasc Imaging. 2021;14(1):246-255.
79. Clerc OF, Cuddy SAM, Robertson M, et al. Cardiac Amyloid Quantification Using 124I-Evuzamitide (124I-P5+14) Versus 18F-Florbetapir: A Pilot PET/CT Study. JACC Cardiovasc Imaging. 2023;16(11):1419-1432.
80. Wall JS, Martin EB, Lands R, et al. Cardiac Amyloid Detection by PET/CT Imaging of Iodine (124I) Evuzamitide (124I-p5+14): A Phase 1/2 Study. JACC Cardiovasc Imaging. 2023;16(11):1433-1448.
81. Kong Y, Cao L, He B, et al. Head-to-head comparison of $^{[18F]}$florbetapir and $^{[18F]}$FDG PET for the early detection of amyloidosis in systemic amyloidosis and plasma cell dyscrasias. Eur J Radiol. 2025;189:112188.
82. Campi C, Briani C, Salvalaggio A, et al. Semi-Quantification of Myocardial Uptake of Bone-Seeking Agents in Suspected Cardiac Amyloidosis. J Cardiovasc Dev Dis. 2023;10(5):184.
83. Treglia G, Martinello C, Dondi F, et al. Prevalence of Incidental Findings Suspicious for Transthyretin Cardiac Amyloidosis among Patients Undergoing Bone Scintigraphy: A Systematic Review and a Meta-Analysis. J Clin Med. 2023;12(17):5698.

84. Tini G, Milani P, Zampieri M, et al. Diagnostic pathways to wild-type transthyretin amyloid cardiomyopathy: a multicentre network study. Eur J Heart Fail. 2023;25(6):845-853.
85. Porcari A, Razvi Y, Cappelli F, et al. Clinical Phenotype and Prognosis of Asymptomatic Patients With Transthyretin Cardiac Amyloid Infiltration. JAMA Cardiol. 2025;10(5):437-445.
86. Cappelli F, Gallini C, Costanzo EN, et al. Lung uptake during 99mTc-hydroxymethylene diphosphonate scintigraphy in patient with TTR cardiac amyloidosis: An underestimated phenomenon. Int J Cardiol. 2018;254:346-350.
87. Monfort A, Rivas A, Banydeen R, et al. Pulmonary 99mTc-HMDP uptake correlates with restrictive ventilatory defects and abnormal lung reactance in transthyretin cardiac amyloidosis patients. Respir Res. 2022;23(1):72.
88. Patel RK, Bandera F, Venneri L, et al. Cardiopulmonary Exercise Testing in Evaluating Transthyretin Amyloidosis. JAMA Cardiol. 2024;9(4):367-376.
89. Hutt DF, Fontana M, Burniston M, et al. Prognostic utility of the Perugini grading of 99mTc-DPD scintigraphy in transthyretin (ATTR) amyloidosis and its relationship with skeletal muscle and soft tissue amyloid. Eur Heart J Cardiovasc Imaging. 2017 Dec 1;18(12):1344-1350.
90. Castano A, Haq M, Narotsky DL, et al. Multicenter Study of Planar Technetium 99m Pyrophosphate Cardiac Imaging: Predicting Survival for Patients With ATTR Cardiac Amyloidosis. JAMA Cardiol. 2016;1(8):880-889.
91. Rettl R, Calabretta R, Duca F, et al. DPD Quantification Correlates With Extracellular Volume and Disease Severity in Wild-Type Transthyretin Cardiac Amyloidosis. JACC Adv. 2024;3(10):101261.
92. Salvalaggio A, Cipriani A, Righetto S, et al. Incidental cardiac uptake of 99mTc-diphosphonates is predictive of poor outcome: data from 9616 bone scintigraphies. J Nucl Cardiol. 2022;29(6):3419-3425.
93. Porcari A, Fontana M, Canepa M, et al. Clinical and Prognostic Implications of Right Ventricular Uptake on Bone Scintigraphy in Transthyretin Amyloid Cardiomyopathy. Circulation. 2024;149(15):1157-1168.
94. Papathanasiou M, Kessler L, Bengel FM, et al. Regression of Myocardial ^{99m}Tc-DPD Uptake After Tafamidis Treatment of Cardiac Transthyretin Amyloidosis. J Nucl Med. 2023;64(7):1083-1086.

95. Rettl R, Wollenweber T, Duca F, et al. Monitoring tafamidis treatment with quantitative SPECT/CT in transthyretin amyloid cardiomyopathy. Eur Heart J Cardiovasc Imaging. 2023;24(8):1019-1030.
96. Razvi Y, Porcari A, Hutt DF, et al. Uncertain Clinical Relevance of Serial Bone Scintigraphy Findings in Treated Transthyretin Amyloid Cardiomyopathy. JACC Cardiovasc Imaging. 2025:S1936-878X(25)00249-9.
97. Choi YJ, Koh Y, Lee HJ, et al. Independent Prognostic Utility of 11C-Pittsburgh Compound B PET in Patients with Light-Chain Cardiac Amyloidosis. J Nucl Med. 2022;63(7):1064-1069.
98. Clerc OF, Datar Y, Cuddy SAM, et al. Prognostic Value of Left Ventricular 18F-Florbetapir Uptake in Systemic Light-Chain Amyloidosis. JACC Cardiovasc Imaging. 2024;17(8):911-922.
99. Datar Y, Clerc OF, Cuddy SAM, et al. Quantification of right ventricular amyloid burden with 18F-florbetapir positron emission tomography/computed tomography and its association with right ventricular dysfunction and outcomes in light-chain amyloidosis. Eur Heart J Cardiovasc Imaging. 2024;25(5):687-697.
100. Vergaro G, Aimo A, Genovesi D, et al. Estimated total amyloid burden from 18F-florbetaben PET predicts all-cause mortality in light-chain cardiac amyloidosis. Eur Heart J Cardiovasc Imaging. 2024:jeae332.
101. Salimi Y, Shiri I, Mansouri Z, et al. Artificial intelligence-based cardiac transthyretin amyloidosis detection and scoring in scintigraphy imaging: multi-tracer, multi-scanner, and multi-center development and evaluation study. Eur J Nucl Med Mol Imaging. 2025;52(7):2513-2528.
102. Al Taha Z, Alibazoglu D, Sabbour H, et al. Attacking the Achilles heel of cardiac amyloid nuclear scintigraphy: How to reduce equivocal and false positive studies. J Nucl Cardiol. 2023;30(5):1922-1934.
103. Chevance V, Damy T, Tacher V, et al. Myocardial iodine concentration measurement using dual-energy computed tomography for the diagnosis of cardiac amyloidosis: a pilot study. Eur Radiol. 2018;28(2):816-823.
104. Treibel TA, Bandula S, Fontana M, et al. Extracellular volume quantification by dynamic equilibrium cardiac computed tomography in cardiac amyloidosis. J Cardiovasc Comput Tomogr. 2015;9(6):585-92.
105. Scully PR, Patel KP, Saberwal Bet al. Identifying Cardiac Amyloid in Aortic Stenosis: ECV Quantification by CT in TAVR Patients. JACC Cardiovasc Imaging. 2020;13(10):2177-2189.

106.Gama F, Rosmini S, Bandula S, et al. Extracellular Volume Fraction by Computed Tomography Predicts Long-Term Prognosis Among Patients With Cardiac Amyloidosis. JACC Cardiovasc Imaging. 2022;15(12):2082-2094.
107.Deux JF, Nouri R, Tacher V, et al. Diagnostic Value of Extracellular Volume Quantification and Myocardial Perfusion Analysis at CT in Cardiac Amyloidosis. Radiology. 2021;300(2):326-335.
108.Popp S, Beitzke D, Strassl A, et al. Evaluation of Extracellular Volume and Coronary Artery Disease in Cardiac Amyloidosis Using Photon-Counting CT. Invest Radiol. 2025.
109.De Michieli L, De Gaspari M, Sinigiani G, et al. Chest pain in cardiac amyloidosis: occurrence, causes and prognostic significance. Int J Cardiol. 2023;389:131204.
110.Meng Q, Zhao L, Sun X, et al. Development and validation of a radiomics model for detecting cardiac amyloidosis at coronary computed tomography angiography. Eur Heart J Cardiovasc Imaging. 2025;26(6):1039-1048.

PART II: ORIGINAL CONTRIBUTIONS

Chapter 5. Relative apical sparing in cardiac amyloidosis is not always explained by an amyloid gradient.

This chapter is based on the manuscript: *De Gaspari M*, Sinigiani G*, De Michieli L, Della Barbera M, Rizzo S, Thiene G, Iliceto S, Perazzolo Marra M, Mele D, Basso C, Cipriani A. Relative apical sparing in cardiac amyloidosis is not always explained by an amyloid gradient. Eur Heart J Cardiovasc Imaging. 2023;24(9):1258-1268.*

5.1 Introduction

Amyloidosis includes an under-diagnosed but increasingly recognized group of disorders characterized by the extracellular deposition of misfolded proteins in one or more organs. Cardiac involvement is the major contributor to prognosis in patients with systemic amyloidosis[1,2] and is mainly caused by the immunoglobulin light chains (AL) and transthyretin (ATTR) misfolding and amyloidogenesis[3,4]. A high index of suspicion is needed to achieve the correct diagnosis, and two-dimensional (2D) echocardiography is considered a cornerstone for the identification and follow-up of patients with known or suspected cardiac amyloidosis (CA)[5,6]. The most renowned echocardiographic markers of CA are the increased left ventricular (LV) wall thickness with severe LV diastolic dysfunction and restrictive filling pattern.5 In early disease stage of CA, LV ejection fraction (LVEF) is generally preserved. However, LV longitudinal strain (LS), measurable using 2D speckle-tracking echocardiography[7], can be significantly impaired and also characterized by a typical relative apical sparing (RELAPS) pattern[8]. RELAPS is common in patients with CA and is included among the 'red flags' useful for the differential diagnosis with other causes of increased LV wall thickness[9]. Despite the increasing focus on this specific marker of CA, an etiological clarification for this echocardiographic sign is yet to be determined. A base-to-apex gradient in myocardial amyloid burden has been previously proposed as a possible explanation of the RELAPS pattern[10,11], but serial clinicopathological correlations are missing. Hence, the aim of the present study was to investigate the histopathological basis of the RELAPS phenomenon in whole heart specimens of patients affected by CA.

5.2 Methods

Study design and population

The study included consecutive patients who died at the University Hospital of Padua with an established in vivo diagnosis of CA from July 2005 to November 2021 and underwent complete autopsy. Exclusion criterion was non-availability of the whole heart specimen or inadequate preservation. Written informed consent was obtained from all participants for echocardiography. Consent to autopsy by the patient's family is not required in Italy.

Pathology

During the post-mortem dissection, a first mid-ventricular transverse section (a so-called short-axis section) was made in the unfixed heart. A standard gross examination of the heart was performed. The hearts were routinely fixed with 10% buffered formalin. After fixation, two additional transverse sections at the level of the ventricles were performed so that, overall, a basal, mid-ventricular, and apical slice were obtained. Each transverse section for all specimens was entirely processed for histology, with LV samples matching the standard model used for 2D echocardiography[12]. The samples were routinely processed for histology and paraffin embedded. For evaluation of amyloid deposition, three μm-thick serial sections were obtained for haematoxylin–eosin and sulphated alcian blue stain, as previously described[13]. For each cardiac specimen, the localization of amyloid fibrils was determined, in terms of prevalent interstitial pattern (PIP) or prevalent vascular pattern (PVP). Amyloid distribution was assessed by a histomorphometric quantitative analysis. The extent of amyloid was expressed as percentage of the examined myocardial area. Each LV sample (except for the septal ones) was subdivided in four layers: subepicardial, mid-mural, subendocardial, and trabecular. The interventricular septum (IVS) samples were instead partitioned in three layers: right ventricular (RV)-side, mid-mural, and LV-side. The presence of replacement-type fibrosis was similarly quantified in each ventricular sample by a histomorphometric quantitative analysis and expressed as a percentage of myocardial area.

Amyloid typing

Amyloid typing was obtained by immune electron microscopy on formalin-fixed paraffin-embedded blocks after dewaxing and resin-embedding. Selected sections were then processed for post-embedding immunogold. The primary antibodies used were anti-human kappa light chains, anti-human lambda light chains, and anti-human TTR.

Echocardiography

Echocardiographic images were acquired using a Vivid 7 or Vivid 9 ultrasound system (GE Medical Systems, Milwaukee, USA), and analysis was independently carried out in post-processing by a trained cardiologist blinded to the pathology findings. Inadequate image quality was defined in the presence of a frame rate <40 frames per second or inability to visualize or perform adequate speckle-tracking analysis on more than two myocardial segments. IVS thickness, LV end-diastolic diameter (LVEDD), and posterior wall (PW) thickness were measured on 2D images at the level of the mitral valve leaflet tips in diastole. LVEF was calculated using the biplane Simpson method. Diastolic function was evaluated using the E/A and E/e′ ratios, with conventional and tissue Doppler traces recorded in the apical four-chamber view. All measurements were in accordance with the American Society of Echocardiography guidelines[12]. Peak systolic LS assessment was performed using the EchoPAC software v. 113 (GE Medical Systems, Milwaukee, USA). The three standard apical four-chamber, two-chamber, and long-axis views were used for LS measurements. A polar plot of segmental peak systolic LS values was generated by the software. Global LS (GLS) was calculated using the average of the segmental LS values. Strain values for the six basal, six mid, and five apical segments of the LV were averaged to obtain three regional LS values (basal, mid, and apical). Relative apical LS was calculated as relative apical LS = average apical LS/(average basal LS + average mid LS), and a value of 1 was used as a cut-off for the presence of RELAPS[8]. Qualitative assessment (i.e. visually identified RELAPS) was not considered. Considering that echocardiographic RELAPS is a pattern of LS and to avoid any bias due to single segmental analysis, an adjunctive pattern analysis of the relationship between LS and segmental

amyloid deposition was performed; accordingly, every LS polar plot was visually compared with the correspondent LV segmental amyloid deposition polar diagram.

Statistical analysis

Continuous variables were expressed as median with 25th and 75th percentiles (Q1–Q3) and analysed by Student's t-test (or analysis of variance) or Mann–Whitney U test for parametric and non-parametric variables, respectively. Categorical variables were expressed as absolute numbers and percentages and were compared using the $\chi 2$ test or Fisher exact test, when appropriate. Pearson and Spearman correlation analysis were used to test the association between continuous variables. Friedman test was applied for comparison of means between subgroups. All statistical analyses were performed using IBM SPSS Statistics 27.0 package and Jamovi (version 2.3).

5.3 Results

Among 2932 consecutive autopsies performed during the study period, CA was diagnosed in 67 patients (2.3%) and the heart specimen was available for further examination in 27 cases (18 males; median age 71 years, range 45–93 years). Amyloid typing by immunogold technique on transmission electron microscopy performed on formalin-fixed paraffin-embedded cardiac samples after autopsy identified 17 cases of AL-CA (63%) and 10 ATTR-CA (37%).

Histopathology

Detailed gross and histopathological data are reported in **Table 1**. At gross examination, heart weight ranged from 400 to 1400 g, with a median value of 605 g. The basal LV section had the greatest median ventricular wall thickness (15 mm), compared with the mid-ventricular (13 mm) and apical section (9 mm). At histology, amyloid deposition was observed with PIP in 21 cases (78%), whereas a PVP was documented in 6 cases (22%). Pattern of deposition was further characterized in interstitial segmental in 18 cases (67%) and interstitial diffuse in 9 (33%). No evidence of major epicardial coronary artery involvement by amyloid deposits was observed.

Table 1. General and histopathological characteristics of the study population.

	All (Study population) N = 27	**PIP N = 21**	**PVP N = 6**	**p**	**AL-CA N = 17**	**ATTR-CA N = 10**	**p**
Age (years) (range)	71 (45 – 93)	71 (45 – 88)	69 (61 – 93)	0.64	63 (57 – 66)	83 (79 – 88)	0.001
Sex	M: 18 (67) F: 9 (33)	M: 13 (62) F: 8 (38)	M: 5 (83) F: 1 (17)	0.63	M: 13 (76) F: 4 (24)	M: 5 (550) F: 5 (50)	0.22
CA subtype	AL: 17 (63) ATTR: 10 (37)	AL: 12 (57) ATTR: 9 (43)	AL: 5 (68) ATTR: 1 (17)	0.36	AL: 17 (100) ATTR: 0	AL: 0 ATTR: 10 (100)	-
Gross analysis							
Heart weight, g	605 (510–700)	605 (510-700)	600 (500-650)	0.88	575 (505 – 640)	685 (550 – 750)	0.10
LV thickness							
Basal, mm	15 (13–16)	16 (15–16)	13 (11–14)	0.012	15 (13–16)	16 (13–16)	0.60
Mid-ventricular, mm	13 (11–14)	13 (12–15)	11 (9–12)	0.015	12 (10–13)	13 (13–14)	0.29
Apical, mm	9 (7–11)	10 (8–11)	8 (7–8)	0.24	9 (8–11)	9 (7–10)	0.46
Histomorphometric analysis							
Amyloid burden per segment, %	25.30 (6.72 – 57.54)	46.16 (14.64-60.57)	3.69 (2.54-6.10)	<0.001	24.13 (6.81-51.56)	43.58 (7.71-49.18)	0.07
Fibrosis burden per segment, %	0.50 (0.00 – 1.33)	0.31 (0.00 – 1.11)	1.81 (0.96 – 3.68)	<0.001	0.52 (0.00 – 1.32)	0.45 (0.00 – 1.54)	0.69

Categorical values are reported as n (%), continuous values are reported as median (25th-75th). Abbreviations: M=male; F=female; AL=light-chain amyloidosis; ATTR= transthyretin amyloidosis; CA=cardiac amyloidosis; LV=left ventricular; PIP=prevalent interstitial pattern; PVP=prevalent vascular pattern.

Table 2. Amyloid burden quantification at histology.

	N	Basal	Mid-ventricular	Apical	p
All	27	25.38 (11.35-59.04)	26.70 (6.90-56.07)	18.80 (4.02-59.35)	0.03
Trabecular		29.75 (19.38-65.25)	27.00 (9.88-61.38)	31.67 (5.17-60.83)	0.11
Subendocardial		22.75 (10.69-61.19)	25.75 (8.06-60.50)	19.31 (4.50-59.31)	0.07
Mid-mural		26.25 (9.25-53.56)	24.13 (6.88-53.19)	17.38 (3.81-55.06)	0.001
Subepicardial		26.25 (9.50-53.75)	28.38 (8.31-54.13)	20.00 (3.56-56.69)	0.011
PIP	21	42.60 (17.02-59.71)	46.55 (16.27-58.02)	45.96 (11.53-62.82)	0.09
Trabecular		48.50 (28.00-67.75)	55.50 (22.00-63.00)	50.70 (14.08-67.42)	0.16
Subendocardial		48.25 (16.38-62.50)	53.38 (16.13-63.00)	50.25 (13.75-63.69)	0.14
Mid-mural		42.38 (16.13-57.25)	41.50 (14.38-53.63)	39.63 (7.38-58.38)	0.09
Subepicardial		33.63 (15.00-56.00)	38.38 (20.21-56.12)	38.50 (9.13-59.56)	0.07
PVP	6	4.03 (2.93-7.94)	4.07 (2.28-6.44)	3.48 (2.42-4.15)	0.14
Trabecular		5.25 (3.50-14.31)	5.13 (3.31-13.31)	5.17 (3.42-5.92)	0.61
Subendocardial		3.88 (2.69-7.69)	4.06 (2.66-6.31)	3.75 (2.81-4.50)	0.40
Mid-mural		3.50 (2.06-5.41)	3.56 (2.25-4.59)	2.63 (2.06-3.56)	0.30
Subepicardial		4.31 (3.31-5.69)	3.63 (2.66-4.50)	2.38 (2.00-3.31)	0.31
ATTR-CA	10	49.15 (13.94-71.57)	35.81 (7.71-64.82)	37.13 (4.44-65.61)	0.008
Trabecular		60.63 (24.31-80.19)	42.88 (8.63-69.63)	44.17 (4.00-76.08)	0.048
Subendocardial		47.50 (13.40-73.00)	35.19 (6.88-66.88)	38.50 (3.50-68.56)	0.007
Mid-mural		46.81 (11.81-68.22)	30.88 (6.68-60.34)	29.63 (4.25-66.06)	0.014
Subepicardial		41.06 (11.25-70.31)	36.00 (8.72-62.63)	32.63 (3.25-62.13)	0.027
AL-CA	17	23.03 (7.94-53.26)	26.70 (9.84-51.83)	18.80 (4.03-48.66)	0.14
Trabecular		28.00 (14.25-60.50)	27.00 (15.75-57.50)	24.67 (5.95-54.58)	0.31
Subendocardial		21.75 (8.75-55.00)	25.75 (10.00-53.50)	19.88 (4.50-53.56)	0.74
Mid-mural		24.13 (5.63-44.37)	24.13 (8.60-43.50)	17.38 (3.63-47.25)	0.62
Subepicardial		20.13 (5.88-51.25)	28.38 (9.13-51.50)	20.00 (3.68-47.56)	0.83

All values are reported in median (25^{th}-75^{th}) of percentages. Abbreviations: AL=light-chain amyloidosis; ATTR= transthyretin amyloidosis; CA=cardiac amyloidosis; PIP=prevalent interstitial pattern; PVP=prevalent vascular pattern

Histopathology: segmental analysis

Overall median amyloid infiltration per each ventricular segment was 25.3% (6.72–57.54), and it was greater in patients with PIP compared with those with PVP (46.16% vs. 3.69%, P < 0.001) and in ATTR-CA vs. AL-CA (43.58% vs. 24.13%) (although not statistically significant, P = 0.07). Fibrosis per each ventricular segment was 0.5% (0–1.33), similar between ATTR- and AL-CA (0.45% vs. 0.52%, P = 0.69), and greater in patients with PVP compared with those with PIP (1.81% vs. 0.31%, P < 0.001).

Amyloid burden quantification analysis divided per basal, mid-ventricular, and apical segments and subepicardial, mid-mural, subendocardial, and trabecular layers is reported in **Table 2**.

In the whole population, amyloid burden was significantly greater in the basal (25.38%) and mid-ventricular levels (26.70%) compared with the apical ones (18.80%) (P = 0.030) (**Figure 1**).

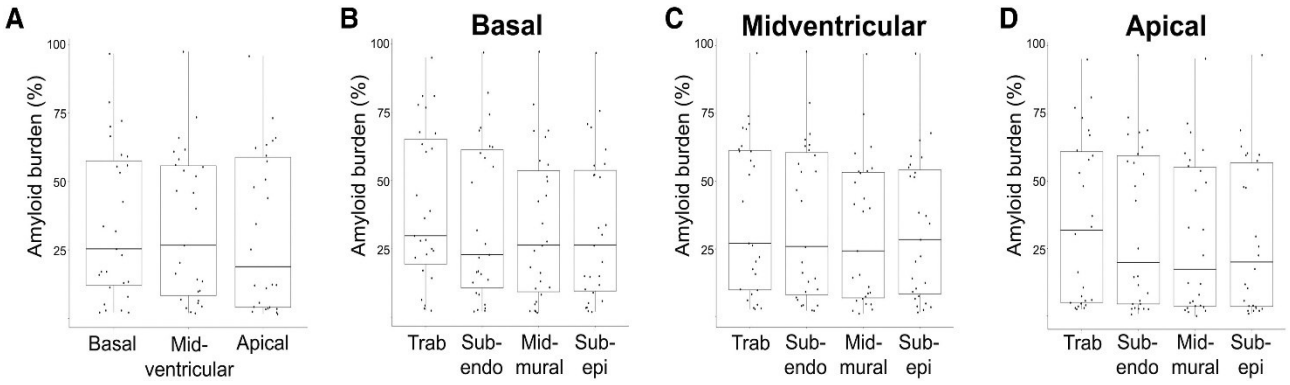

Figure 1. Longitudinal and transmural amyloid distribution at histology
A) Amyloid burden at histology in different ventricular levels (basal vs. mid-ventricular vs. apical, p = 0.03). B) Transmural distribution of amyloid burden at histology in the basal level, C) in the mid-ventricular level, D) in the apical level (B,C,D p < 0.001).
Abbreviations: trab = trabecular layer; sub-endo = subendocardial layer; sub-epi = subepicardial layer.

The amyloid distribution was diffusely low in 11, diffusely high in 7, heterogeneous in 4, and with a base-to-apex gradient in 5.

In patients with ATTR-CA, amyloid burden was significantly greater in the basal level (49.15%), compared with the mid-ventricular (35.81) and apical ones (37.13%) (P = 0.008), and the difference was confirmed in all layers. However, when considering separately patients with PIP, PVP, or with

AL-CA only, no differences among segments were detected, neither overall nor according to different layers (**Table 2**). In all groups, a transmural gradient in amyloid burden was found, with more deposits in the trabecular and subendocardial layers compared with the mid-mural and subepicardial ones (**Table 2** and **Figure 1**).

Echocardiography study

Detailed 2D echocardiography data including LS evaluation were available in 11/27 patients (n = 8 with PIP and n = 3 with PVP; n = 7 with AL-CA and n = 4 with ATTR-CA) and are showed in Table 3. No LV segments were excluded in the analysis. No differences in all echo parameters among PIP vs. PVP groups or AL-CA vs. ATTR-CA were detected. The speckle-tracking analysis in all patients revealed a reduced GLS (−8%), with a RELAPS phenomenon observed in 8/11 (73%). A significant base-to-apex gradient of GLS was found in the whole echo population ($P < 0.001$), PIP ($P = 0.010$), AL-CA ($P = 0.021$), and ATTR-CA ($P = 0.039$) subgroups (**Table 3**).

Echocardiography–histopathology correlation

A significant correlation between amyloid burden and IVS and PW thickness was observed ($r = 0.83$ and $r = 0.73$, respectively; $P < 0.001$ for both; see **Figure 2**). While no significant inverse correlation between global amyloid burden and LVEF was found ($r = −0.267$, $P = 0.428$), a direct correlation between segmental amyloid burden and GLS in each segment was evident ($r = 0.409$, $P = 0.018$), with even more significant values when only PIP patients were considered ($r = 0.616$, $P = 0.001$) (**Figure 2E and F**).

Table 3. Echocardiographic results.

	All (Echo subgroup) N = 11	**PIP N = 8**	**PVP N = 3**	**p**	**AL-CA N = 7**	**ATTR-CA N = 4**	**p**
LVEDVi, ml/m^2	51 (47 – 66)	49 (47 – 57)	66 (62 – 96)	0.13	62 (47 – 66)	49 (47 – 94)	0.85
LVEF, %	54 (41 – 56)	55 (48 – 56)	41 (27 – 59)	0.77	53 (41 – 56)	56 (40 – 57)	0.64
IVSd, mm	17 (14 – 18)	18 (14 – 19)	14 (11 – 18	0.38	17 (14 – 18)	17 (13 – 21)	0.63
LVEDD, mm	45 (39 – 57)	42 (37 – 52)	51 (45 – 59)	0.28	44 (35 – 51)	52 (43 – 61)	0.26
PWTd, mm	13 (11 – 17)	14 (12 – 18)	12 (9 – 16)	0.38	13 (11 – 17)	14 (11 – 18)	0.85
RWT	0.63 (0.46 – 0.72)	0.66 (0.55 – 0.75)	0.53 (0.31 – 0.63)	0.13	0.63 (0.53 – 0.77)	0.56 (0.42 – 0.69)	0.71
LV Mass indexed (gr/mq)	146 (112 – 194)	148 (104 – 191)	132 (122 – 175)	0.84	137 (112 – 150)	188 (108 – 414)	0.35
E/e’	20 (14 – 33)	15 (13 – 23)	33 (18 – 35)	0.27	20.2 (13.6 – 33.0)	18.8 (13.1 – 33.0)	1.00
E/A	1.8 (1.2 – 3.0)	1.8 (1.2 – 3.6)	1.5 (0.5 – 2.5)	0.64	1.8 (1.1 – 2.5)	3.1 (1.2 – 4.9)	0.51
GLS (-%)	8.0 (4.3 – 12.3)	4.9 (2.8 – 7.5)	1.7 (0.5 – 13.2)	0.63	3.7 (1.7 – 7.3)	5.4 (1.9 – 9.9)	0.79
GLS basal (-%)	5.5 (2.5 – 7.5)	6.0 (3.0 – 7.5)	3.5 (1.0 – 12.5)	1.00	5.5 (3.5 – 7.5)	5.0 (0 – 9.5)	0.79
GLS mid-ventricular (-%)	8.0 (5.5 – 9.0)	8.0 (6.5 – 8.5)	5.5 (1.5 – 14.0)	0.49	7.0 (5.5 – 9.0)	8.0 (6.3 – 11.0)	0.65
GLS apical (-%)	12.0 (11.0 – 18.0)	12.0 (11.0 – 16.0)	15.0 (9.0 – 19.0)	0.63	14.0 (11.0 – 18.0)	11.5 (8.5 – 15.0)	0.41
RELAPS (%)	8 (73)	6 (75)	2 (67)	1.00	6 (86)	2 (50)	0.49

All values are reported in median (25th-75th). Abbreviations AL=light-chain amyloidosis; ATTR= transthyretin amyloidosis; CA=cardiac amyloidosis; GLS= global longitudinal strain; IVSd= interventricular septum in diastole; LVEDD= left ventricular end-diastolic diameter; LVEDVi= left ventricular end-diastolic volume index; LVEF= left ventricular ejection fraction; PIP=prevalent interstitial pattern; PVP=prevalent vascular pattern; PWTd= posterior wall thickness in diastole; RWT= relative wall thickness; RELAPS= relative apical sparing.

Table 4. Clinical and pathological details of the study population (11 patients with echocardiography).

Pattern	Sex	Age of death	Time echo – death (months)	Amyloid type	Specific therapy	History of ACS or CAD	Cause of death	HR (bpm)	SBP in echo (mmHg)	DPB in echo (mmHg)	IVS thickness (mm)	PW thickness (mm)	iEDV (ml/mq)	EF (%)	Echo pattern	Amyloid histological pattern	Amyloid histological burden
Normal or mildly reduced LS – Diffuse low amyloid	F	82	5	ATTRwt	No	Yes	Septic shock (Endocarditis)	80	130	80	11	9	45	46	LS normal or mildly reduced	PIP	Diffuse low
	M	65	10	AL lambda	CyBorD	No	Septic shock	63	140	70	14	12	62	59	LS normal or mildly reduced	PVP	Diffuse low
Severely reduced LS – Diffuse high amyloid	M	75	5	ATTRwt	No	No	Acute heart Failure	65	135	75	26	21	138	25	LS diffusely reduced	PIP	Diffuse high
RELAPS – Amyloid gradient	F	88	1	ATTRwt	No	Yes	ACS-STE	65	145	70	14	13	51	57	RELAPS	PIP	Base-to-apex gradient
	M	79	2	AL lambda	No	No	Acute heart Failure	92	125	80	18	16	66	41	RELAPS	PVP	Base-to-apex gradient
RELAPS – No amyloid gradient	F	73	< 1*	AL lambda	No	No	Cardiogenic shock	80	120	80	11	9	96	27	RELAPS	PVP	Diffuse low
	F	83	10	ATTRwt	No	No	Acute heart failure	96	130	80	22	15	47	56	RELAPS	PIP	Diffuse high
	M	57	1	AL lambda	CyborD	No	Acute heart Failure	93	100	60	18	19	52	43	RELAPS	PIP	Diffuse high
	F	59	1	AL lambda	CyBorD	No	SCD (Refractory FV)	86	110	70	14	11	38	53	RELAPS	PIP	Diffuse low
	M	66	1	AL lambda	BorD	No	SCD (EMD)	56	115	80	17	17	50	54	RELAPS	PIP	Heterogeneous
	M	73	< 1**	AL lambda	No	No	Acute peritonitis	90	100	60	18	13	63	56	RELAPS	PIP	Diffuse high

* 2 weeks before the death. ** 3 weeks before the death. Abbreviations: F = female, M = male; AL = light chain amyloidosis; ATTR = transthyretin amyloidosis; ATTRwt = ATTR wild – type; CyBordD = cyclophosphamide, bortezomid and dexamethasone; ACS = acute coronary syndrome; CAD = coronary artery disease; IVS = interventricular septum; PW = posterior wall of the left ventricle; iEDV = indexed end-diastolic volume; EF = ejection fraction; EMD= electromechanical dissociation; PIP, prevalent interstitial pattern; PVP, prevalent vascular pattern.

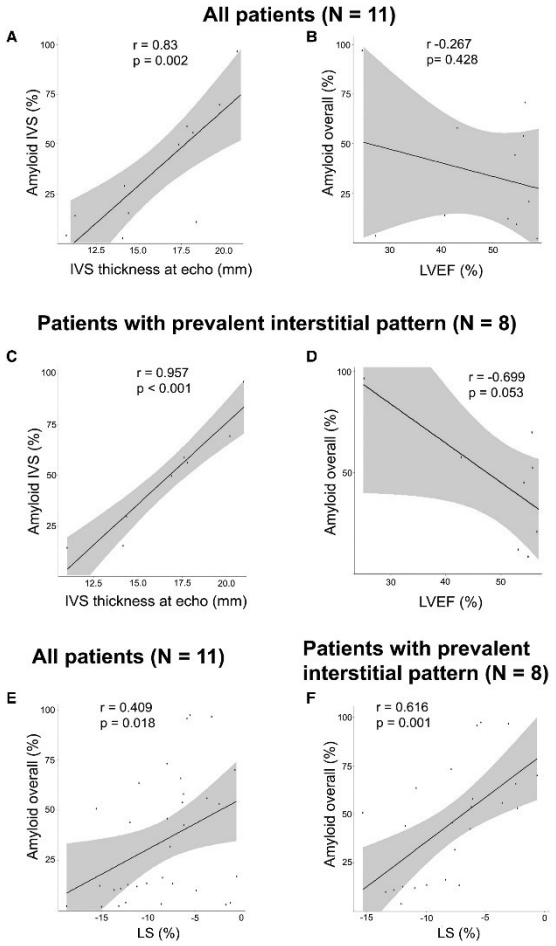

Figure 2. Clinicopathological correlations between echocardiographic parameters and amyloid burden at histology**.** A) Correlation between histologically-assessed amyloid deposition at the level of the interventricular septum (IVS) and the IVS thickness evaluated at echocardiography. B) Correlation between left ventricular (LV) amyloid burden at histology and left ventricular ejection fraction (LVEF). C-D) The same correlations as in A-B but restricted to patients with a prevalent interstitial pattern of amyloid deposition. E) Correlation segment by segment between LV amyloid deposition at base, mid-ventricular and apical level and global longitudinal strain (GLS) at echocardiography. (F) The same correlation as in E restricted to patients with a prevalent interstitial pattern of amyloid deposition.

When comparing values of LS and histological amyloid burden in the LV (**Figure 3**, **Table 4**), two patients, who had normal or mildly reduced LS and no evidence of RELAPS at 2D echocardiography, were characterized by diffuse low percentages of amyloid deposition. One patient, who had severely reduced LS and no evidence of RELAPS at 2D echocardiography, showed diffuse high percentages of amyloid deposition. Among the eight patients with the RELAPS phenomenon at 2D echocardiography, two (25%) showed a gradient of amyloid deposition, greater in the basal and middle than in the apical segments, and six patients had no histological gradient of amyloid deposition. More in detail, three patients had a diffusely high

amyloid burden; two patients had a diffusely low amyloid burden, and one patient had a heterogeneous amyloid build-up. Furthermore, we assessed the correlation between transmural gradient and RELAPS or subendocardial-only content and RELAPS without evidence of statistically significant differences.

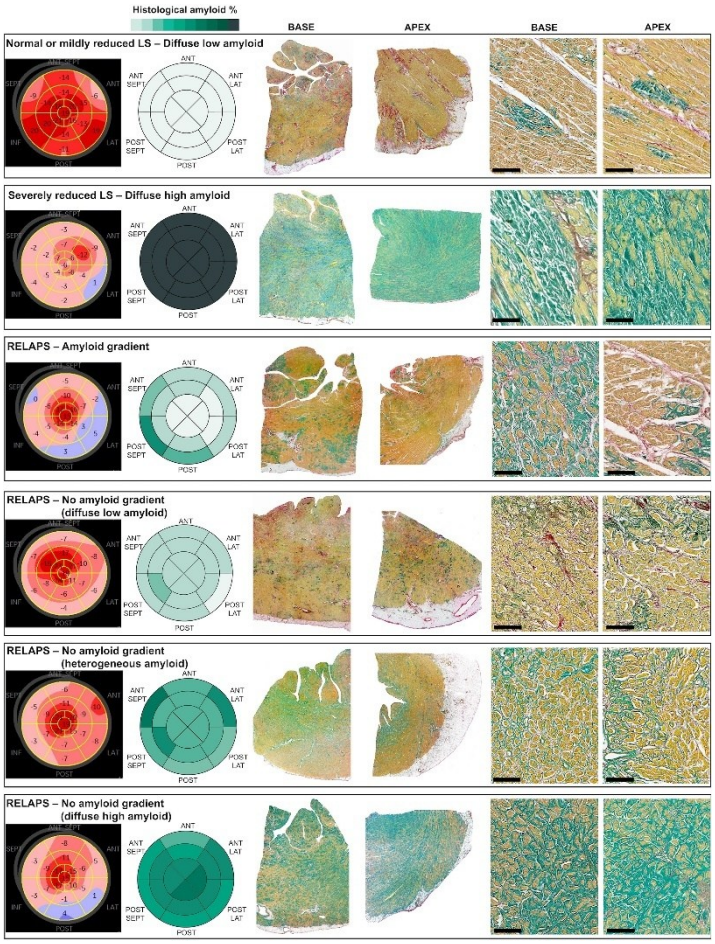

Figure 3. Echo-histological patterns of amyloid distribution. Different patterns of correlation between echocardiographic findings and histologically-assessed amyloid distribution are represented: normal or mildly reduced LS – diffuse low amyloid, without RELAPS at echocardiography and with diffuse low percentages of amyloid deposition at histology; severely reduced LS – diffuse high amyloid, without RELAPS at echocardiography and with diffuse high percentages of amyloid deposition at histology; RELAPS – amyloid gradient, with RELAPS phenomenon and a base-to-apex gradient of amyloid deposition; and RELAPS – no amyloid gradient, with diffusely low amyloid deposition, heterogeneous amyloid deposition and diffuse high amyloid deposition. All patterns are illustrated with a sequence of echocardiography longitudinal strain bull's eye polar, histological bull's eye equivalent of amyloid deposition, panoramic view of basal and apical LV sections and close-up of the same sections (scale bar 100 μm).

5.4 Discussion

The aim of our clinicopathological study was to investigate the histopathological basis of the RELAPS phenomenon in whole heart specimens of patients affected by CA. The main study results were (i) the amyloid burden as assessed at the microscope was significantly greater in the basal and mid-ventricular than in the apical levels (base-to-apex gradient); (ii) a transmural gradient in amyloid burden was also present, with more deposits in the trabecular and subendocardial compared with the mid-mural and subepicardial layers; (iii) the amyloid deposition was observed both in the interstitium and in the intramyocardial vessels, but in about one-fourth of cases, the deposition was prevalent in the vessels, a finding predominantly observed in AL-CA; and (iv) 2D echocardiography data, besides confirming a significant correlation between amyloid burden and LV wall thickness, showed a RELAPS phenomenon in nearly three-quarters of cases and a significant base-to-apex gradient of LS in the whole echo population. A direct correlation between segmental amyloid burden and LS in each segment was evident, with even more significant values when only patients with PIP were considered. Myocardial mass was higher than normal, with thickened LV ventricular wall in nearly all cases. At echocardiography, increased LV wall thickness with preserved EF and severe diastolic dysfunction was found, in keeping with the classical phenotype reported for CA[5,6,9].

Despite their intrinsic heterogeneity, AL-CA and ATTR-CA did not manifest significant differences except for the age at presentation. The well-known dissimilarities mainly related to age at diagnosis (higher in ATTR-CA), LV wall thickness (higher in ATTR-CA), and survival (worse in AL-CA)[4,14] are mostly unidentifiable in our study population, most probably due to its small size and study design. However, a non-significant trend is recognizable with ATTR-CA having greater mean heart weight and mass and a slightly more severe amyloid burden per segment. A greater difference in the amyloid and fibrosis burden per segment can be clearly recognized when comparing the two deposition patterns (PIP and PVP), with PVP related to less amyloid accumulation but more severe (even if minimally) myocardial fibrosis.

Three main hypotheses have been advanced to explain the RELAPS phenomenon so far: (i) differences in amyloid level deposition, greater in the base than in the apex; (ii) differences in myocytes and extracellular matrix orientation between base and apex; and (iii) greater tendency towards apoptosis and remodelling in basal regions, due to turbulent flow in the LV outflow tract[10,15]. According to the hypothesis of amyloid base-to-apex gradient, the presence of less amyloid deposition at the apex may preserve cardiac myocyte contraction and deformation properties, leading to the relative sparing of apical LS.

Phelan et al. first suggested the amyloid base-to-apex gradient theory, after the echocardiographic observation of a thicker LV wall at the basal and mid-ventricular segments than at the apex in patients with CA. However, no histology validation analysis was available. Similar results were proposed by Ternacle et al., who studied with 2D strain echocardiography and cardiac magnetic resonance a series of patients with CA, showing that LV LS impairment reflected the amyloid burden and late-gadolinium enhancement was associated with LV LS impairment. Of note, a strong negative correlation between the amyloid burden measured by histopathology and segmental LV LS in different types of CA was also highlighted. Although only three explanted hearts were available, amyloid deposits were more abundant in the basal and mid-ventricular sections, which were those with greater LGE and poorer LS. A similar histopathological explanation for the RELAPS substrate has been provided only by Sawada et al.[11] with a single case report showing a base-to-apex gradient of amyloid deposition, even if with limited methodology (a single histological section was sampled at each level, namely basal, mid-ventricular, and apical). Bravo et al.[16] by studying a series of patients with AL-CA with 2D echocardiography, 18F-florbetapir positron emission tomography, and cardiac magnetic resonance postulated that the RELAPS is explained by regional differences in total mass of the amyloid deposition rather than the proportion of amyloid deposits. In other words, the total amyloid mass was disproportionately greater towards the basal and mid-ventricular segments than the apex.

In the present clinicopathological study, we specifically addressed the role of the amyloid deposition carrying out for the first time a detailed histomorphometric analysis matching the standard model used for 2D echocardiography. At the level of any single LV segment—not considering if basal, medium, or apical—a significant correlation between percentage of amyloid deposition and LS was found. In addition, in our study, the GLS analysis showed more propensity of AL-CA to develop RELAPS. A contributing role of intramyocardial vessel amyloid deposition is possible, suggesting that RELAPS might be an epiphenomenon of complex interactions among different patterns of deposition, myocardial structure, and consequent adaptation.

Overall, we found that the amyloid burden assessed at histology was significantly greater in the basal and mid-ventricular levels than in the apical one, irrespectively of deposition pattern (PIP or PVP). In detail, the comparative analysis of LS and amyloid burden led to identify four echo-histological patterns, i.e. normal or mildly reduced LS with diffuse low amyloid burden, severely reduced LS with diffuse high amyloid burden, RELAPS with amyloid gradient, and RELAPS without amyloid gradient, the latter with diffuse low, heterogenous, or diffuse high amyloid deposition. Thus, while a base-to-apex gradient of amyloid burden always accounts for the RELAPS phenomenon at 2D echocardiography, this marker was not always explained by a gradient of amyloid in the heart, as demonstrated by histopathological correlation. Furthermore, by comparing the three cases without RELAPS vs. the eight cases with RELAPS, our results are not supporting the theory that the absence of RELAPS should be considered a marker of advanced disease due to the apical LS impairment.

A possible role of transmural amyloid gradient with prevalent subendocardial involvement together with the peculiar vulnerability of the subendocardium to ischaemia[17] should be taken into consideration. A previous extensive histomorphometric analysis demonstrated a similar transmural gradient of amyloid deposition, with trabecular and subendocardial layers being the most infiltrated[18]. This region of the heart is crucial in regulating the contraction and mechanics, suggesting this additional pathophysiological pathway to explain the RELAPS phenomenon. As

previously hypothesized by Dorbala et al.[19], since the majority of longitudinal fibres are subendocardial and this area of the myocardium is most vulnerable to ischaemia, predominant amyloid deposition in this region could play a role in longitudinal impairment.

Furthermore, as suggested by Rapezzi and Fontana[15], it is possible that the diverse fibre orientation at the apex compared with the base and the preferential involvement of specific fibre subtypes could contribute to the echocardiographic phenomenon of RELAPS. Anatomic studies of the LV fibre architecture have clearly demonstrated the physiological regional variation, showing the clock-wise spiralling of the fibres forming the apex[20].

The presence itself of the misfolded proteins has been hypothesized as a cause of direct damage to the cardiomyocytes via apoptotic cell death leading to cardiac dysfunction and subsequent heart failure[21]. Unfortunately, apoptosis is difficult to evaluate at histology in a quantitative way, since the most frequently used method (called TUNEL) is burdened by high controversy[22]. Moreover, our retrospective study of fixed hearts coming from the pathology archives does not allow to perform a reliable investigation of cardiomyocyte apoptosis in the current population. Recently, the RELAPS pattern has been reported as quite frequent in patients with severe symptomatic aortic stenosis[23,24], even in the absence of pathologically demonstrated CA and with reversibility after surgery[25]. These findings are supportive of a putative role of pronounced LV remodelling with predominant IVS thickening at basal level. The role of myocardial fibrosis remains controversial, since the percentage of replacement-type fibrosis could not be reversed by surgery. The recent demonstration of GLS improvement and RELAPS disappearance in treated AL-CA[26] could further support the role of LV remodelling and toxic myocardial damage from circulating amyloid precursors[27]. Further clinicopathological correlation studies are needed to elucidate the pathological substrates of RELAPS in different clinical settings.

Limitations

Our study has some limitations inherent to its retrospective nature with a relatively small number of heart specimens from patients in which GLS analysis was available. Unfortunately, echocardiogram

was available in less than half of the population. However, the population is unique, taking into account the need to find whole preserved specimens with the possibility to investigate multiple sections from base to apex. Overall, by considering the skewed distribution of RELAPS (yes/no), the different aetiology of CA (AL/ATTR), and level of severity of amyloid deposition, it is hard to express any definite conclusion about negative finding.

5.5 Conclusions

The present clinicopathological study demonstrated that amyloid is variably distributed in the heart of patients affected by CA, with vascular involvement being more frequent in AL-CA. The amyloid burden at histology was significantly greater in the basal and mid-ventricular levels compared with the apex and in the subendocardial layers compared with the subepicardial ones (i.e. longitudinal and transmural gradients). A direct correlation between segmental amyloid burden and LS in each segment is evident. The RELAPS phenomenon at echocardiography is present in nearly half of cases and is not always explained by a base-to-apex gradient of amyloid burden at histopathology, suggesting that RELAPS might be an epiphenomenon of complex interactions among amyloid infiltration, myocardial structure, and adaptation.

5.6 References

1. Kumar S, Dispenzieri A, Lacy MQ, Hayman SR, Buadi FK, Colby C et al. Revised prognostic staging system for light chain amyloidosis incorporating cardiac biomarkers and serum free light chain measurements. J Clin Oncol 2012;30:989–95.
2. Grogan M, Scott CG, Kyle RA, Zeldenrust SR, Gertz MA, Lin G et al. Natural history of wild-type transthyretin cardiac amyloidosis and risk stratification using a novel staging system. J Am Coll Cardiol 2016;68:1014–20.
3. Buxbaum JN, Dispenzieri A, Eisenberg DS, Fändrich M, Merlini G, Saraiva MJM et al. Amyloid nomenclature 2022: update, novel proteins, and recommendations by the International Society of Amyloidosis (ISA) Nomenclature Committee. Amyloid 2022; 29:213–9.
4. Rapezzi C, Merlini G, Quarta CC, Riva L, Longhi S, Leone O et al. Systemic cardiac amyloidoses. Circulation 2009;120:1203–12.
5. Falk RH, Quarta CC, Dorbala S. How to image cardiac amyloidosis. Circ Cardiovasc Imaging 2014;7:552–62.

6. Falk RH. Diagnosis and management of the cardiac amyloidoses. Circulation 2005;112: 2047–60.
7. Tsang W, Lang RM. Echocardiographic evaluation of cardiac amyloid. Curr Cardiol Rep 2010;12:272–6.
8. Phelan D, Collier P, Thavendiranathan P, Popović ZB, Hanna M, Plana JC et al. Relative apical sparing of longitudinal strain using two-dimensional speckle-tracking echocardiography is both sensitive and specific for the diagnosis of cardiac amyloidosis. Heart 2012; 98:1442–8.
9. Garcia-Pavia P, Rapezzi C, Adler Y, Arad M, Basso C, Brucato A et al. Diagnosis and treatment of cardiac amyloidosis: a position statement of the ESC Working Group on Myocardial and Pericardial Diseases. Eur Heart J 2021;42:1554–68.
10. Ternacle J, Bodez D, Guellich A, Audureau E, Rappeneau S, Lim P et al. Causes and consequences of longitudinal LV dysfunction assessed by 2D strain echocardiography in cardiac amyloidosis. JACC Cardiovasc Imaging 2016;9:126–38.
11. Sawada N, Daimon M, Abe H, Ushiku T, Kato TS, Morita H et al. An autopsy case of cardiac amyloidosis with heterogeneous deposition of amyloid protein: a possible mechanism for relative apical sparing of longitudinal strain. CASE (Phila) 2020;4: 54–6.
12. Lang RM, Badano LP, Mor-Avi V, Afilalo J, Armstrong A, Ernande L et al. Recommendations for cardiac chamber quantification by echocardiography in adults: an update from the American Society of Echocardiography and the European Association of Cardiovascular Imaging. J Am Soc Echocardiogr 2015;28:1–39.e14.
13. Pomerance A, Slavin G, McWatt J. Experience with the sodium sulphate-alcian blue stain for amyloid in cardiac pathology. J Clin Pathol 1976;29:22–6.
14. Cipriani A, De Michieli L, Porcari A, Licchelli L, Sinigiani G, Tini G et al. Low QRS voltages in cardiac amyloidosis. JACC CardioOncol 2022;4:458–70.
15. Rapezzi C, Fontana M. Relative left ventricular apical sparing of longitudinal strain in cardiac amyloidosis: is it just amyloid infiltration? JACC Cardiovasc Imaging 2019;12: 1174–6.
16. Bravo PE, Fujikura K, Kijewski MF, Jerosch-Herold M, Jacob S, El-Sady MS et al. Relative apical sparing of myocardial longitudinal strain is explained by regional differences in total amyloid mass rather than the proportion of amyloid deposits. JACC Cardiovasc Imaging 2019;12:1165–73.
17. Algranati D, Kassab GS, Lanir Y. Why is the subendocardium more vulnerable to ischemia? A new paradigm. Am J Physiol Heart Circ Physiol 2011;300:H1090–1100.
18. Leone O, Longhi S, Quarta CC, Ragazzini T, De Giorgi LB, Pasquale F et al. New pathological insights into cardiac amyloidosis: implications for non-invasive diagnosis. Amyloid 2012;19:99–105.

19. Dorbala S, Vangala D, Bruyere J, Quarta C, Kruger J, Padera R et al. Coronary microvascular dysfunction is related to abnormalities in myocardial structure and function in cardiac amyloidosis. JACC Heart Fail 2014;2:358–67.
20. Greenbaum RA, Ho SY, Gibson DG, Becker AE, Anderson RH. Left ventricular fibre architecture in man. Br Heart J 1981;45:248–63.
21. Mishra S, Guan J, Plovie E, Seldin DC, Connors LH, Merlini G et al. Human amyloidogenic light chain proteins result in cardiac dysfunction, cell death, and early mortality in zebrafish. Am J Physiol Heart Circ Physiol 2013;305:H95–103.
22. Grasl-Kraupp B, Ruttkay-Nedecky B, Koudelka H, Bukowska K, Bursch W, Schulte-Hermann R. In situ detection of fragmented DNA (tunel assay) fails to discriminate among apoptosis, necrosis, and autolytic cell death: a cautionary note. Hepatology 1995;21:1465–8.
23. Ferreira VV, Rosa SA, Pereira-da-Silva T, Rodrigues I, Gonçalves AV, Mendonça T et al. Prevalence and prognostic impact of apical sparing contractility pattern in patients with aortic stenosis referred for transcatheter aortic valve implantation. Am J Cardiovasc Dis 2021;11:283–94.
24. Robin G, Cognet T, Bouisset F, Cariou E, Méjean S, Pradel S et al. Toulouse Amyloidosis Research Network Collaborators. Value of longitudinal strain to identify wild-type transthyretin amyloidosis in patients with aortic stenosis. Circ J 2021;85:1494–504.
25. Abecasis J, Lopes P, Santos RR, Maltês S, Guerreiro S, Ferreira A et al. Prevalence and significance of relative apical sparing in aortic stenosis: insights from an echo and cardiovascular magnetic resonance study of patients referred for surgical aortic valve replacement. Eur Heart J Cardiovasc Imaging 2023;24:1033–42.
26. Cohen OC, Ismael A, Pawarova B, Manwani R, Ravichandran S, Law S et al. Longitudinal strain is an independent predictor of survival and response to therapy in patients with systemic AL amyloidosis. Eur Heart J 2022;43:333–41.
27. Merlini G. AL amyloidosis: from molecular mechanisms to targeted therapies. Hematology 2017;2017:1–12.

Chapter 6. Atrial electrofunctional predictors of incident atrial fibrillation in cardiac amyloidosis.

This chapter is based on the manuscript: *Sinigiani G, De Michieli L, Porcari A, Zocchi C, Sorella A, Mazzoni C, Bisaccia G, De Luca A, Di Bella G, Gregori D, Perfetto F, Merlo M, Sinagra G, Iliceto S, Perazzolo Marra M, Corrado D, Ricci F, Cappelli F, Cipriani A. Atrial electrofunctional predictors of incident atrial fibrillation in cardiac amyloidosis. Heart Rhythm. 2024;21(6):725-732.*

6.1 Introduction

Atrial fibrillation (AF) is the most frequent sustained arrhythmia in patients with cardiac amyloidosis (CA), which is an infiltrative cardiomyopathy characterized by the deposition of misfolded protein in the heart[1]. Two main types of CA are acknowledged: immunoglobulin light-chain (AL) and transthyretin (ATTR) CA. In AL, the amyloid fibrils are formed by a monoclonal immunoglobulin light chain produced by a low-proliferating bone marrow plasma cell clone. Conversely, ATTR is derived from misfolding of transthyretin protein, a carrier of thyroxine and retinol-binding protein mainly produced by the liver. ATTR is further subdivided into wild type and hereditary types, depending on the absence or presence of variants in the transthyretin gene. AF can be detected in up to two-thirds of CA patients, far more commonly in those with ATTR-CA than AL-CA[2].

Patients with CA poorly tolerate AF occurrence, and those affected are exposed to a greater risk of heart failure hospitalizations[3]. Moreover, AF exacerbates the existing elevated risk of intracardiac thrombi and systemic embolisms in this population[4]. Therefore, early AF detection is key for timely initiation of anticoagulant therapy that in CA is not dependent on the CHA2DS2-VASc score[5]. Previous studies have identified certain factors associated with a greater risk for development of AF (eg, older age, advanced ATTR-CA stage, heart failure, left ventricular ejection fraction, left atrial size, and right atrial pressure)[6,7]. However, none of these studies considered P-wave indices on the electrocardiogram, including assessment of interatrial block (IAB), or functional evaluation of the atria by cardiac magnetic resonance (CMR) imaging. The objective of this study was to identify

baseline clinical parameters, including electrocardiographic and CMR imaging findings, to predict incident AF in a multicenter cohort of patients with AL- and ATTR-CA.

6.2 Methods

This is a multicenter observational study performed in 4 referral centers for CA in Italy: Padua University Hospital, Padua; Careggi University Hospital, Florence; SS Annunziata University Hospital, Chieti; and Trieste University Hospital, Trieste. The local regional institutional review board approved the study, and the participating centers obtained local institutional review board approvals for the retrospective collection of anonymous data. The research reported in this paper adhered to the Declaration of Helsinki as revised in 2013, and informed consent was obtained according to the local review board policies.

Study design and study population

All patients in sinus rhythm with a definitive diagnosis of AL- and ATTR-CA referred for a clinical CMR study between March 2017 and March 2022 were included in the study. The diagnosis of CA was established according to the European Society of Cardiology position paper[5]. Because of the small number of patients with hereditary ATTR in our cohort, we analyzed ATTR-CA patients as a unique group. Standard 12-lead electrocardiography performed within 3 months of CMR examination was necessary for inclusion. Exclusion criteria were a previous diagnosis of AF, including paroxysmal, and all standard contraindications to performance of a CMR examination as described in more detail in the Supplemental Methods.

The indication for the CMR study in the centers involved was for diagnostic purposes. Specifically, CMR was requested for clinical suspicion of cardiomyopathy or demonstration of cardiac involvement. Patients' baseline was set at the time of CMR execution at participating centers. The clinical data recorded within ±3 months from the baseline included all the following: medical history and physical examination, electrocardiography, and laboratory examinations.

Clinical data collection

Careful clinical history was collected, including New York Heart Association class and National Amyloidosis Centre stage. Electrocardiographic IAB was defined as follows: partial IAB, P-wave duration ≥120 ms without a negative deflection in the inferior leads (II, III, aVF); or advanced IAB, P-wave duration ≥120 ms and biphasic (positive/negative) morphology in the inferior leads[8,9]. Low QRS voltages were defined as QRS amplitude <5 mm (0.5 mV) in all peripheral leads, including both negative and positive components[10]. Further details about clinical evaluation, electrocardiography, and biomarkers are described in the Supplemental Methods.

CMR imaging protocol and imaging analysis

CMR imaging was performed with 1.5T systems (Magnetom Avanto [Siemens Medical Systems, Erlangen, Germany], Gyroscan NT and Intera [Philips Healthcare, Andover, MA], and CVi, HD release [GE Healthcare, Milwaukee, WI]). All images were analyzed with dedicated software (cvi42, version 5.13.7; Circle Cardiovascular Imaging Inc, Calgary, Canada). Left and right atrial end-diastolic areas, volumes, ejection fraction, and stroke volume were calculated using 4- and 2-chamber views, as reported by Petersen and coworkers[11]. For the left atrium, the biplane area-length method was used, with atrial endocardial borders manually contoured in 4- and 2-chamber views, excluding the appendage and the pulmonary veins[12]. Maximum area was contoured, as shown in the Supplemental Figure, in the frame immediately before mitral valve opening, whereas minimum area was contoured in the frame immediately after the mitral valve closure. From these, left atrial volume (LAV) was calculated by the formula volume = (0.85 · area2)/length. Atrial ejection fraction was derived with the formula left atrial ejection fraction (LAEF) = (LAVmax – LAVmin)/LAVmax, as previously reported[12]. For the right atrium, given the lack of multiple dedicated views, the area-length method was applied. Left and right ventricular end-diastolic volumes, ejection fractions, stroke volumes, and masses were measured from the short-axis cine images. Left ventricular late gadolinium enhancement (LGE) pattern was qualitatively classified as subendocardial and transmural[13]. Left ventricular LGE presence was qualitatively assessed in 4-, 2-, and 3-chamber views. Intrareader and interreader reproducibility of left atrial indices and other

details about CMR imaging protocol and postprocessing analysis are described in the Supplemental Methods.

Outcomes and statistical analysis

The primary end point was incident AF of any type (paroxysmal, persistent, or permanent) at follow-up. Secondary end points included ischemic stroke, hospitalization for heart failure, and death. All patients were followed up in the heart failure or amyloidosis outpatient clinic every 6 months. AF was diagnosed by standard electrocardiography recorded at each visit, hospitalization or emergency department admission, and 24-hour Holter electrocardiography performed yearly. AF was defined by current guidelines[14]. Survival analysis was calculated with day 1 set as the day the CMR study was performed at the referral center. End points were obtained from follow-up visits and medical records.

Correlation analysis was performed with Cox regression. For statistically continuous variables significant at multivariate Cox regression, a receiver operating characteristic curve was calculated, and the best cutoff was obtained through the Youden index. Subsequently, a score based on the presence of the detected risk factors was calculated. For both factors and score, cumulative incidence curves with Kaplan-Meier method and Gray test were drawn. Further details of statistical methods are given in the Supplemental Methods.

6.3 Results

Of 703 patients diagnosed with CA in the 4 involved centers between March 2017 and March 2022, 140 (19.9%) underwent CMR. Of them, 96 (40 AL-CA, 56 ATTR-CA, of whom 11 had hereditary ATTR) had no previous history of AF and constituted the study population. Baseline characteristics are shown in **Table 1** and in Supplemental Table 1. Intraobserver and interobserver variability of left atrial parameters on CMR is shown in Supplemental Table 2.

Table 1. Baseline characteristics of population according to the onset of atrial fibrillation.

	Overall N = 96	**AF N = 30**	**No AF N = 66**	**p**
Age (years)	74 (66 – 79.5)	79 (72 – 82)	73 (62 – 77)	<0.001
Sex	M: 66 (69) F: 30 (31)	M: 24 (80) F: 6 (20)	M: 42 (64) F: 14 (36)	0.11
Amyloidosis type				
AL	40 (41)	4 (13)	36 (55)	<0.001
ATTR	56 (59)	26 (87)	30 (45)	<0.001
NYHA class				
NYHA I/II	80 (73)	27 (90)	53 (81)	0.38
NYHA III/IV	16 (17)	3 (10)	13 (19)	0.38
CHA_2DS_2VASc score				
$CHA_2DS_2VASc < 3$	50 (52)	11 (37)	39 (59)	0.041
$CHA_2DS_2VASc \geq 3$	46 (48)	19 (63)	27 (41)	0.041
Electrocardiogram				
LBBB	12 (13)	3 (10)	9 (14)	0.62
LAFB	30 (31)	13 (43)	17 (26)	0.09
RBBB	14 (15)	2 (7)	12 (18)	0.14
P wave (msec)	100 (90 – 120)	120 (88 – 130)	100 (88 – 120)	0.08
PQ interval (msec)	194 (162 – 220)	200 (174 – 235)	191 (159 – 220)	0.32
QRS interval (msec)	102 (90 – 118)	106 (90 – 119)	101 (90 – 119)	0.43
Low QRS voltages	34 (35)	14 (47)	20 (30)	0.12
Anterior pseudoinfarction	30 (31)	12 (40)	18 (27)	0.21
Inferior pseudoinfarction	23 (24)	8 (27)	15 (23)	0.68
Partial interatrial block	28 (29)	14 (47)	14 (21)	0.011
Advanced interatrial block	7 (7)	5 (17)	2 (3)	0.017
Blood exams				
NTproBNP (ng/L) *	883 (330 – 1265)	1890 (966 – 3871)	1370 (491 – 2513)	0.048
eGFR (ml/min/m^2)	62.5 (45 – 78)	66 (56 – 79)	79 (67 – 91)	0.046
Cardiac magnetic resonance				
LA area (cm^2)	26 (21 – 30)	29 (25 – 32)	25 (20 – 30)	0.17
RA area (cm^2)	21 (18 – 27)	27 (20 – 31)	21 (18 – 24)	0.61
LA EDVI (ml/m^2)	44 (34 – 56)	51 (40 – 61)	43 (33 – 53)	0.018
RA EDVI (ml/m^2)	39 (31 – 53)	43 (36 – 61)	35 (29 – 45)	0.014
LA EF (%)	36 (26 – 47)	29 (24 – 36)	41 (28 – 52)	0.004
LA SVi (ml/m^2)	17 (12 – 20)	16 (12 – 20)	17 (12 – 21)	0.69
RA EF (%)	36 (27 – 48)	33 (25 – 42)	39 (28 – 49)	0.38
RA SVi (ml/m^2)	15 (11 – 20)	15 (13 – 19)	14 (9 – 20)	0.11
IVS (mm)	16 (14 – 18)	17 (15 – 19)	15 (14 – 18)	0.1
LV mass indexed (g/m^2)	89 (69 – 115)	102 (82 – 134)	83 (67 – 105)	0.045
LV EDVi (ml/m^2)	73 (62 – 87)	82 (71 – 102)	71 (58 – 80)	0.027
LV EF (%)	58 (50 – 65)	50 (43 – 61)	61 (52 – 65)	0.13
LV SVi (ml/m^2)	40 (35 – 47)	41 (36 – 48)	40 (34 – 46)	0.37
RV EDVi (ml/m^2)	66 (54 – 79)	75 (60 – 84)	66 (54 – 77)	0.97
RV EF (%)	59 (52 – 66)	60 (49 – 66)	59 (53 – 65)	0.64
RV SVi (ml/m^2)	39 (33 – 46)	39 (36 – 46)	39 (33 – 46)	0.96
LA LGE	72 (75)	28 (93)	44 (69)	0.009
RA LGE	60 (63)	24 (80)	36 (57)	0.031
LV LGE	89 (93)	30 (100)	59 (91)	0.09
RV LGE	61 (64)	23 (77)	38 (59)	0.10
Subendocardial LGE	38 (40)	13 (43)	25 (42)	0.93
Transmural LGE	54 (56)	19 (63)	35 (59)	0.71
Pericardial effusion	30 (31)	11 (37)	19 (29)	0.47
Pleural effusion	25(26)	8 (27)	17 (26)	0.96
Follow up				
Heart Failure	18 (19)	12 (40)	6 (9)	< 0.001
Death	17 (18)	7 (23)	10 (15)	0.33
Ischemic stroke	6 (6)	4 (14)	2 (3)	0.047

Quantitative variables expressed as median value (25th – 75th percentile). Qualitative variables expressed as absolute number (%).
Abbreviations: AL= light chain amyloidosis; ATTR= Transthyretin amyloidosis; EDVi = end diastolic volume indexed; EF = ejection fraction; eGFR = estimated glomerular filtration rate; IVS = interventricular septum; LA = left atrium; LAFB = left anterior fascicular block; LBBB = left bundle branch block; LGE = late gadolinium enhancement; LV = left ventricle; NAC = National Amyloidosis Centre; NTproBNP = N-Terminal proBNP* (available in 55); NYHA = New York Heart Association; RA = right atrium; RBBB = right bundle branch block; RV = right ventricle; sPAP = systolic pulmonary artery pressure; SVi = stroke volume indexed.

Incident AF and follow-up

During a median follow-up time of 18 months (Q1–Q3, 7–29 months), 30 patients (29%) had incident AF. Compared with those without AF, patients with incident AF were significantly older (79 vs 73 years); they were more frequently diagnosed with ATTR-CA (n = 26, 87%) and more frequently showed IAB, either partial (47% vs 21%; P = .011) or advanced (17% vs 3%; P = .017). Based on CMR findings, patients with incident AF had significantly higher left atrial (51 vs 43 mL/m2; P = .018) and right atrial (43 vs 35 mL/m2; P = .014) end-diastolic volume indexed. They also exhibited a reduced LAEF (29% vs 41%; P = .004) and presented more frequently with left atrial LGE (93% vs 69%; P = .009) and right atrial LGE (80% vs 57%; P = .031). Regarding secondary end points, heart failure hospitalizations (40% vs 9%; P < .001) and ischemic stroke (14% vs 3%; P = .047) were more frequent in patients with incident AF compared with those without. Clinical characteristics of patients with ischemic stroke are reported in Supplemental Table 3. No differences in all-cause mortality between the 2 groups were observed (P = .33).

Predictors of incident AF

Univariable analyses and the derived multivariable model are shown in **Table 2**. The presence of IAB of any grade emerged as an independent predictor of incident AF (hazard ratio [HR], 2.211; 95% CI, 1.03–4.75; P = .041), together with age (HR, 1.059; 95% CI, 1.002–1.118; P = .042) and LAEF (HR, 0.967; 95% CI, 0.936–0.998; P = .044). These findings were further confirmed after proportional hazards assumption (Supplemental Table 4) and competing risk analysis for all-cause mortality (Supplemental Table 5). As shown in **Figure 1**, the hazard of experiencing incident AF progressively increased with the reduction of LAEF values. The cutoffs of LAEF and age for the prediction of incident AF, also confirmed by the receiver operating characteristic curve, were 40% (area under the curve, 0.31; P = .004) and 78 years (area under the curve, 0.73; P < .001), respectively. The presence of either LAEF <40% or age >78 years in combination with the presence of IAB of any grade conferred an increased risk for incident AF (HR, 2.64 [95% CI, 1.264–5.51; P = .01] and HR, 2.42 [95% CI, 1.096–5.34; P = .029], respectively). The increased risk also emerged

for the contemporary presence of any 2 risk factors (HR, 2.19; 95% CI, 1.06–4.52; P = .034), but the highest risk was found in the presence of the 3 parameters (HR, 3.44; 95% CI, 1.523–7.77; P = .003). As shown in **Figure 2**, cumulative incidence of AF at 12 months was significantly higher in patients with IAB of any type (20% [95% CI, 12%–28%] vs 11.5% [95% CI, 5%–18%]; log-rank P < .001), age >78 years (30% [95% CI, 21%–39%] vs 8.5% [95% CI, 3%–14%]; log-rank P = .001), or LAEF <40% (19% [95% CI, 11%–27%] vs 10% [95% CI, 4%–16%]; log-rank P = .021) than without. After combination of the 3 parameters (IAB of any type, age >78 years, LAEF <40%), the highest risk of incident AF was found in the presence of all of them (40% [95% CI, 30%–50%] at 12 months) compared with 2, 1, or none (20% [95% CI, 12%–28%] vs 8.5% [95% CI, 3%–14%] vs 7.6% [95% CI, 2.3%–13%]; log-rank P < .001; **Figure 3**). Furthermore, as shown in **Figure 4**, age >78 years, IAB of any type, and LAEF <40% showed incremental predictive value when sequentially added to a basal model (ie, absence of any of the 3).

Table 2. Predictors of incident atrial fibrillation during 60-month follow-up.

	Univariate Analysis		Multivariable Analysis	
	HR (95% CI)	**p**	**HR (95% CI)**	**p**
Age (years)	1.078 (1.026 – 1.133)	0.003	1.059 (1.002 – 1.118)	0.042
Male sex	1.96 (0.79 – 4.81)	0.14		
AL	0.167 (0.058 – 0.482)	0.001		
History of stroke	0.95 (0.13 – 7.01)	0.96		
History of heart Failure	1.24 (0.59 – 2.61)	0.58		
Hypertension	1.83 (0.89 – 3.71)	0.1		
P wave (msec)	1.01 (0.92 – 1.02)	0.44		
PQ interval (msec)	1.00 (0.99 – 1.01)	0.84		
QRS interval (msec)	1.09 (0.96 – 1.02)	0.22		
Low QRS voltages	2.10 (1.01 – 4.39)	0.048		
Partial interatrial block	2.096 (1.020 – 4.306)	0.044		
Advanced interatrial block	3.657 (1.364 – 9.805)	0.01		
Interatrial block of any grade	3.352 (1.582 – 7.102)	0.002	2.211 (1.03 – 4.75)	0.041
NTproBNP (ng/L)	1 (1 – 1)	0.09		
eGFR (ml/min/m^2)	0.980 (0.962 – 0.999)	0.039		
LA EDVI (mL/m^2)	1.025 (1.001 – 1.049)	0.041		
RA EDVI (mL/m^2)	1.024 (1.004 – 1.045)	0.019		
LA EF (%)	0.961 (0.932 – 0.991)	0.011	0.967 (0.936 – 0.998)	0.044
RA EF (%)	0.99 (0.96 – 1.02)	0.52		
LV EDVi (mL/m^2)	1.01 (0.99 – 1.02)	0.39		
LV EF (%)	0.98 (0.94 – 1.01)	0.19		
RV EDVi (mL/m^2)	1 (0.99 – 1.01)	0.86		
RV EF (%)	0.98 (0.95 – 1.02)	0.31		
LA LGE	4.608 (1.092 – 19.45)	0.038		
RA LGE	2.04 (0.83 – 5.01)	0.12		

Abbreviations as in Table 1.

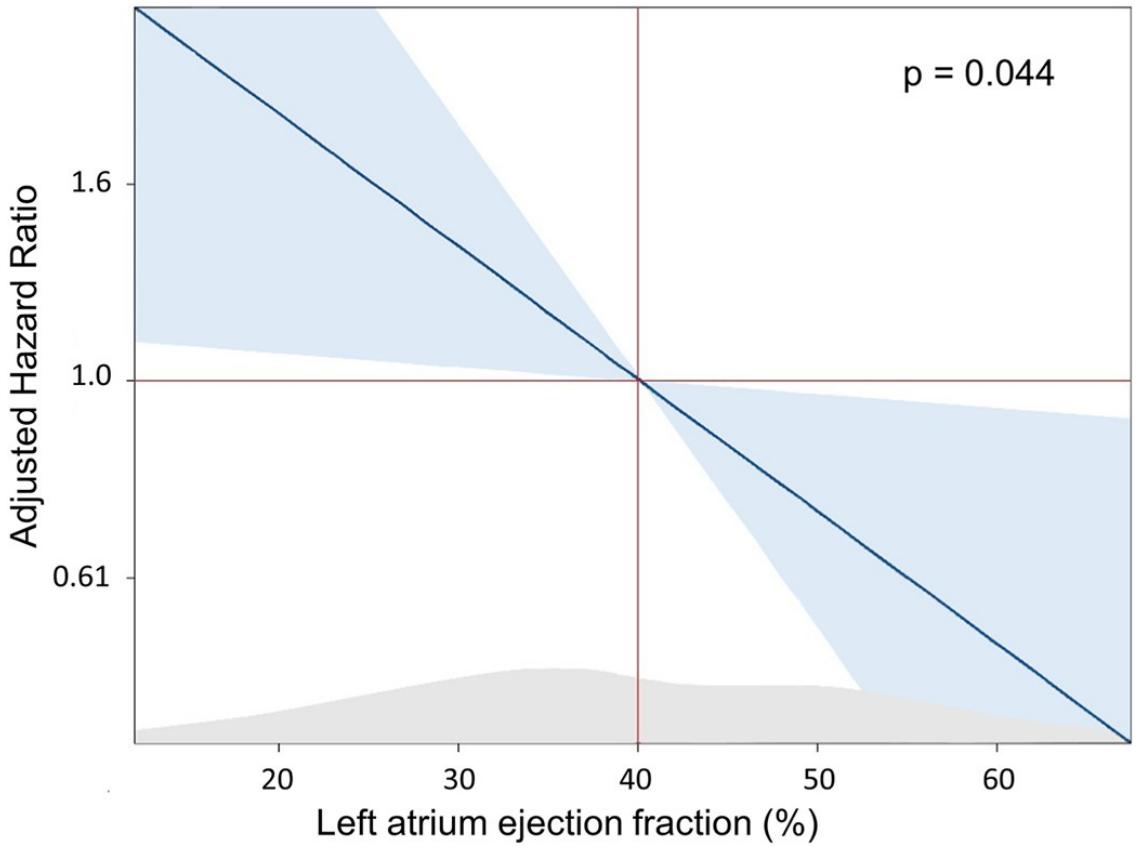

Figure 1. Hazard risk of incident atrial fibrillation according to left atrium ejection fraction, adjusted for age and interatrial block of any grade. Light blue = confidence interval; grey zone = distribution of left atrium ejection fraction in our cohort.

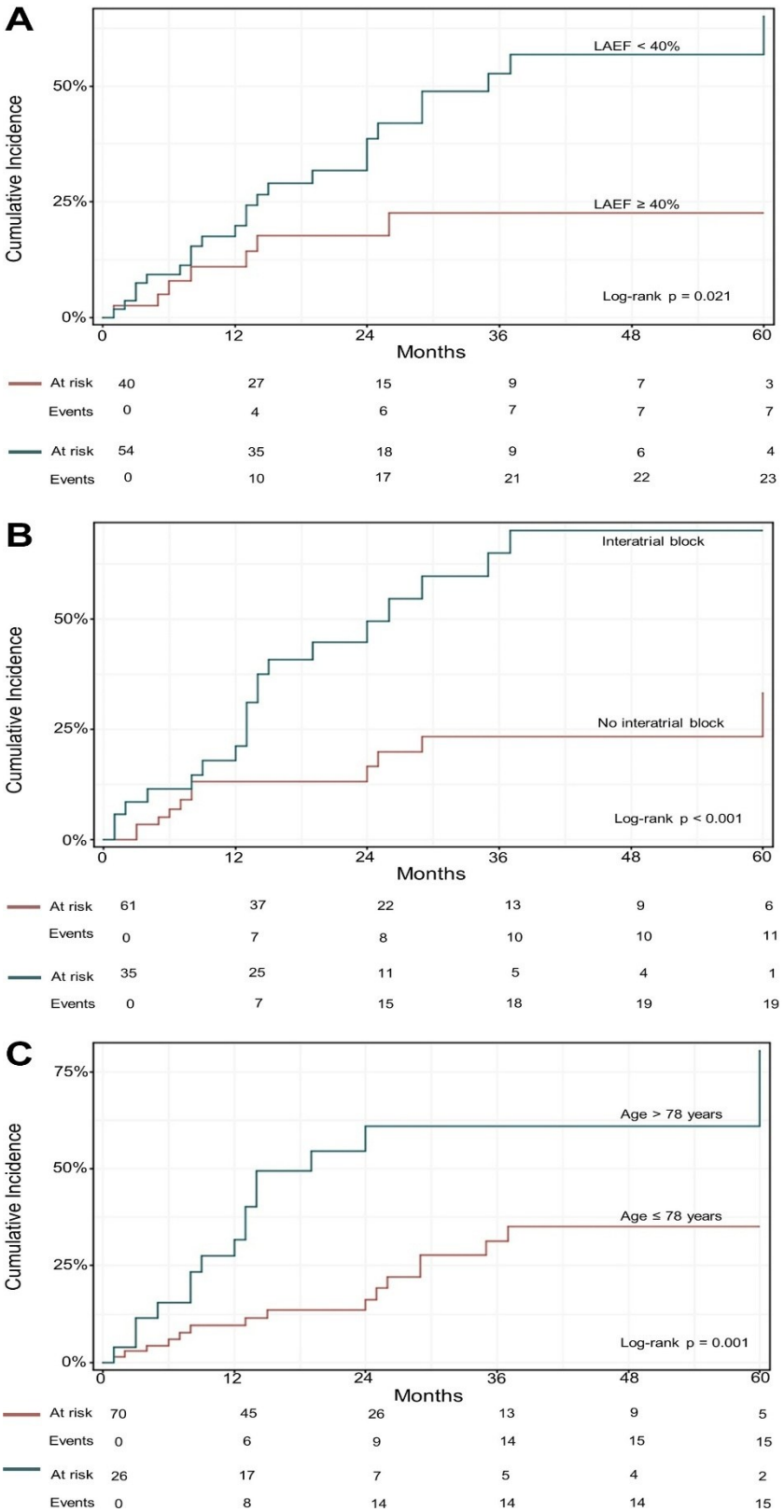

Figure 2. Cumulative incidence of atrial fibrillation according to the presence of left atrium ejection fraction (LAEF) ≤40% (panel A, top), interatrial block of any grade (panel B, middle), or age ≥78 years (panel C, bottom).

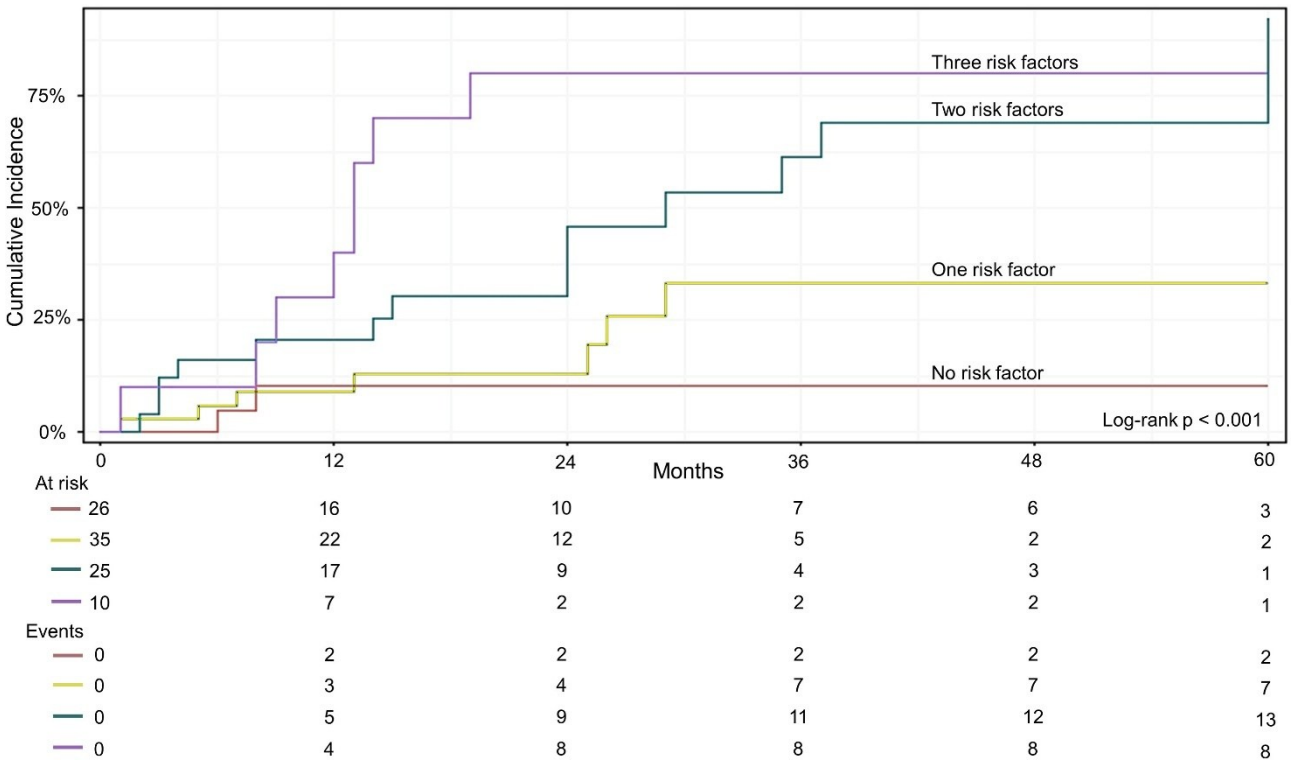

Figure 3. Cumulative incidence of atrial fibrillation according to the different combined presence of left atrium ejection fraction <40%, interatrial block of any grade, age >78 years.

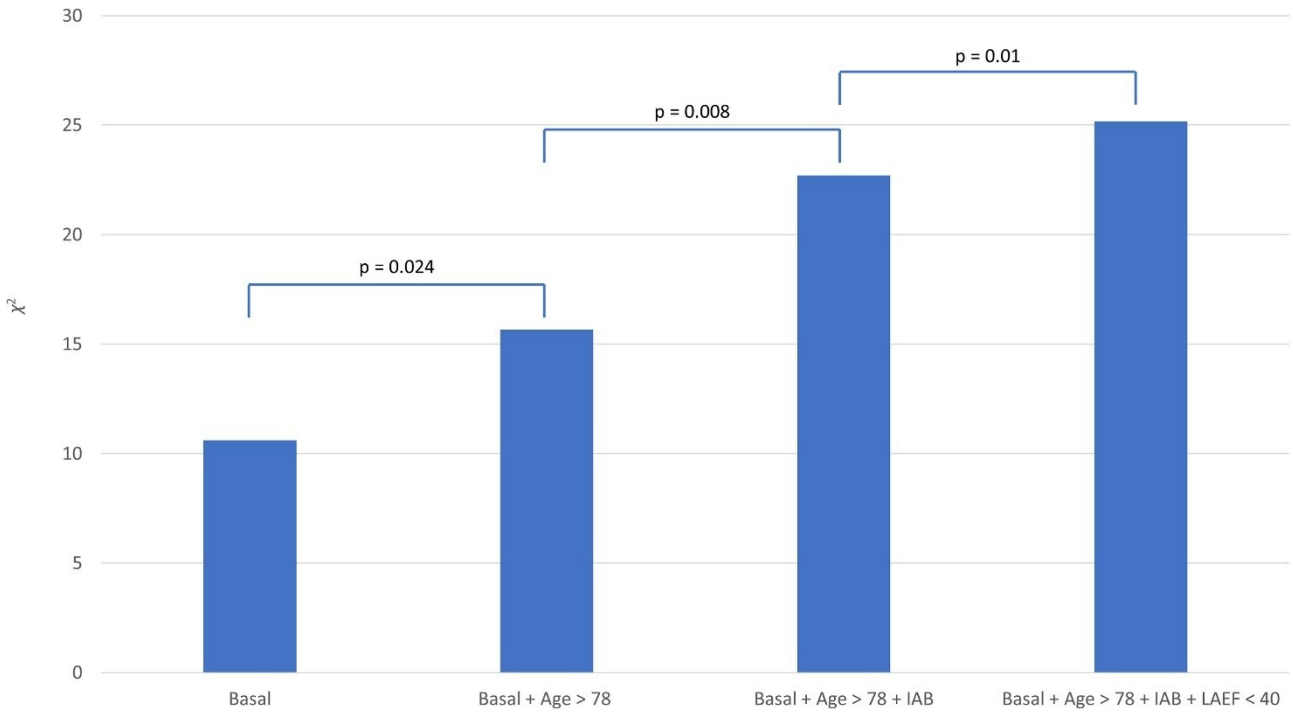

Figure 4. Incremental prognostic value of age >78 years, interatrial block (IAB) of any grade and left atrium ejection fraction (LAEF) <40%, when hierarchical added to a basal model.

6.4 Discussion

This study was designed to investigate the electrical and functional predictors of incident AF in patients with CA by electrocardiography and CMR imaging. The main findings were as follows. First, electrocardiographic IABs, either partial or advanced, are frequent in patients with CA, being detected in 29% and 7% of our cohort, respectively. Second, during a median 1.5-year follow-up, new-onset AF occurred in almost one-third of sinus rhythm patients with CA. Third, IABs and LAEF calculated by CMR emerged as independent predictors of incident AF. Fourth, in the individual CA patient, the combined presence of IAB (any type), age >78 years, and LAEF <40% led to the highest risk of incident AF.

AF is the most frequent arrhythmia in CA, with a prevalence ranging from 15% to 88% of patients and incidence up to 15% per year[6,15–17]. In our study, which included only sinus rhythm CA patients undergoing CMR, we observed an incidence of about 18% per year. This rate is in keeping with that of Sanchis and coworkers,16 who observed 36% new-onset AF during a 2-year follow-up (15% per year), but differs from that of Longhi and coworkers,6 who conversely reported 2.1% per year. The differences encountered may reasonably be due to different study sample size and CA subtype distribution, in particular a higher prevalence of wild-type ATTR in our cohort.

In patients with CA, AF is a significant contributor of heart failure symptoms and a well-established risk factor for stroke[6,18] and bradyarrhythmias worthy of pacemaker implantation[19]. Identifying prognostically relevant markers of AF is therefore crucial to allow early diagnosis and to prompt all strategies that in turn may prevent the risk for development of heart failure hospitalizations and thromboembolic events. Age, male sex, ATTR-CA, renal function, and atrial remodeling were previously demonstrated as significant predictors of AF in CA[6,7,17,20–22]. Our results are consistent with this, in particular with regard to age and ATTR subtype. The major novelty, however, is represented by the prognostic role of IABs and CMR LAEF as independent predictors of incident AF in CA. IABs are associated with AF and stroke in the general population[23] and have been associated with reduced left atrial function on echocardiography of patients with CA[24]. In our CA

cohort, partial IAB was detected in 29% of patients and advanced IAB in 7%, both more frequently in ATTR-CA than in AL-CA. From a pathogenetic point of view, tissue abnormalities involving the myocardium of the atria, such as fibrosis and amyloid deposition, may contribute to IAB and AF occurrence and perpetuation by altering the normal pattern of propagation and inducing discontinuous slow conduction, which plays a key role in the context of reentrant circuits[25–27]. Structural and functional changes in the left atrium are well-known risk factors for AF development in the general population[28]. In particular, elevated LAV and decreased left atrial reservoir and conduit functions measured with feature-tracking CMR have been associated with incident AF[29]. In patients with CA, impairment of left atrial contractile function evaluated with CMR imaging is common, is not influenced by CA cause, and is associated with poor outcome[30]. Our data seem concordant and confirm the prognostic role of left atrial dysfunction because of both atrial infiltration by amyloid fibrils and atrial volume and pressure overload due to restrictive hemodynamics, which could lead to atrial fibrosis, resulting in further atrial electrical heterogeneity favoring AF onset[27,31].

Finally, the presence of IAB together with old age and reduced LAEF was associated with the highest risk of incident AF in patients with CA, both AL and ATTR related. Therefore, our results strongly support the combined use of electrocardiography and CMR, not only to assess QRS voltages, amyloid burden, and disease severity but also to stratify the risk of patients for development of AF during follow-up. High-risk patients could undergo close and long-term monitoring with implantable devices or be encouraged to wear smart technologies for a systematic screening of AF[32] (**Graphical Abstract**).

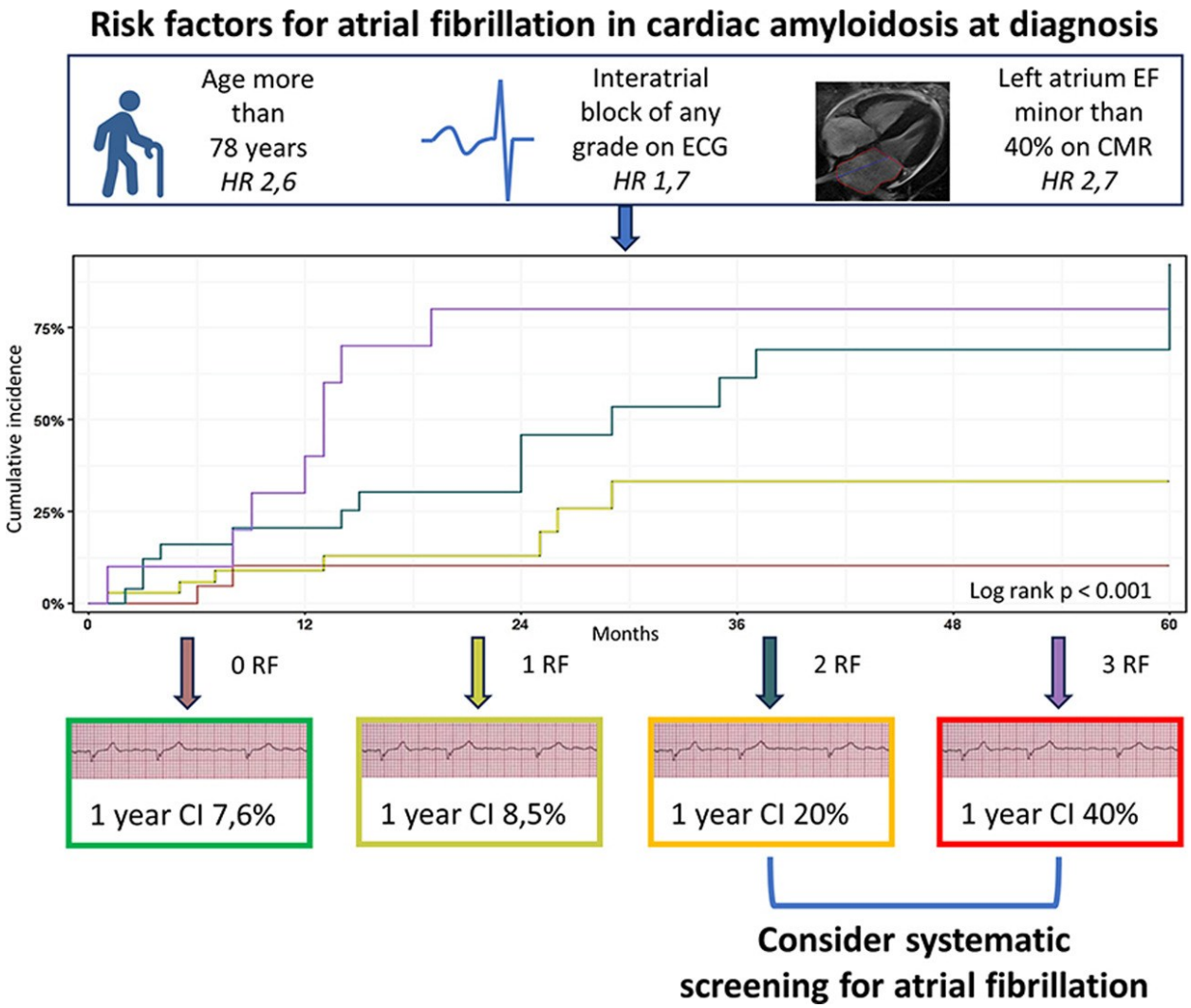

Graphical Abstract. Risk factors for atrial fibrillation onset in cardiac amyloidosis at diagnosis. Abbreviations: CI = cumulative incidence; CMR = cardiac magnetic resonance; ECG = electrocardiogram; EF = ejection fraction; HR = hazard ratio; RF = risk factor

Limitations

This study has some limitations. First, it is retrospective and multicentric, with a relatively small population that allows limited statistical power and does not allow a comprehensive, systematic analysis of factors associated with AF onset. Furthermore, an in-depth separate analysis of AL-CA and ATTR-CA subpopulations was not possible. Nevertheless, the strictness of the inclusion criteria is to be considered. CMR for diagnostic purposes is not mandatory in the diagnostic pathway, and the high prevalence of AF at diagnosis of patients significantly and inevitably restricted the recruitable population. Second, despite the availability of data about disease-modifying therapy, the exiguous number of patients treated does not allow assessment of a possible impact on the risk of

arrhythmia onset. Third, as mentioned, the unavailability of continuous rhythm monitoring devices limited our sensitivity to detect subclinical and asymptomatic AF events. However, therapeutic management of infrequent and short AF episodes in the general population is still a debated topic in the literature[33,34]. Fourth, although data regarding cardiac troponin levels have been collected, significant heterogeneity between centers emerged, caused by poor standardization and high variability in assays (regular sensitivity or high sensitivity) and troponin type (T or I) use over time, so these data were omitted from the analysis. Consequently, we could not apply the Mayo Clinic staging system to better characterize the disease severity of patients with AL-CA.

6.5 Conclusions

In patients with AL-CA and ATTR-CA, IABs are common and together with advanced age and reduced LAEF on CMR are independent predictors of incident AF. Patients with these features might benefit from closer AF screening strategies during follow-up.

6.6 References

1 Fontana M, Ćorović A, Scully P, et al. Myocardial Amyloidosis: The Exemplar Interstitial Disease. JACC Cardiovasc Imaging. 2019;12(11Pt2):2345-2356.

2 Martini N, Sinigiani G, De Michieli L, et al. Electrocardiographic features and rhythm disorders in cardiac amyloidosis. Trends Cardiovasc Med. 2023Feb 24:S1050-1738(23)00024-5.

3 Thakkar S, Patel HP, Chowdhury M, et al. Impact of Arrhythmias on Hospitalizations in Patients With Cardiac Amyloidosis. Am J Cardiol. 2021 Mar 15;143:125-130.

4 Martinez-Naharro A, Gonzalez-Lopez E, Corovic A, et al. High Prevalence of Intracardiac Thrombi in Cardiac Amyloidosis. J Am Coll Cardiol. 2019Apr 9;73(13):1733-1734.

5 Garcia-Pavia P, Rapezzi C, Adler Y, et al. Diagnosis and treatment of cardiac amyloidosis: a position statement of the ESC Working Group on Myocardial and Pericardial Diseases. Eur Heart J. 2021Apr21;42(16):1554-1568.

6 Longhi S, Quarta CC, Milandri A, et al. Atrial fibrillation in amyloidotic cardiomyopathy: prevalence, incidence, risk factors and prognostic role. Amyloid. 2015;22(3):147-55.

7 Donnellan E, Wazni OM, Hanna M, et al. Atrial Fibrillation in Transthyretin Cardiac Amyloidosis: Predictors, Prevalence, and Efficacy of Rhythm Control Strategies. JACC Clin Electrophysiol. 2020Sep;6(9):1118-1127.

8 Bayés de Luna A, Platonov P, Cosio FG, et al. Interatrial blocks. A separate entity from left atrial enlargement: a consensus report. J Electrocardiol. 2012Sep;45(5):445-51.
9 Baranchuk A, Villuendas R, Bayes-Genis A, et al. Advanced interatrial block: a well-defined electrocardiographic pattern with clinical arrhythmological implications. Europace. 2013Dec;15(12):1822.
10 Cipriani A, De Michieli L, Porcari A, et al. Low QRS Voltages in Cardiac Amyloidosis: Clinical Correlates and Prognostic Value. JACC CardioOncol. 2022Sep7;4(4):458-470.
11 Petersen SE, Khanji MY, Plein S, et al. European Association of Cardiovascular Imaging expert consensus paper: a comprehensive review of cardiovascular magnetic resonance normal values of cardiac chamber size and aortic root in adults and recommendations for grading severity. Eur Heart J Cardiovasc Imaging. 2019Dec1;20(12):1321-1331.
12 Kanagala P, Arnold JR, Cheng ASH, et al. Left atrial ejection fraction and outcomes in heart failure with preserved ejection fraction. Int J Cardiovasc Imaging. 2020Jan;36(1):101-110.
13 Fontana M, Pica S, Reant P, et al. Prognostic Value of Late Gadolinium Enhancement Cardiovascular Magnetic Resonance in Cardiac Amyloidosis. Circulation. 2015Oct 20;132(16):1570-9.
14 Hindricks G, Potpara T, Dagres N, et al. 2020 ESC Guidelines for the diagnosis and management of atrial fibrillation developed in collaboration with the European Association for Cardio-Thoracic Surgery (EACTS): The Task Force for the diagnosis and management of atrial fibrillation of the European Society of Cardiology (ESC) Developed with the special contribution of the European Heart Rhythm Association (EHRA) of the ESC. Eur Heart J. 2021Feb1;42(5):373-498.
15 Bukhari S, Khan SZ, Bashir Z. Atrial Fibrillation, Thromboembolic Risk, and Anticoagulation in Cardiac Amyloidosis: A Review. J Card Fail. 2023Jan;29(1):76-86.
16 Sanchis K, Cariou E, Colombat M, et al. Atrial fibrillation and subtype of atrial fibrillation in cardiac amyloidosis: clinical and echocardiographic features, impact on mortality. Amyloid. 2019Sep;26(3):128-138.
17 Mints YY, Doros G, Berk JL, et al. Features of atrial fibrillation in wild-type transthyretin cardiac amyloidosis: a systematic review and clinical experience. ESC Heart Fail. 2018Oct;5(5):772-779.
18 Bukhari S, Barakat AF, Eisele YS, et al. Prevalence of Atrial Fibrillation and Thromboembolic Risk in Wild-Type Transthyretin Amyloid Cardiomyopathy. Circulation. 2021Mar30;143(13):1335-1337.

19 Porcari A, Rossi M, Cappelli F, et al. Incidence and risk factors for pacemaker implantation in light-chain and transthyretin cardiac amyloidosis. Eur J Heart Fail. 2022Jul;24(7):1227-1236.
20 Gramley F, Lorenzen J, Knackstedt C, et al. Age-related atrial fibrosis. Age (Dordr). 2009Mar;31(1):27-38.
21 Henein MY, Suhr OB, Arvidsson S, et al. Reduced left atrial myocardial deformation irrespective of cavity size: a potential cause for atrial arrhythmia in hereditary transthyretin amyloidosis. Amyloid. 2018Mar;25(1):46-53.
22 Choi YJ, Kim D, Rhee TM, et al. Left atrial reservoir strain as a novel predictor of new-onset atrial fibrillation in light-chain-type cardiac amyloidosis. Eur Heart J Cardiovasc Imaging. 2023May31;24(6):751-758.
23 Tse G, Wong CW, Gong M, et al. Predictive value of inter-atrial block for new onset or recurrent atrial fibrillation: A systematic review and meta-analysis. Int J Cardiol. 2018;250:152-156.
24 Lindow T, Lindqvist P. The Prevalence of Advanced Interatrial Block and Its Relationship to Left Atrial Function in Patients with Transthyretin Cardiac Amyloidosis. J Clin Med. 2021Jun23;10(13):2764.
25 Kottkamp H. Human atrial fibrillation substrate: towards a specific fibrotic atrial cardiomyopathy. Eur Heart J. 2013Sep;34(35):2731-8.
26 Cheniti G, Vlachos K, Pambrun T, et al. Atrial Fibrillation Mechanisms and Implications for Catheter Ablation. Front Physiol. 2018 Oct17;9:1458.
27 Miragoli, M. · Glukhov, A.V. Atrial fibrillation and fibrosis: beyond the cardiomyocyte centric view. Biomed Res Int. 2015; 2015, 798768
28 Hoit BD. Left atrial size and function: role in prognosis. J Am Coll Cardiol. 2014 Feb18;63(6):493-505.
29 Habibi M, Samiei S, Ambale Venkatesh B, et al. Cardiac Magnetic Resonance-Measured Left Atrial Volume and Function and Incident Atrial Fibrillation: Results From MESA (MultiEthnic Study of Atherosclerosis). Circ Cardiovasc Imaging. 2016;9(8):10.1161/CIRCIMAGING.115.004299e004299.
30 Aquaro GD, Morini S, Grigoratos C, at al. Electromechanical dissociation of left atrium in patients with Cardiac Amyloidosis by Magnetic Resonance: Prognostic and clinical correlates. Int J Cardiol Heart Vasc. 2020Sep14;31:100633.
31 Xintarakou A, Tzeis S, Psarras S, et al. Atrial fibrosis as a dominant factor for the development of atrial fibrillation: facts and gaps. Europace. 2020Mar1;22(3):342-351.

32 Svennberg E, Tjong F, Goette A, et al. How to use digital devices to detect and manage arrhythmias: an EHRA practical guide. Europace. 2022Jul15;24(6):979-1005.
33 Svendsen JH, Diederichsen SZ, Højberg S, et al. Implantable loop recorder detection of atrial fibrillation to prevent stroke (The LOOP Study): a randomised controlled trial. Lancet. 2021Oct23;398(10310):1507-1516.
34 Kirchhof P, Toennis T, Goette A, et al. Anticoagulation with Edoxaban in Patients with Atrial High-Rate Episodes. N Engl J Med. 2023Sep28;389(13):1167-1179

Chapter 7. Right ventricular to pulmonary artery uncoupling is an early predictor of poor outcome in wild-type transthyretin amyloid cardiomyopathy

This chapter is based on the manuscript: *Sinigiani G, De Michieli L, d'Addazio M, Portalone L, De Gaspari M, Lupi A, Zorzi A, Tona F, Basso C, Perazzolo Marra M, Iliceto S, Corrado D, Nistri S, Mele D, Cipriani A. Right ventricular to pulmonary artery uncoupling is an early predictor of poor outcome in wild-type transthyretin amyloid cardiomyopathy. Int J Cardiovasc Imaging. 2025;41(6):1119-1130.*

7.1 Introduction

Wild-type transthyretin amyloid cardiomyopathy (wtATTR-CM) is a sporadic non-inherited cardiac disease characterized by the deposition of misfolded transthyretin in the heart, causing a progressive disruption of cardiac structure and function[1,2,3]. This condition is typically characterized by increased left ventricular (LV) wall thickness and stiffness, predisposing to impaired diastolic function and heart failure with preserved ejection fraction (HFpEF)[2]. A significant epidemiological increase of this condition has been observed in recent times, due to the adoption of non-invasive diagnostic algorithms[4], and patients are currently more frequently early diagnosed, showing no or mild symptoms, lower disease stage, and more favourable structural abnormalities at diagnosis[5]. At the same time, novel disease-modifying agents have been identified to stop or delay the progression of wtATTR-CM[6], so that there is an urgent clinical need to identify early predictors of poor outcome that could prompt the initiation of ATTR-targeted therapy, also in asymptomatic or early stages patients.

The right ventricle (RV) to pulmonary artery (PA) coupling is defined as the ratio of RV function to pulmonary vascular afterload and is traditionally assessed by means of echocardiography using the ratio between tricuspid annular plane systolic excursion (TAPSE) and systolic pulmonary artery pressure (sPAP)[7,8,9]. Recently, other ratios using RV strain function indexes have been proposed and validated[10,11,12,13]. The RV-PA uncoupling has emerged as a strong prognostic factor in patients with HF[14,15,16,17,18,19,20] and also in historical mixed cohorts of light-chain and ATTR cardiomyopathy patients[7,8]. However, little evidence is available about its pathophysiological and

clinical meaning in wtATTR – CM only, particularly in contemporary cohorts, including early diagnosed and less sick patients[5].

7.2 Methods

Study design and study population

The Cardiac Amyloidosis Outpatient Clinic of University Hospital of Padua (Italy) is a tertiary centre for evaluation of all patients with established or suspected amyloid cardiomyopathy. At the time of the first visit, all patients undergo a routine clinical evaluation, including family and personal history, physical examination, biomarkers analysis, resting 12-lead ECG, and 2-dimensional transthoracic echocardiography. This is a single-centre observational longitudinal study, enrolling a consecutive series of patients with a definitive diagnosis of wtATTR-CM, established according to the Gillmore algorithm[4], between January 2018 and January 2023. All first echocardiographic exams of these patients performed in our Institution were retrieved and re-analysed focusing on RV-PA uncoupling assessment. Exclusion criteria were inadequate image quality for strain analysis (frame rate < 50 frames per seconds or inability to accurately visualize the RV from base to apex or to perform adequate speckle - tracking analysis on any RV segments), insufficient data for a reliable assessment of systolic pulmonary artery pressure, and history of severe chronic obstructive pulmonary disease, severe obstructive sleep apnoea syndrome or pulmonary embolism. All patients underwent genetic testing, and those diagnosed with hereditary ATTR-CM were not included in this study, due to the low prevalence in our region[21], the highly variable phenotypes[22] and the different clinical and echocardiographic features compared with wtATTR-CM[23]. Patients were systematically followed up from the date of our first cardiologic evaluation (baseline), to avoid any time referral bias. The clinical data recorded within ± 1 months from the baseline included all the following: (I) medical history and physical examination, (II) ECG and (III) laboratory exams. The local regional Institutional Review Board approved the study, and the investigators obtained local institutional review board approvals for the retrospective collection

of anonymous data. The study was conducted according to the Declaration of Helsinki, and informed consent was obtained according to the local review board policies.

Clinical History, electrocardiography and biomarkers

Careful clinical history, ongoing medical therapy, and data regarding New York Heart Association (NYHA) class and National Amyloidosis Centre (NAC) stage[24] at baseline, including NAC Ia stage[25], were collected. Tafamidis in Italy was approved in October 2021, and the Italian Medicines Agency authorized its reimbursement exclusively in patients with ATTRwt-CM and NYHA class I or II[26]. Disease modifying therapy at baseline or during the follow up was noted. Further details are provided in Supplemental Materials.

Echocardiography

Echocardiographic images were acquired using a Vivid 9 ultrasound system (General Electric Medical System, Milwaukee, USA), and analysis was independently carried out in post – processing by a trained cardiologist blinded to patients' history using the EchoPAC software v.204 (General Electric Medical System, Milwaukee, USA). American Society of Echocardiography and the European Association of Cardiovascular Imaging recommendations[27,28] were careful followed. TAPSE was measured using M-mode echocardiography at tricuspid annulus level. Longitudinal strain (LS) was quantified using a region of interest including both right ventricle free wall (RVFW), with adequate width to cover its thickness, and interventricular septum (IVS). RVFW longitudinal strain (RVFWLS) was measured as the average of the strain values of the three segments of the RVFW; RV four-chamber LS (RV4CLS) was measured as the average of the strain values of the six segments of the RVFW and IVS[29]. Right atrium longitudinal strain (RALS) was calculated as established in literature[28], limited to reservoir phase due to high prevalence of atrial fibrillation in our cohort. Systolic pulmonary artery pressure (sPAP) was calculated using the formula: 4*(peak velocity of TR)2 + estimated right atrial pressure. The latter was derived on the inferior vena cava diameter and collapsibility[30]. RV-PA uncoupling parameters (i.e.,

RVFWLS/sPAP and RV4CLS/sPAP) were positivized for easier comprehension. Further details are provided in Supplemental Materials.

Outcomes and statistical analysis

Continuous baseline characteristics were expressed as median with 25th and 75th percentiles [Q1 – Q3] and were compared using the Mann – Whitney test. Categorical variables were expressed as absolute numbers and percentages and were compared using the chi-square ($\chi 2$) test. The primary endpoint was the composite of all-cause death and HF hospitalisation. The latter was defined as an admission to hospital for HF symptoms and need for intravenous diuretic therapy. Survival analysis was performed with a Cox proportional hazards regression, with univariable and multivariable models. The number of variables entered into the multivariable model was limited according to the number of events, based on the principle of not having more than one variable every 10 events. Thus, multiple models were built to test the predictive value of RV systolic function parameters and RV-PA uncoupling values, adjusting for covariates that were both statistically significant at univariate analysis ($p<0.05$) and selected on the basis of their clinical relevance coupled with absence of collinearity. Candidate predictors included HF presentation, defined as HF hospitalization requiring intravenous diuretic therapy before the diagnosis, N-terminal pro-brain natriuretic peptide (NT-proBNP) and furosemide intake >50 mg[24,31,32]. To correctly assess the impact of disease modifying therapy, a dedicated time – dependent Cox's regression analysis was carried out. Overfitting was eventually tested with a 10-fold cross validation of each model, by comparison of original and cross-validated C-index with a threshold in difference of 0.5. For independent predictors, median values were used to draw the primary endpoint cumulative incidence curves using the Kaplan Meier method and the log-rank test. For estimating the incremental prognostic value of the RV-PA uncoupling indexes over the uncoupled RV systolic function parameters, the time-dependent areas under the curve (AUC) of the corresponding ROCs of each were evaluated and compared as previously defined[33]. All tests were 2-tailed, and a $p<0.05$

was considered statistically significant. Statistical analyses were conducted using the SPSS software version 26.0 statistical package and the RStudio software version 4.3.1.

7.3 Results

Study population

Among 202 patients diagnosed with cardiac amyloidosis between January 2018 and January 2023, 135 (68%) had a diagnosis of wtATTR-CM. After exclusion of those patients with inadequate image quality (n=35), 100 (74%) constituted the study population. Baseline characteristics are shown in **Table 1**. Most patients were male (n=91, 91%) with a median age of 81 (75 – 85) years, a NYHA class I or II (n=82, 82%) and a NAC stage I or II (n=85, 85%). The majority was treated with disease modifying therapy (n=53, 53%), with a median time from diagnosis of 3 (1 – 8) months, and a median follow up in therapy of 15 (10 – 18) months. Considering echocardiogram data, median values of E/A and E/e' ratios were 2.1 (1.1 to 2.7) and 16.1 (13.4 – 19.4). Median values of RVFWLS and RV4CLS were -16.5% and -12.1%. On segmental analysis of the RVFW, LS were -14% (-19 to -10), -18% (-25 to -11) and -16% (-23 to -12) for basal, mid, and apical segments, respectively (**Figure 1, panel A**). Regarding RV-PA coupling non-invasive parameters, median values of TAPSE/sPAP, RVFWLS/sPAP and RV4CLS/sPAP were 0.45 mm/mmHg, 0.46 %/mmHg and 0.33 %/mmHg, respectively. Intra- and inter-readers intraclass correlation coefficients (ICC) are provided in Supplemental Table 2. A moderate correlation (Spearman's R -0.37, -0.36 and -0.37) was found between E/e' ratio and TAPSE/sPAP, RVFWLS/sPAP and RV4CLS/sPAP, respectively.

Primary endpoint and follow-up

During a median follow-up time of 16 months (Q1-Q3: 12–24), the primary endpoint occurred in 37 (37%) patients. All-cause death and heart failure hospitalization occurred in 22 (22%) and 25 (25%) patients, respectively. Compared with those without, patients with primary endpoint had a significantly higher prevalence of HF presentation (69% vs 44%, p = 0.020), and were more frequently treated with furosemide (84% vs 60%, p = 0.015) at higher dose (50 mg vs 25 mg, p =

0.006), and less frequently with disease modifying therapy drugs (32% vs 65%, p = 0.002) (Table 1). Considering laboratory test, patients with primary endpoint had higher high sensitivity troponin I value (92 vs 60 ng/L, p = 0.020), but no significantly differences emerged for N terminal pro-brain natriuretic peptide (NT-proBNP) (1921 vs 1610 ng/L, p = 0.1) or estimated glomerular filtration rate (eGFR) (57 vs 62 ml/min/m2, p = 0.3). On echocardiography, they had more frequently a LV restrictive filling pattern (41% vs 21%, p = 0.032), with higher E/A ratio (2.6 vs 1.5, p = 0.028) and left atrium volume indexed (59.4 ml/m2 vs 49.7 ml/m2, p = 0.031). No significant differences among groups emerged in LV ejection fraction (51% vs 53%, p = 0.4) or LV global longitudinal strain (-11% vs -11%, p = 0.6). Compared with those without, patients with primary endpoint had significantly lower RALS (10.0% vs 15.1%, p = 0.034), significantly higher RV end-diastolic indexed area and sPAP (12.4 cm2/m2 vs 11.4 cm2/m2, p = 0.008 and 39 mmHg vs 30 mmHg, p = 0.003) and more impaired RV systolic function, either evaluated with TAPSE (15.1 mm vs 17.1 mm, p = 0.038) or RVFWLS (-15.0% vs -17.9%, p = 0.043). RV-PA uncoupling parameters such as TAPSE/sPAP, RVFWLS/sPAP and RV4CLS/sPAP were significantly lower in patients with primary endpoint, compared with those without (0.38 vs 0.50 mm/mmHg, p = 0.001; 0.39 vs 0.49 %/mmHg, p = 0.001; 0.28 vs 0.39 %/mmHg, p = 0.006).

When considering only NAC Ia patients (n=18), primary endpoint occurred in 6 patients (33%) (**Table 2**). RV-PA uncoupling parameters such TAPSE/sPAP, RVFWLS/sPAP and RV4CLS/sPAP were significantly lower in patients with primary endpoint, compared with those without (0.41 vs 0.78 mm/mmHg, p = 0.013; 0.47 vs 0.79 -%/mmHg, p = 0.042; 0.32 vs 0.61 -%/mmHg, p = 0.041, respectively).

Prognostic value of RV-PA uncoupling

Univariable analyses and all derived multivariable models are presented in **Table 2** and **Table 3**. RV-PA uncoupling emerged as independent predictor of composite endpoint, evaluated with TAPSE/sPAP (HR 0.04, 95% CI 0.01–0.24, p < 0.001), RVFWLS/sPAP (HR 0.07, 95% CI 0.01–0.41, p = 0.003) or RV4CLS/sPAP (HR 0.06, 95% CI 0.01–0.53, p = 0.011) ratios, and were

confirmed after proportional hazards assumption analysis. Using median values for discriminating the composite endpoint (**Figure 2**), 12-months cumulative incidence was significantly higher in patients with TAPSE/sPAP ≤ 0.45 mm/mmHg (24% vs 16%, log–rank p 0.018), RVFWLS/sPAP ≤ 0.46 %/mmHg (29% vs 12%, log-rank p = 0.003) or RV4CLS/sPAP ≤ 0.33 %/mmHg (27% vs 14%, log-rank p = 0.018), respectively. To further investigate and compare the predictive value of RV-PA uncoupling data with RV function parameters alone, a time-dependent ROC curve analysis was performed. At 36 months, time dependent AUC for TAPSE, RVFWLS and RV4CLS were 0.65, 0.64 and 0.66, respectively. On the other hand, time dependent AUC for RVFWLS/sPAP, RV4CLS/sPAP, TAPSE/sPAP were 0.76, 0.77 and 0.79, respectively, without significantly differences between them (all p values >0.05, Figure 3). Nevertheless, these values were significantly higher than that of RV function parameters considered alone, resulting in a further incremental prognostic accuracy for the composite endpoint (all adjusted p values <0.05). The same held true when compared with diastolic function parameters and daily high furosemide doses.

7.4 Discussion

This study was designed to investigate the prognostic value of RV-PA uncoupling in a modern cohort of patients with wtATTR-CM. The main results were the following: i) RV-PA uncoupling, evaluated with either RVFWLS/sPAP, RV4CLS/sPAP, or TAPSE/sPAP, was independently associated with the risk of the composite outcome of all-cause death or HF hospitalisation in patients with wtATTR-CM; ii) in the earliest stage of disease, RV-PA uncoupling remained associated with poor outcome; iii) RV-PA uncoupling indexes, such as RVFWLS/sPAP, RV4CLS/sPAP, or TAPSE/sPAP, showed incremental value in outcome prediction over TAPSE, RV4CLS, RVFWLS and sPAP, considered as separate parameters.

The recent development of non-invasive algorithms for the diagnosis of ATTR-CM, together with the rapidly evolving therapeutic landscape, has transformed wtATTR-CM from a rare and untreatable condition to a more prevalent disease, now diagnosed at earlier and milder stages. As was observed in the ATTRibute-CM[34] and HELIOS-B trial[35], patients are now less likely to have

cardiovascular events than in the ATTR-ACT trial era[36], so that it is of great importance to identify early predictors of outcome in modern cohorts of wtATTR-CM patients, that can help risk stratify them and guide the prompt initiation of disease-modifying therapy.

The use of non–invasive surrogates of RV-PA uncoupling for prognosis prediction is not novel in the literature. Guazzi et al. investigated the independent prognostic significance of TAPSE/sPAP in 387 patients with different HFpEF aetiologies and found that TAPSE/sPAP <0.35 mm/mmHg was independently associated with the risk of combined endpoint of HF hospitalisation or all-cause death[37]. Same results were demonstrated in our cohort, although with a higher TAPSE/sPAP cut-off value (0.45 mm/mmHg). Discrepancy could be due to lower sPAP data in our population, far less characterized by patients with chronic pulmonary diseases.

RV-PA uncoupling can be assessed also by means of RV strain function indexes, such as RVFWLS and RV4CLS[10,11,12,13], which are as known less angle- and volume dependent than TAPSE, and have a higher sensitivity for detecting subclinical RV systolic dysfunction. Bosch et al. investigated the contribution of RV dysfunction in 219 patients with HFpEF and found that RVFWLS/sPAP was independently associated with the risk of composite endpoint of all-cause mortality and HF hospitalisation[15]. This was confirmed by our study results, although with some difference in RVFWLS/sPAP cut-off value (lower in our cohort), possibly due to different pathophysiology of RV dysfunction in ATTR-CM compared to other HFpEF aetiologies. Indeed, other than pulmonary hypertension secondary to LV disease, in ATTR-CM there might be a direct contribution in RV systolic impairment also caused by myocardial amyloid deposition[38]. This pathophysiological mechanism is also suggested by the only moderate correlation between diastolic function and RV-PA parameters in our cohort.

The prognostic role of RV-PA uncoupling has been recently studied in patients with CA. In a mixed AL-CA and ATTR-CM cohort, Tomasoni et al. showed that the TAPSE/PASP ratio (median value 0.45 mm/mmHg) is a strong and independent predictor of all-cause death or HF hospitalisation, providing incremental risk prediction beyond TAPSE or sPAP considered alone[7]. A subsequent

study confirmed these findings, although in a smaller mixed AL-CA and ATTR-CM cohort[8]. Our study results refined and expanded the prognostic role of RV-PA uncoupling in a modern cohort of ATTR-CM. To the best of our knowledge, this is the first study to focus on wtATTR-CM only and to apply and investigate multiple indexes of RV-PA uncoupling in this setting. Compared with the above-mentioned studies[7,8], our wtATTR-CM patients were mostly characterised by earlier and milder disease stages (85% in NAC stage < 2, 18% in NAC stage Ia and 82% in NYHA class < II). Nonetheless, RV-PA uncoupling, either using M-mode or strain-based RV systolic function parameters, remained an independent predictor of poor outcome, thus suggesting that the maladaptation of RV-PA afterload could be a relatively early phaenomenon in the natural history of ATTR-CM, possibly driven by initial amyloid deposition in the basal segments of RV[39,40]. The early and major involvement of basal regions of RV could also explain the non-incremental prognostic accuracy for poor prognosis of speckle-tracking based uncoupling indexes compared to M-mode one (**Figure 1, panel B**). The different regional amyloid deposition in RV could also account for the overall reduced RALS in our cohort.

According to our study results, the evaluation of RV-PA uncoupling may aid in individual risk assessment and treatment selection. The higher risk of HF hospitalisation and mortality in asymptomatic, early stage (NAC Ia) patients with RV-PA uncoupling signs would support the need of immediate and more aggressive therapy, including not only disease-modifying, but also conventional HF drugs. Since wtATTR-CM mostly affects the older population[5] and encompasses a wide spectrum of disease severity, a more comprehensive staging system beyond NYHA class and classical biomarkers is needed to improve prognostic precision and optimize treatment strategies for individual patients.

Limitations

This study has some limitations. First, the design is observational and single-centre, with a relatively small sample size (albeit in line with previous studies on the same topic[41,42,43,44]), that may limit statistical power and generalizability of the findings. Nevertheless, methodological approach

and data analysis depth are to be considered, together with the peculiar characteristics of our cohort, including mostly early diagnosed and less sick wtATTR-CM patients, thus reflecting more faithfully the current real – world population of patients[5]. Second, despite the availability of data about disease-modifying therapy, the evaluation of its efficacy could be affected by the small sample size and different timing of prescription between patients during follow up. Nevertheless, the most appropriate data analysis was employed, and the emerged early prognostic value of the RV-PA uncoupling assessment could highlight the necessity of further studies specifically addressing this important topic.

7.5 Conclusions

In a modern cohort of patients with wtATTR-CM, RV-PA uncoupling emerged as an early and strong predictor of outcome, being independently associated with the risk of HF hospitalisation or all – cause death. No differences in risk prediction were observed among M-mode and strain-based RV function parameters. The evaluation of RV-PA uncoupling should be considered in the clinical practice for risk stratification and prognosis assessment of patients with wtATTR-CM, with potential implications treatment strategies definition.

7.6 References

1. Wechalekar AD, Gillmore JD, Hawkins PN. Systemic amyloidosis. Lancet. 2016;387:2641-2654.
2. Fontana M, Ćorović A, Scully P, et al. Myocardial Amyloidosis: The Exemplar Interstitial Disease. JACC Cardiovasc Imaging. 2019;12:2345-2356.
3. Quarta CC, Kruger JL, Falk RH. Cardiac amyloidosis. Circulation. 2012;126:e178-82.
4. Gillmore JD, Maurer MS, Falk RH, et al. Nonbiopsy Diagnosis of Cardiac Transthyretin Amyloidosis. Circulation. 2016;133:2404-12.
5. Ioannou A, Patel RK, Razvi Y, et al. Impact of Earlier Diagnosis in Cardiac ATTR Amyloidosis Over the Course of 20 Years. Circulation. 2022;146:1657-1670.
6. Aimo A, Castiglione V, Rapezzi C, et al. RNA-targeting and gene editing therapies for transthyretin amyloidosis. Nat Rev Cardiol. 2022;19:655-667.
7. Tomasoni D, Adamo M, Porcari A, et al. Right ventricular to pulmonary artery coupling and outcome in patients with cardiac amyloidosis. Eur Heart J Cardiovasc Imaging. 2023;24:1405-1414.

8. Palmiero G, Monda E, Verrillo F, et al. Prevalence and clinical significance of right ventricular pulmonary arterial uncoupling in cardiac amyloidosis. Int J Cardiol. 2023;388:131147.
9. Pestelli G, Fiorencis A, Trevisan F, et al. New measures of right ventricle-pulmonary artery coupling in heart failure: An all-cause mortality echocardiographic study. Int J Cardiol. 2021;329:234-241.
10. Richter MJ, Rako ZA, Tello K. Ratio between right ventricular strain and systolic pulmonary artery pressure as a surrogate for right ventricular to pulmonary arterial coupling: validation against the gold standard. Eur Heart J Cardiovasc Imaging. 2023;24:e50-e52.
11. Brener MI, Grayburn P, Lindenfeld J, et al. Right Ventricular-Pulmonary Arterial Coupling in Patients With HF Secondary MR: Analysis From the COAPT Trial. JACC Cardiovasc Interv. 2021;14:2231-2242.
12. Iacoviello M, Monitillo F, Citarelli G, et al. Right ventriculo-arterial coupling assessed by two-dimensional strain: A new parameter of right ventricular function independently associated with prognosis in chronic heart failure patients. Int J Cardiol. 2017;241:318-321.
13. Ünlü S, Bézy S, Cvijic M, et al. Right ventricular strain related to pulmonary artery pressure predicts clinical outcome in patients with pulmonary arterial hypertension. Eur Heart J Cardiovasc Imaging. 2023;24:635-642.
14. Guazzi M, Bandera F, Pelissero G, et al. Tricuspid annular plane systolic excursion and pulmonary arterial systolic pressure relationship in heart failure: an index of right ventricular contractile function and prognosis. Am J Physiol Heart Circ Physiol. 2013;305:H1373-81.
15. Bosch L, Lam CSP, Gong L, et al. Right ventricular dysfunction in left-sided heart failure with preserved versus reduced ejection fraction. Eur J Heart Fail. 2017;19:1664-1671.
16. Lyhne MD, Kabrhel C, Giordano N, et al. The echocardiographic ratio tricuspid annular plane systolic excursion/pulmonary arterial systolic pressure predicts short-term adverse outcomes in acute pulmonary embolism. Eur Heart J Cardiovasc Imaging. 2021;22:285-294.
17. Trousselle L, Eggenspieler F, Huttin O, Pace N, Nazeyrollas P, Faroux L, et al. Echocardiographic assessment of right ventricular function and right ventriculoarterial coupling in tricuspid regurgitation. Int J Cardiovasc Imaging. 2024;40(11):2247-2259.
18. Roccabruna A, Fortuni F, Comuzzi A, Armani I, Bolzan B, Franchi E, et al. Right ventricular-pulmonary artery coupling in patients undergoing cardiac resynchronization therapy. Int J Cardiovasc Imaging. 2024;40(11):2325-2334.
19. Mendes LF, Brandão M, Diaz SO, Almeida MC, Barros AS, Saraiva F, et al. Impact of right ventricle-pulmonary artery coupling in patients undergoing transcatheter aortic valve implantation. Int J Cardiovasc Imaging. 2024;40(8):1745-1753.

20. Lillo R, Graziani F, Ingrasciotta G, Przbybylek B, Iannaccone G, Locorotondo G, et al. Right ventricle systolic function and right ventricle-pulmonary artery coupling in patients with severe aortic stenosis and the early impact of TAVI. Int J Cardiovasc Imaging. 2022;38(8):1761-1770.
21. Russo M, Obici L, Bartolomei I, et al. ATTRv amyloidosis Italian Registry: clinical and epidemiological data. Amyloid. 2020;27:259-265.
22. Rapezzi C, Quarta CC, Obici L, et al. Disease profile and differential diagnosis of hereditary transthyretin-related amyloidosis with exclusively cardiac phenotype: an Italian perspective. Eur Heart J. 2013;34:520-8.
23. Quarta CC, Solomon SD, Uraizee I, et al. Left ventricular structure and function in transthyretin-related versus light-chain cardiac amyloidosis. Circulation. 2014;129:1840-9.
24. Gillmore JD, Damy T, Fontana M, et al. A new staging system for cardiac transthyretin amyloidosis. Eur Heart J. 2018;39:2799-2806.
25. Law S, Bezard M, Petrie A, et al. Characteristics and natural history of early-stage cardiac transthyretin amyloidosis. Eur Heart J. 2022;43:2622-2632.
26. Italian Agency of Pharmacy determina n. 15, published in G.U. 250/2021.
27. Lang RM, Badano LP, Mor-Avi V, et al. Recommendations for cardiac chamber quantification by echocardiography in adults: an update from the American Society of Echocardiography and the European Association of Cardiovascular Imaging. J Am Soc Echocardiogr. 2015;28:1-39.e14.
28. Badano LP, Kolias TJ, Muraru D, et al. Standardization of left atrial, right ventricular, and right atrial deformation imaging using two-dimensional speckle tracking echocardiography: a consensus document of the EACVI/ASE/Industry Task Force to standardize deformation imaging. Eur Heart J Cardiovasc Imaging. 2018;19:591-600.
29. Badano LP, Muraru D, Parati G, et al. How to do right ventricular strain. Eur Heart J Cardiovasc Imaging. 2020;21:825-827.
30. Rudski LG, Lai WW, Afilalo J, et al. Guidelines for the echocardiographic assessment of the right heart in adults: a report from the American Society of Echocardiography endorsed by the European Association of Echocardiography, a registered branch of the European Society of Cardiology, and the Canadian Society of Echocardiography. J Am Soc Echocardiogr. 2010;23:685-713.
31. Cheng RK, Levy WC, Vasbinder A, et al. Diuretic Dose and NYHA Functional Class Are Independent Predictors of Mortality in Patients With Transthyretin Cardiac Amyloidosis. JACC CardioOncol. 2020;2:414-424.

32. Tini G, Milani P, Zampieri M, et al. Diagnostic pathways to wild-type transthyretin amyloid cardiomyopathy: a multicentre network study. Eur J Heart Fail. 2023;25:845-853.
33. Blanche P, Dartigues JF, Jacqmin-Gadda H. Estimating and comparing time-dependent areas under receiver operating characteristic curves for censored event times with competing risks. Stat Med. 2013;32:5381-97.
34. Gillmore JD, Judge DP, Cappelli F, et al. Efficacy and Safety of Acoramidis in Transthyretin Amyloid Cardiomyopathy. N Engl J Med. 2024;390(2):132-142.
35. Fontana M, Berk JL, Gillmore JD, Witteles RM, Grogan M, Drachman B, et al. Vutrisiran in Patients with Transthyretin Amyloidosis with Cardiomyopathy. N Engl J Med. 2024.
36. Maurer MS, Schwartz JH, Gundapaneni B, et al. Tafamidis Treatment for Patients with Transthyretin Amyloid Cardiomyopathy. N Engl J Med. 2018;379:1007-1016.
37. Guazzi M, Dixon D, Labate V, et al. RV Contractile Function and its Coupling to Pulmonary Circulation in Heart Failure With Preserved Ejection Fraction: Stratification of Clinical Phenotypes and Outcomes. JACC Cardiovasc Imaging. 2017;10:1211-1221.
38. Knight DS, Zumbo G, Barcella W, et al. Cardiac Structural and Functional Consequences of Amyloid Deposition by Cardiac Magnetic Resonance and Echocardiography and Their Prognostic Roles. JACC Cardiovasc Imaging. 2019;12:823-833.
39. De Gaspari M, Sinigiani G, De Michieli L, et al. Relative apical sparing in cardiac amyloidosis is not always explained by an amyloid gradient. Eur Heart J Cardiovasc Imaging. 2023;24:1258-1268.
40. Porcari A, Fontana M, Canepa M, et al. Clinical and Prognostic Implications of Right Ventricular Uptake on Bone Scintigraphy in Transthyretin Amyloid Cardiomyopathy. Circulation. 2024;149:1157-1168.
41. Ozbay B, Satyavolu BS, Rearick C, et al. Right Ventricular Strain Improves the Echocardiographic Diagnosis and Risk Stratification of Transthyretin Cardiac Amyloidosis Among Other Phenotypes of Left Ventricular Hypertrophy. J Am Soc Echocardiogr. 2024;26:S0894-7317(24)00319-5.
42. Moñivas Palomero V, Durante-Lopez A, Sanabria MT, et al. Role of Right Ventricular Strain Measured by Two-Dimensional Echocardiography in the Diagnosis of Cardiac Amyloidosis. J Am Soc Echocardiogr. 2019;32:845-853.e1.
43. Pradel S, Magne J, Jaccard A, et al. Left ventricular assessment in patients with systemic light chain amyloidosis: a 3-dimensional speckle tracking transthoracic echocardiographic study. Int J Cardiovasc Imaging. 2019;35:845-854.

44. Licordari R, Minutoli F, Recupero A, et al. Early Impairment of Right Ventricular Morphology and Function in Transthyretin-Related Cardiac Amyloidosis. J Cardiovasc Echogr. 2021;31:17-22.

Table 1 – Population characteristics stratified according to composite endpoint occurrence

Variable	Total population N=100	No Endpoint N=63	Endpoint N=37	p
Clinical characteristics				
Age (years)	81 (75–85)	80 (75–84)	81 (76 – 85)	0.4
Male sex (%)	91 (91)	56 (89)	35 (95)	0.5
NYHA class >II (%)	18 (18)	10 (16)	8 (22)	0.6
HF presentation (%)	52 (54)	27 (44)	25 (69)	**0.020**
COPD (%)	9 (9)	8 (15)	1 (3)	0.3
OSAS (%)	1 (1)	1 (2)	0 (0)	0.9
NAC stage I (%)	63 (63)	44 (70)	19 (51)	0.06
NAC stage II (%)	22 (22)	11 (17)	11 (30)	0.1
NAC stage III (%)	15 (15)	8 (15)	7 (19)	0.8
Medical therapy				
Furosemide (%)	69 (69)	38 (60)	31 (84)	**0.015**
Dose of furosemide (mg)	25 (0 – 50)	25 (0 – 50)	50 (25 – 100)	**0.006**
β–blockers (%)	53 (53)	36 (57)	17 (46)	0.3
ACE-i/ARBs/ARNI (%)	50 (50)	31 (49)	19 (51)	1
SGLT2i (%)	5 (5)	3 (8)	2 (6)	0.9
MRA (%)	39 (39)	21 (33)	18 (49)	0.1
Disease modifying therapy (%)	53 (53)	41 (65)	12 (32)	**0.002**
Time of DMT starting from diagnosis (months)	3 (1 – 8)	3 (1 – 8)	6 (1 – 11)	0.4
Electrocardiogram characteristics				
AF (%)	49 (49)	30 (48)	19 (51)	0.8
LQRSV (%)	31 (31)	23 (38)	8 (22)	0.1
QRS duration (ms)	118 (101 – 144)	111 (99 – 143)	135 (117 – 147)	**0.007**
Biochemical characteristics				
NTproBNP (ng/L)	1777 (815 – 4896)	1610 (745 – 4221)	1921 (928 – 6010)	0.1
eGFR (ml/min/m2)	60 (50 – 77)	62 (53 – 77)	57 (45 – 75)	0.3
Hs-TnI (ng/L)	78 (41 – 138)	60 (36 – 121)	92 (54 – 234)	**0.020**
Echocardiogram characteristics				
IVS (mm)	18 (16 – 20)	18 (15 – 20)	18 (16 – 20)	0.9
PW (mm)	15 (14 – 17)	16 (14 – 18)	15 (14 – 17)	0.6
RWT	0.72 (0.59 – 0.83)	0.74 (0.57 – 0.86)	0.70 (0.59 – 0.80)	0.3
LV mass (gr)	307 (258 – 387)	284 (250 – 387)	314 (269 – 388)	0.4
LV EDVi (ml/m2)	56 (46 – 67)	54 (47 – 64)	60 (43 – 72)	0.3
LV EF (%)	52 (44 – 57)	53 (43 – 58)	51 (44 – 56)	0.4
LV SVi (ml/m2)	27.2 (22.2 – 33.1)	29 (23 – 35)	27 (22 – 33)	0.9
LV GLS (-%)	11 (8 – 13)	11 (8 – 13)	11 (7 – 12)	0.6
E/A	2.1 (1.1 – 2.7)	1.5 (0.9 – 2.7)	2.6 (2.1 – 2.8)	**0.028**
E/e’	16.1 (13.4 – 19.4)	15.8 (11.9 – 19.4)	16.7 (14.4 – 19.2)	0.1
E/e’>14 (%)	68 (69)	37 (60)	31 (86)	**0.007**
Restrictive filling pattern (%)	28 (28)	13 (21)	15 (41)	**0.032**
LAVi (ml/m2)	52.5 (42.3 – 65.4)	49.7 (41.9 – 60.5)	59.4 (47.0 – 70.9)	**0.031**
RAVi (ml/m2)	45.5 (34.4 – 57.1)	43.4 (33.6 – 56.1)	50.2 (38.7 – 63.2)	0.06
RALS (%)	13.1 (8.1 – 15.9)	15.1 (8.9 – 16.1)	10.0 (5.3 – 13.8)	**0.034**
RV thickness (mm)	7.0 (4.2 – 9.0)	7 (4 – 8)	7 (5 – 9)	0.3
RV EDAi (cm2/m2)	11.6 (9.8 – 12.9)	11.4 (9.6 – 12.5)	12.4 (10.6 – 14.3)	**0.008**
TAPSE (mm)	16.5 (13.0 – 20.0)	17.1 (14.0 – 20.4)	15.1 (12.1 – 19.2)	**0.038**
RV FAC (%)	35.5 (30.0 – 41.8)	36 (30 – 42)	33 (31 – 42)	0.8
RVFWLS (-%)	16.5 (12 – 21.5)	17.9 (13 – 22)	15.0 (11 – 20)	**0.043**
RV4CLS (-%)	12.1 (9.1 – 16.6)	12.5 (9.2 – 16.8)	11 (8 – 15.3)	0.2
sPAP (mmHg)	35 (26 – 45)	30 (22 – 42)	39 (33 – 47)	**0.003**
TAPSE/sPAP (mm/mmHg)	0.45 (0.33 – 0.72)	0.50 (0.36 – 0.83)	0.38 (0.27 – 0.52)	**0.001**
RVFWLS/sPAP (%/mmHg)	0.46 (0.31 – 0.72)	0.49 (0.35 – 0.87)	0.39 (0.27 – 0.52)	**0.001**
RV4CLS/sPAP (%/mmHg)	0.33 (0.23 – 0.52)	0.39 (0.26 – 0.62)	0.28 (0.20 – 0.42)	**0.006**
Trivial TR (%)	34 (34)	29 (46)	5 (14)	**0.001**
Mild TR (%)	45 (45)	22 (35)	23 (62)	**0.010**
Moderate TR (%)	20 (20)	12 (19)	8 (22)	0.8
Severe TR (%)	1 (1)	0 (0)	1 (3)	0.4
Severe MR (%)	0 (0)	0 (0)	0 (0)	1
Severe AS (%)	1 (1)	0 (0)	1 (3)	0.4
Severe pericardial effusion (%)	1 (1)	1 (2)	0 (0)	1
Pleural effusion (%)	8 (8)	4 (6)	4 (11)	0.5

Quantitative variables expressed as median value (25^{th}–75^{th} percentile). Qualitative variables expressed as absolute number (%). Abbreviations: ACE-i=Angiotensin converter enzyme inhibitor; AF=atrial fibrillation; ARBs=angiotensin receptor blockers; ARNI=angiotensin receptor neprilysin receptor inhibitors; AS=aortic stenosis; COPD=chronic obstructive pulmonary disease; DMT=disease modifying therapy; EDAi=end diastolic area indexed; EDVi=end diastolic volume indexed; EF=ejection fraction; eGFR=estimated glomerular filtration rate; FAC=fractional area change; GLS=global longitudinal strain; HF=heart failure; Hs–TnI=high sensitivity troponin I; IVS=interventricular septum; LAVi=left atrium volume

indexed; LQRSV=low QRS voltages; LV=left ventricle; MR=mitral regurgitation; MRA=mineralocorticoids receptor antagonist; NAC=National Amyloid Centre; NYHA=New York Heart Association; NTproBNP=N-Terminal pro brain natriuretic peptide; OSAS=obstructive sleep apnoea syndrome; PW=posterior wall; RALS= right atrium longitudinal strain; RAVi=right atrium volume indexed; RVFWLS=RV free wall longitudinal strain; RV4CLS=RV 4-chamber longitudinal strain; RWT=relative wall thickness; SGLT2i=Sodium glucose transporter 2 inhibitors; sPAP=systolic pulmonary artery pressure; SVi=stroke volume indexed; RV=right ventricle; TAPSE=tricuspid annulus plane systolic excursion; TR=tricuspid regurgitation.

Table 2 – RV-PA coupling characteristics according to endpoint occurrence in patients with wtATTR-CM stage NAC Ia.

	No endpoint N = 12	**Endpoint N = 6**	**p**
TAPSE/sPAP (mm/mmHg)	0.78 (0.60 – 0.90)	0.41 (0.37 – 0.45)	**0.013**
RVFWLS/sPAP (%/mmHg)	0.79 (0.61 – 0.96)	0.47 (0.32 – 0.61)	**0.042**
RV4CLS/sPAP (%/mmHg)	0.61 (0.43 – 0.82)	0.32 (0.20 – 0.44)	**0.041**

Abbreviations as in Table 1.

Table 3 – Univariable analysis for composite endpoint predictors at 60-months follow up according to Cox's regression.

	Univariate analysis	
	HR (95% CI)	**p**
Age	1 (0.95 – 1.05)	0.9
Sex	0.64 (0.15 – 2.66)	0.5
HF presentation	2.73 (1.31 – 5.69)	**0.007**
LQRSV	0.59 (0.27 – 1.29)	0.2
QRS duration	1.02 (1.00 – 1.03)	**0.012**
NTproBNP	1.00 (1.00 – 1.00)	**0.004**
eGFR	0.99 (0.97 – 1)	0.2
TnI	1.01 (1.00 – 1.01)	0.1
Furosemide > 50 mg	2.87 (1.46 – 5.62)	**0.002**
Disease modifying therapy*	0.48 (0.22 – 1.07)	0.07
RWT	0.27 (0.05 – 1.56)	0.1
LV EF	0.98 (0.95 – 1.01)	0.3
LV Svi	1.00 (0.96 – 1.04)	0.8
LV GLS	1.07 (0.98 – 1.16)	0.1
E/A	1.77 (1.09 – 2.87)	**0.020**
E/e'	1.02 (0.97 – 1.07)	0.4
E/e' > 14	3.19 (1.24 – 8.23)	**0.016**
Restrictive filling pattern	1.74 (0.90 – 3.36)	0.1
RALS	0.92 (0.83 – 1.00)	**0.048**
RV EDAi	1.16 (1.05 – 1.29)	**0.005**
TAPSE	0.92 (0.86 – 0.99)	**0.032**
FAC	0.98 (0.94 – 1.02)	0.3
RVFWLS	0.94 (0.89 – 0.99)	**0.022**
RV4CLS	0.93 (0.86 – 1.00)	**0.043**
sPAP	1.04 (1.02 – 1.07)	**0.001**
TAPSE/sPAP	0.004 (0.01 – 0.21)	**<0.001**
RVFWLS/sPAP	0.12 (0.03 – 0.52)	**0.005**
RV4CLS/sPAP	0.06 (0.01 – 0.43)	**0.005**

Table 4 – Multivariable models for prediction of composite endpoint at 60 months follow up according to Cox's regression.

	Model 1		**Model 2**		**Model 3**		**Model 4**		**Model 5**		**Model 6**	
	HR (95% CI)	**p**	**HR (95% CI)**	**p**	**HR (95% CI)**	**p**	**HR (95% CI)**	**p**	**HR (95% CI)**	**p**	**HR (95% CI)**	**p**
HF presentation	1.39 (0.61 – 3.18)	0.4	1.34 (0.57 – 3.16)	0.5	1.36 (0.56 – 3.28)	0.5	1.30 (0.59 – 2.85)	0.5	1.12 (0.50 – 2.55)	0.8	1.12 (0.49 – 2.57)	0.8
NTproBNP	1.00 (1.00 – 1.00)	0.5	1.00 (1.00 – 1.00)	0.2	1.00 (1.00 – 1.00)	0.2	1.00 (1.00 – 1.00)	0.7	1.00 (1.00 – 1.00)	0.7	1.00 (1.00 – 1.00)	0.5
Furosemide >50 mg	2.62 (1.23 – 5.62)	**0.013**	2.42 (1.13 – 5.19)	**0.023**	2.47 (1.15 – 5.27)	**0.020**	3.38 (1.55 – 7.35)	**0.002**	2.77 (1.28 – 5.96)	**0.009**	2.74 (1.27 – 5.88)	**0.010**
TAPSE	0.94 (0.86 – 1.02)	0.2										
RVFWLS			0.97 (0.91 – 1.03)	0.3								
RV4CLS					0.97 (0.89 – 1.06)	0.5						
TAPSE/sPAP							0.04 (0.01 – 0.24)	**<0.001**				
RVFWLS/sPAP									0.07 (0.01 – 0.41)	**0.003**		
RV4CLS/sPAP											0.06 (0.01 – 0.53)	**0.011**
Model C-index	0.71		0.69		0.69		0.74		0.73		0.72	
CV model C-index	0.69		0.65		0.68		0.73		0.70		0.70	

Abbreviations as in Table 2 plus CV=cross-validat

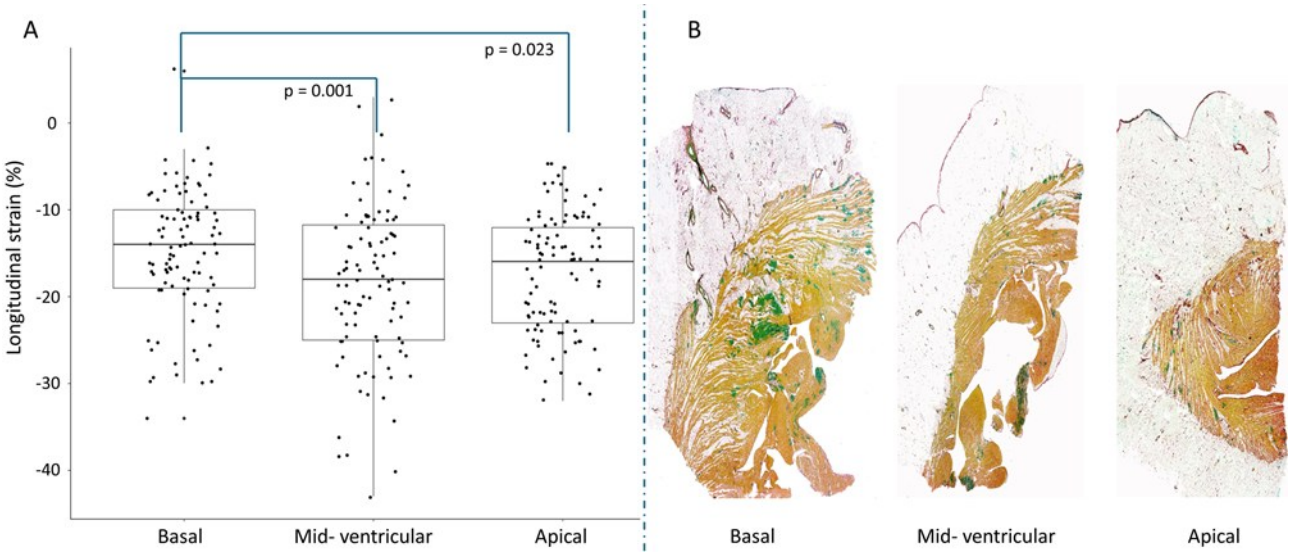

Figure 1. Right ventricular (RV) free wall longitudinal strain and amyloid infiltration. Panel A. Longitudinal strain values calculated in the basal segments of the RV free wall are significantly lower than mid-ventricular and apical ones. Panel B. Histological panoramic view of the RV free wall of a 81-year-old female patient with wtATTR-CM, showing larger amyloid infiltration (sulphated alcian blue stain) in the basal segments, compared with the mid-ventricular and apical ones.

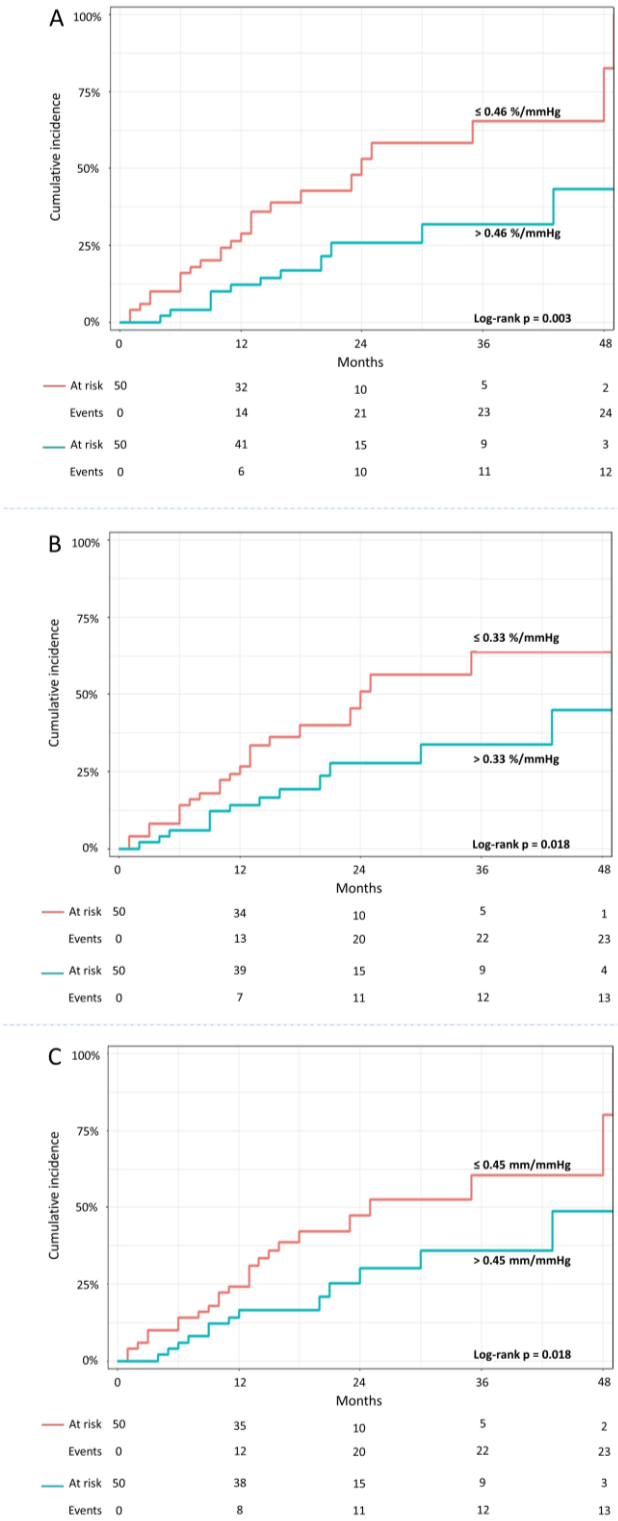

Figure 2. Cumulative incidence of composite endpoint according to the presence of RVFWSL/sPAP ≤0.46%/mmHg (A), RV4CLS/sPAP ≤0.33%/mmHg (B) or TAPSE/sPAP ≤0.45mm/mmHg (C), showing bad outcome in patients with worse RV-PA coupling ratios. Abbreviations: RV4CLS=right ventricular four-chamber strain (including the septum); RVFWLS=right ventricular free-wall longitudinal strain; sPAP=systolic pulmonary artery pressure; TAPSE=tricuspid annulus plane systolic excursion.

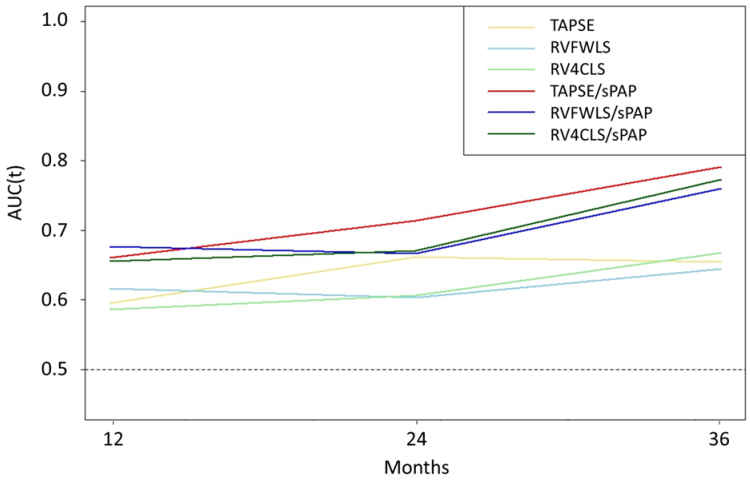

Figure 3. Time dependent AUC analysis, showing significant differences in prognostic value among RV systolic function indexes and RV-PA coupling ratios.

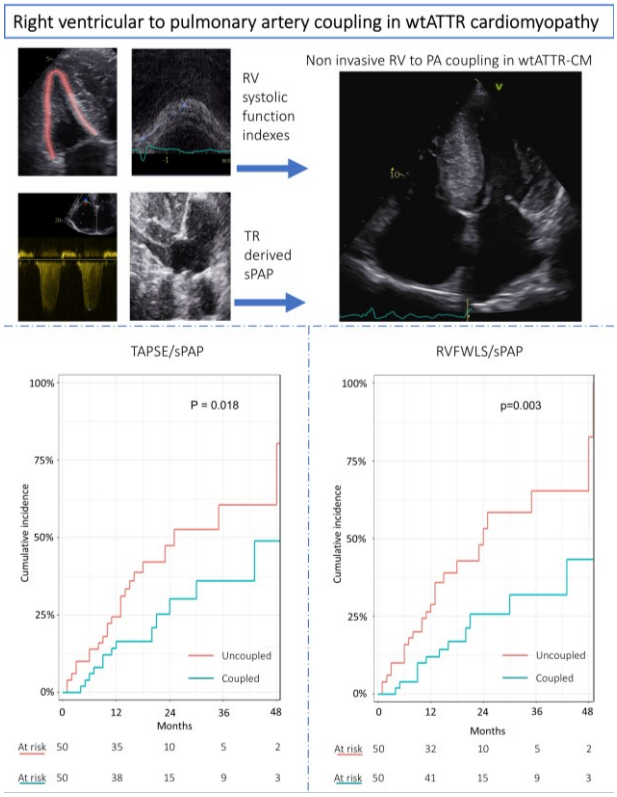

Central illustration. Prognostic value of non-invasive right to pulmonary artery coupling in wild-type transthyretin cardiomyopathy. Bad outcome is observed in patients with worse RV-PA coupling ratios.

Chapter 8. Outcome and disease progression in NYHA class I and II patients with wild-type transthyretin cardiomyopathy treated with tafamidis

This chapter is based on the manuscript: *Sinigiani G, Sanna GD, Aimo A, Porcari A, Bonacchi G, De Michieli L, Milani P, Vergaro G, Tini G, Baldan M, Martire P, Beghini A, Tomasoni D, Palmiero G, Ossola P, Musca F, Zampieri M, Guidi Colombi G, Serenelli M, Cemin R, Iseppi M, Moretti M, Giacomin E, Negri F, Driussi M, Nuvolone M, Zanoletti M, Bianco M, Chinaglia A, Faro D, Ruotolo I, Longhi S, Monte IP, Lorenzoni G, Gregori D, Imazio M, Canepa M, Ricci F, Merlo M, Perazzolo Marra M, Limongelli G, Musumeci B, Perlini S, Cappelli F, Metra M, Corrado D, Sinagra G, Emdin M, Palladini G, Cipriani A. Outcome and Disease Progression in NYHA Functional Class I and II Patients With Wild-Type Transthyretin Cardiomyopathy Treated With Tafamidis. JACC Heart Fail. 2025;13(8):102549.*

Wild-type transthyretin amyloid cardiomyopathy (ATTRwt-CM) is a progressive cardiac disease caused by the deposition of misfolded transthyretin (TTR) in the myocardium, leading to increased wall thickness, diastolic dysfunction and heart failure (HF). Tafamidis, a TTR stabilizer, reduced all-cause mortality and functional deterioration in the ATTR-ACT trial, particularly in early-stage patients, and received a class I recommendation in the 2021 European HF guidelines for patients with ATTRwt-CM and New York Heart Association (NYHA) Class I or II. Although real-world studies have confirmed the benefit of tafamidis, mortality and clinical progression remain relevant, underscoring the need for better tools to identify patients at higher risk of poor outcomes[1]. Furthermore, no objective tools are currently validated to monitor disease progression under tafamidis treatment. Expert consensus recommends multidomain assessment—clinical, biochemical, and imaging-based—but their application and prognostic value in tafamidis-treated cohorts are still poorly defined[2]. Recent data from untreated cohorts demonstrated that NT-proBNP elevation, kidney function decline, and outpatient diuretic intensification (ODI) may serve as markers of disease progression[3-4]. Whether these criteria apply in tafamidis-treated patients remains unclear. This study aimed to investigate outcome in early-stage ATTRwt-CM patients treated with tafamidis, to evaluate the prognostic value of previously proposed progression markers, and to identify baseline features associated with disease progression and poor prognosis despite treatment.

This was a multicenter, longitudinal, observational study conducted in the ATTR-CM outpatient clinic of 19 Italian centers. The study was approved by the coordinating center's ethics committee (AOP3378), with local approvals obtained. It complied with the Declaration of Helsinki, and informed consent was obtained per institutional regulations. We included consecutive patients with a definitive diagnosis of ATTRwt-CM who initiated tafamidis between October 2021 (Italian approval) and December 31st, 2022. Diagnosis was established by biopsy or by non–invasive criteria per European consensus, with TTR genetic testing performed in all patients to exclude hereditary forms. Exclusion criteria were: NYHA class>II, unstable HF requiring diuretic adjustment at tafamidis initiation, enrolment in ATTR–CM trials, or compassionate-use tafamidis. Clinical data were collected at baseline (defined as the day of tafamidis initiation) and at 12 months, including medical history, laboratory exams and echocardiography. The primary endpoint was a composite of all-cause death and HF hospitalization requiring intravenous diuretic administration. Continuous variables were expressed as medians [Q1-Q3] and compared using Wilcoxon rank sum. Categorical variables were compared using chi-square test or Fisher ‘s exact test. Two analyses were performed. First, a time-to-event analysis from baseline using Cox regression, after verifying proportional hazards. For patients without the endpoint, follow up was censored at June 30th, 2024. Multivariable models included variables significant in univariable analysis ($p<0.05$) and those with clinical relevance: HF presentation (defined as the index heart failure event—requiring hospitalization and intravenous diuretic therapy—that led to the diagnosis of ATTRwt-CM and occurred within 12 months prior to enrollment), time from diagnosis to treatment, 6-minute walking test distance (6MWTD), National Amyloidosis Centre (NAC)/Mondor staging system, daily loop diuretic dose, left ventricular ejection fraction (LVEF), E/e’ ratio and tricuspid annulus plane systolic excursion (TAPSE) over systolic pulmonary artery pressure (sPAP) ratio. Second, a 12-month landmark analysis excluded patients with prior events to avoid intervention-related bias. It

assessed the prognostic value of progression markers: worsening NYHA class, NAC/Mondor stage 6MWTD (decrease > 35 meters), eGFR (decrease > 20%), NT-proBNP (absolute increase > 700 ng/L and relative increase >30%), ODI (any initiation or dose increasing of loop diuretic drugs), LV wall thickness (increase ≥ 2 mm), diastolic function (increase ≥ 2 in E/e' ratio), and LVEF (decrease ≥ 5%). Cox regression was repeated from the 12-month timepoint. Model collinearity was assessed with variance inflation factor (VIF), and discrimination with Harrell's C-statistic. Odds and hazard ratios (OR and HRs) were calculated per 1-unit increase (for daily diuretic dose index per 0.5 mg/kg increments). Non-linear associations for diuretic dose were explored using restricted cubic splines. Logistic regression identified baseline factors associated with progression. Survival was assessed using Kaplan-Meier and log-rank tests. Bonferroni correction was applied for multiple comparisons. Statistical analysis was performed using RStudio(v4.4.2).

The study population comprised 683 patients [91% males, median age 78 (73–81) years, 31% >80 years]. Median time from diagnosis to tafamidis start was 6 (2–15) months. One third (n =232, 34%) had prior HF presentation. Most patients were in NYHA class II (85%) and NAC/Mondor stage I (64%). Median values were: 6MWTD 375 m, NT-proBNP 1921 ng/L and eGFR 65 ml/min/m2. Beta-blockers and loop diuretics were used in 59% and 72% of patients, respectively, with median daily furosemide-equivalent dose of 0.32 mg/kg. Over a median follow up of 18 (15–22) months after tafamidis start, the primary endpoint (all-cause death or HF hospitalization) occurred in 97 patients (15%), including 45 (7%) deaths. Primary endpoint cumulative incidence was 9%, 13% and 26% at 12, 18 and 30 months, respectively. All-cause mortality incidence was 3%, 6% and 13%, at same timepoints (**Fig.1,panel A**). Higher baseline daily loop diuretic dose (HR 1.39, 95%CI 1.21–1.59,p<0.001) and NAC/Mondor stage III (HR 2.24, 95%CI 1.08–4.65,p=0.030) were independent associated with the primary endpoint. The relationship between loop diuretic dose indexed and outcome was non-linear (p=0.007), with a significant change-point in HR at 0.35

mg/kg of daily loop diuretic intake [HR from 0 to 0.35 mg/kg=2.26 (95% CI 1.47–3.49); HR from 0.35 to 1.5 mg/kg=2.65 (95% CI 2.08–3.38)]. Patients taking >0.35 mg/kg had a significantly worse outcome (Log-rank p<0.001), especially when combined NAC/Mondor stage III (Log-rank p<0.001) (**Fig.1,panel B**).

At 12 months, HF hospitalization occurred in 37 patients, who showed a markedly increased risk of subsequent death (HR 9.59, 95%CI 4.09–22.5,p<0.001). After excluding these patients and those who died (n=58), 625 patients were eligible for landmark analysis. NT-proBNP progression, eGFR decline and ODI occurred in 146/625 (23%), 117/591 (20%) and 210/625 (34%) patients, respectively. Clinical deterioration included worsening NYHA class in 85/607 (14%), NAC/Mondor stage in 109/591 (18%), 6MWTD in 114/545 (21%), IVS thickness in 86/535 (16%), LV EF in 113/550 (21%) and E/e' ratio in 151/397 (38%). Progression in NYHA class (particularly to class III), any NAC/Mondor stage, eGFR decline, NT-proBNP and ODI were significantly associated with adverse outcomes (**Fig.1,Panel C**). Conversely, imaging-derived markers (IVS, LVEF, and E/e') and age showed no prognostic value. After excluding collinearity between covariates (VIF<5), two multivariable risk models were developed: one including worsening to NYHA class III and NAC/Mondor stage, the other including ODI and worsening in eGFR and NT-proBNP. All variables were independently associated with the primary endpoint. Prognostic accuracy was comparable (Harrell's C 0.71 and 0.72, p=0.2). The contemporary presence of all markers of progression was associated with worse survival (**Fig.1,panel C**). In logistic regression, HF presentation (OR 1.63, 95%CI 1.01–2.64,p=0.046), higher loop diuretic dose (OR 1.95, 95%CI 1.24–3.15,p=0.005) and sPAP (OR 1.03, 95%CI 1.01–1.05,p=0.010) were independently associated with NYHA I/II to III class worsening or any NAC/Mondor worsening at 12-months after therapy start.

This study evaluated outcomes and disease progression in 683 tafamidis-treated ATTRwt-CM patients with NYHA class I–II symptoms. Over a median 18-month follow-up, 15% experienced death or HF hospitalization (9% within the first 12 months). Baseline NAC/Mondor stage III and loop diuretic dose >0.35 mg/kg were associated with worse outcomes. At 12 months, up to one-third showed signs of disease progression. Worsening in NYHA class, NAC/Mondor stage, NT-proBNP, eGFR, and ODI were associated with poor prognosis. Two risk models—one based on clinical progression, the other on biomarkers and ODI—showed comparable accuracy (C-statistics 0.71 and 0.72) and may guide clinical monitoring and therapeutic decision-making in tafamidis-treated patients.

Until recently considered a rare, untreatable disease, ATTRwt-CM is now diagnosed earlier and more often in patients with milder phenotypes. Our cohort, mostly NYHA class I–II and NAC/Mondor stage I, showed 12-, 18-, and 30-month survival rates of 97%, 94%, and 87%, respectively—higher than those observed in earlier trials. Nonetheless, 9% experienced death or HF hospitalization within 12 months. Baseline NAC/Mondor stage III and high daily loop diuretic dose identified high-risk patients. At 12 months, worsening in NYHA class, NT-proBNP, eGFR, and ODI—but not imaging parameters—were associated with adverse outcomes. These findings suggest that disease progression under tafamidis can be assessed primarily through clinical and biochemical markers, as previously reported[3-5], and support earlier diagnosis and individualized treatment strategies in ATTRwt-CM.

This study has limitations. The results apply only to ATTRwt-CM patients in NYHA class I–II. Although some data were missing in the landmark analysis, the overall sample size remained robust. ODI was limited to loop diuretics. The 18-month follow-up may appear short but is likely appropriate for detecting early disease progression in early-stage patients, although longer-term trends and external validation will require further investigation.

In summary, within 12 months of starting tafamidis, 9% of patients experienced HF hospitalization or death, and up to one-third exhibited markers of disease progression. Baseline NAC/Mondor stage III and a high daily loop diuretic dose were independently associated with adverse outcomes. Using a 12-month landmark analysis, we demonstrated that clinical and biochemical worsening over time was associated with subsequent events. Two progression-based models effectively identified high-risk patients may help guide treatment decisions in clinical practice as well as serve as potential endpoints for future clinical trials.

8.1 References

1 Masri A, Bhattacharya P, Medoff B, et al. A Multicenter Study of Contemporary Long-Term Tafamidis Outcomes in Transthyretin Amyloid Cardiomyopathy. JACC CardioOncol. 2025;7:282-293.

2 Garcia-Pavia P, Bengel F, Brito D, et al. Expert consensus on the monitoring of transthyretin amyloid cardiomyopathy. Eur J Heart Fail. 2021;23(6):895-905.

3 Ioannou A, Cappelli F, Emdin M,et al. Stratifying Disease Progression in Patients With Cardiac ATTR Amyloidosis. J Am Coll Cardiol. 2024;83(14):1276–91.

4 Ioannou A, Razvi Y, Porcari A, et al. Kidney Outcomes in Transthyretin Amyloid Cardiomyopathy. JAMA Cardiol. 2024:e244578.

5 Bampatsias D, Wardhere A, Zeldin L, et al. Cardiac disease monitoring measures in patients with transthyretin amyloid cardiomyopathy treated with tafamidis. Heart. 2025 Mar 23:heartjnl-2024-324826.

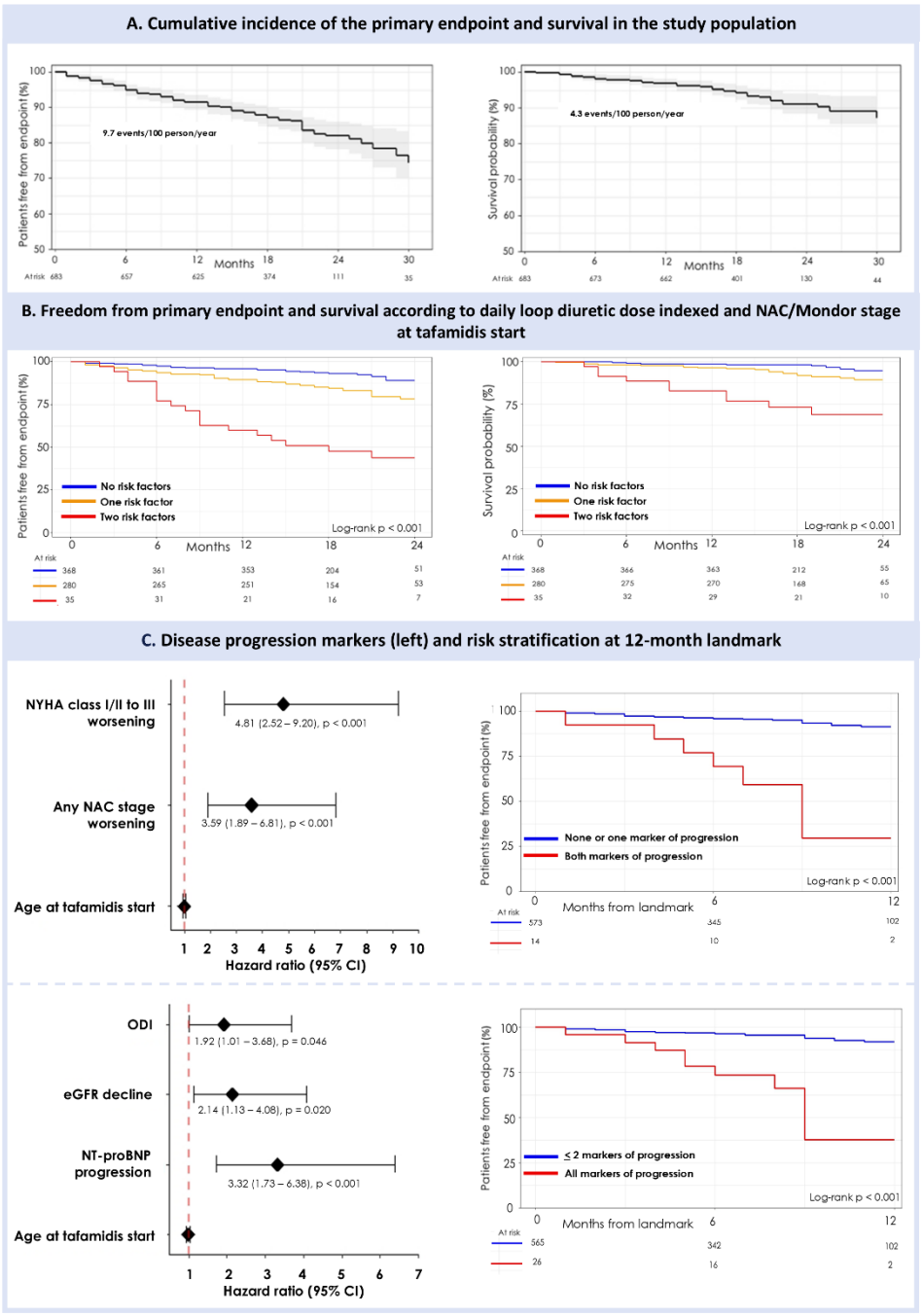

Figure 1. Outcome and Disease Progression in Early Tafamidis-Treated ATTRwt-CM Patients. Panel A: Cumulative incidence of the primary endpoint (left) and survival probability (right) in the overall study population. Panel B: Time to primary endpoint (left) and survival probability (right) stratified by the presence of baseline loop diuretic dose >0.35 mg/kg and NAC/Mondor stage III. Panel C: Independent risk factors for adverse outcomes at 12-month landmark analysis (left). Time to primary endpoint according to concurrent worsening of NYHA class to III and NAC/Mondor stage progression (top right), and according to concurrent NT-proBNP progression, eGFR decline, and outpatient diuretic intensification (ODI) (bottom right).

Chapter 10. Summary of conclusions from original contributions

1. The present clinicopathological study demonstrated that amyloid is variably distributed in the heart of patients affected by CA, with vascular involvement being more frequent in AL-CA. The amyloid burden at histology was significantly greater in the basal and mid-ventricular levels compared with the apex and in the subendocardial layers compared with the subepicardial ones (i.e. longitudinal and transmural gradients). A direct correlation between segmental amyloid burden and LS in each segment is evident. The RELAPS phenomenon at echocardiography is present in nearly half of cases and is not always explained by a base-to-apex gradient of amyloid burden at histopathology, suggesting that RELAPS might be an epiphenomenon of complex interactions among amyloid infiltration, myocardial structure, and adaptation.
2. In patients with AL-CA and ATTR-CA, IABs are common and together with advanced age and reduced LAEF on CMR are independent predictors of incident AF. Patients with these features might benefit from closer AF screening strategies during follow-up.
3. In a modern cohort of patients with wtATTR-CM, RV-PA uncoupling emerged as an early and strong predictor of outcome, being independently associated with the risk of HF hospitalisation or all – cause death. No differences in risk prediction were observed among M-mode and strain-based RV function parameters. The evaluation of RV-PA uncoupling should be considered in the clinical practice for risk stratification and prognosis assessment of patients with wtATTR-CM, with potential implications treatment strategies definition.
4. In summary, within 12 months of starting tafamidis, 9% of patients experienced HF hospitalization or death, and up to one-third exhibited markers of disease progression. Baseline NAC/Mondor stage III and a high daily loop diuretic dose were independently associated with adverse outcomes. Using a 12-month landmark analysis, we demonstrated

that clinical and biochemical worsening over time was associated with subsequent events. Two progression-based models effectively identified high-risk patients may help guide treatment decisions in clinical practice as well as serve as potential endpoints for future clinical trials.